

Electronic band gaps from Quantum Monte Carlo methods

Yubo Yang,¹ Vitaly Gorelov,² Carlo Pierleoni,^{2,3} David M. Ceperley,¹ and Markus Holzmann^{4,5}

¹*Department of Physics, University of Illinois, Urbana, Illinois 61801, USA*

²*Maison de la Simulation, CEA, CNRS, Univ. Paris-Sud,
UVSQ, Université Paris-Saclay, 91191 Gif-sur-Yvette, France*

³*Department of Physical and Chemical Sciences,
University of L’Aquila, Via Vetoio 10, I-67010 L’Aquila, Italy*

⁴*Univ. Grenoble Alpes, CNRS, LPMMC, 3800 Grenoble, France*

⁵*Institut Laue Langevin, BP 156, F-38042 Grenoble Cedex 9, France*
(Dated: November 29, 2021)

We develop a method for calculating the fundamental electronic gap of semiconductors and insulators using grand canonical Quantum Monte Carlo simulations. We discuss the origin of the bias introduced by supercell calculations of finite size and show how to correct the leading and subleading finite size errors either based on observables accessible in the finite-sized simulations or from DFT calculations. Our procedure is applied to solid molecular hydrogen and compared to experiment for carbon and silicon crystals.

I. INTRODUCTION

Insulator and semiconductors are characterized by a non-vanishing *fundamental gap* [1], defined in terms of the ground state energies of a system of fixed ions as the number of electrons is varied:

$$\Delta_{N_e} = E_0(N_e + 1) + E_0(N_e - 1) - 2E_0(N_e) \quad (1)$$

where $E_0(N_e)$ is the ground state energy of an N_e electron system.

Within density functional theory (DFT), it is common to interpret the eigenvalues of the Kohn-Sham equations as excitation energies, the gap being the minimum excitation energy. However, the resulting band gap within the local density approximation (LDA) is typically found too small [2]. This qualitative failure can be alleviated either by hybrid functionals or by adding corrections based on GW many-body perturbation theory, although the precise value depends on the underlying functional and approximation scheme involved [1]. In principle, the fundamental gap can be calculated from any method for ground state energies based on the above formula. High precision methods for correlation energies as, for example, provided by quantum Monte Carlo (QMC) [3–6] or coupled cluster methods [7, 8] can be used. In this paper, we propose a new method for accurate calculations of the fundamental gap within explicitly correlated methods and demonstrate its use with fixed-node Diffusion Monte Carlo (DMC) benchmark studies on solid H₂, C, and Si.

Methods based on correlated many-body wave functions are usually applied to finite sized systems, e. g. limited to supercells containing only few unit cells. QMC calculations of single particle excitations for adding and removing electrons [9–12] crucially rely on the imposed extrapolation law (e.g. 1/ L in [12] opposed to 1/ L^3 in [11] where L denotes the linear extension of the supercell). This introduces considerable uncertainty in the results. Heuristically, single particle excitations are expected to converge slowly for electronic systems, inversely

proportional to L , due to the interaction of charges across the periodic boundaries [13, 14]. Extrapolations with respect to the size of the supercells are then essential to obtain reliable values of the gap in the thermodynamic limit.

Most of the QMC calculations [15–24] have therefore addressed charge neutral, particle-hole excitations, where faster convergence with respect to the size of the supercell is expected. Although the comparison with experiment is appealing [5], a later, more extended DMC study [25] of simple semiconductor materials with larger supercells observed a 1/ L dependance of the gap on the size of the supercell for both, charged single particle and charge-neutral particle-hole excitations. In addition, fixed-node energy differences are not constrained to be upper bounds for particle-hole excitations [26] since orthogonality to the ground state cannot be strictly guaranteed. Furthermore, all QMC calculations so far have addressed excitations at selected symmetry points contained inside the supercell of the simulation. The fundamental gap was then estimated indirectly by introducing a “scissor operator” [27] which assumes a rigid shift of the underlying DFT band structure over the whole Brillouin zone.

In this paper, we show that twisted boundary conditions within the grand canonical ensemble can be used to determine the fundamental gap from QMC without relying on the “scissor” approximation. We prove that to leading order, finite size effects due to two-body correlations are of order 1/ L , and are related to the dielectric constant of the material. Such effects can be understood and corrected for by using the long wavelength properties of the electronic structure factor. For that, we extend the approach described in Ref. [28, 29] which discusses the correction of finite size effects on the ground state energy based on information contained in the static correlation functions of the finite system. Using the static structure factor from simulation, it is possible to obtain estimates of finite size corrections for the band gap, and its asymptotic functional form without the need for explicit studies at different sizes or referring to DFT or to experimental

information external to the QMC calculation.

The paper is organized as follows. In section II, we describe the main ideas behind our new band gap method based on the grand canonical ensemble. In section III, we derive finite size corrections to energy differences based on an explicit many-body wavefunction and exact diagrammatic relations. In section IV, we describe the computational methods used to calculate the fundamental gap. In section V, we show results for H₂, C, and Si crystals and compare with available experimental values of the gap in section VI. Finally in section VII, we summarize general features of the method and outline possible extensions and applications.

II. GRAND-CANONICAL TWIST AVERAGED BOUNDARY CONDITION (GCTABC)

In the following, we consider N_e electrons in a perfect crystal, neglecting both zero point and thermal motion of the ions. A uniform background charge (depending on N_e) is added to assure global charge neutrality when adding or subtracting electrons to a charge neutral system. The fundamental gap, Eq. (1), is unaffected by the background energy, because the background charge needed when adding an electron cancels against the one needed when removing an electron. Periodic boundary conditions of the charge densities are used to eliminate surface effects.

The energetic cost of adding an electron to the system at fixed volume, $V = L^3$, defines the chemical potential

$$\mu_{N_e}^+ = E_0(N_e + 1) - E_0(N_e). \quad (2)$$

A non-vanishing gap implies a discontinuity in the chemical potential from Eq. (1).

It is convenient to work in the grand-canonical ensemble. There, the chemical potential μ is treated as an independent variable and we minimize $E_0(N_e) - \mu N_e$ with respect to N_e at zero temperature and fixed volume. Insulators then represent an incompressible electronic state; for values of μ within the gap, $\partial N_e / \partial \mu = 0$.

To reduce finite size effects, we employ twisted boundary conditions on many-body wave function. as an electron is moved across the supercell, e.g. by moving an electron a distance equal to the size of the box in the x direction:

$$\Psi(\mathbf{r}_1 + L_x \hat{x}) = e^{i\theta_x} \Psi(\mathbf{r}_1). \quad (3)$$

the phase of the many-body wavefunction changes by θ . The ground state energy then depends on the twist angle, $E_0(N_e, \theta)$. Twist averaging can significantly accelerate the convergence to the thermodynamic limit [30]. Within the grand-canonical ensemble [28, 29], the optimal number of electrons $\bar{N}_e(\theta)$ will depend on θ for given chemical potential μ . To fix nomenclature, we define the *mean electronic density*

$$n_e(\mu) = (M_\theta V)^{-1} \sum_\theta \bar{N}_e(\theta), \quad (4)$$

and the *ground-state energy density*

$$e_0(\mu) = (M_\theta V)^{-1} \sum_\theta E_0(\bar{N}_e(\theta), \theta). \quad (5)$$

n_e is determined by minimizing the free energy density

$$f = \frac{1}{M_\theta V} \sum_\theta \min_{N_e} [E_0(N_e, \theta) - \mu N_e], \quad (6)$$

where the sum is over a uniform grid containing M_θ twist angles. For any single electron theory the electronic density $n_e(\mu)$ and the ground state energy density $e_0(\mu)$ coincide exactly with the corresponding thermodynamic limit values for a sufficiently large value of M_θ , e.g. when the sum over twists becomes an integral over the Brillouin zone. Size effects remaining after twist averaging are due to electron-electron correlations.

Figure 1 illustrates $e_0(\mu)$ and $n_e(\mu)$ for solid molecular hydrogen, computed from HSE functional and from QMC (see section IV for details). The value of the band gap can be directly extracted from the width of the incompressible region. Alternatively, if we eliminate μ in favor of n_e , and plot e_0 as a function of n_e , the fundamental gap is obtained by the discontinuity of the derivative, according to Eq. (1).

The definition of the fundamental gap can apply to different symmetry sectors. For a perfect crystal, the total momentum of the electrons modulo reciprocal lattice vectors is conserved, i.e. the crystal momentum. By requiring the total crystal momentum of the electrons to be fixed, e.g. using Bloch type orbitals in the Slater-determinant, the full band structure in the Brillouin zone can be mapped out. For a spin-independent Hamiltonian, one can also impose the total spin to determine the fundamental gap in each spin sector. In practice, the charge gap in the spinless sector can be determined by adding or removing pairs of electrons. The extensions of our definitions and formulas to this case are straightforward, e.g. $\Delta_{N_e} = [E_0(N_e + 2) + E_0(N_e - 2) - 2E_0(N_e)]/2$. We follow this procedure of spin neutral excitations in the remainder of the paper.

III. FINITE SIZE EFFECTS

A. Potential energy

A key quantity in understanding size effects is the long wave length behavior of the static structure factor, $S_{N_e}(\mathbf{k}) = \langle \rho_{-\mathbf{k}} \rho_{\mathbf{k}} \rangle / N_e$ where $\rho_{\mathbf{k}} = \sum_j e^{i\mathbf{k} \cdot \mathbf{r}_j}$ is the Fourier transform of the instantaneous electron density. The structure factor for a homogenous system obeys the bound [1, 18]

$$S_{N_e}(k) \leq \frac{\hbar k^2}{2m\omega_p} \left(1 - \frac{1}{\epsilon_k}\right)^{1/2}, \quad (7)$$

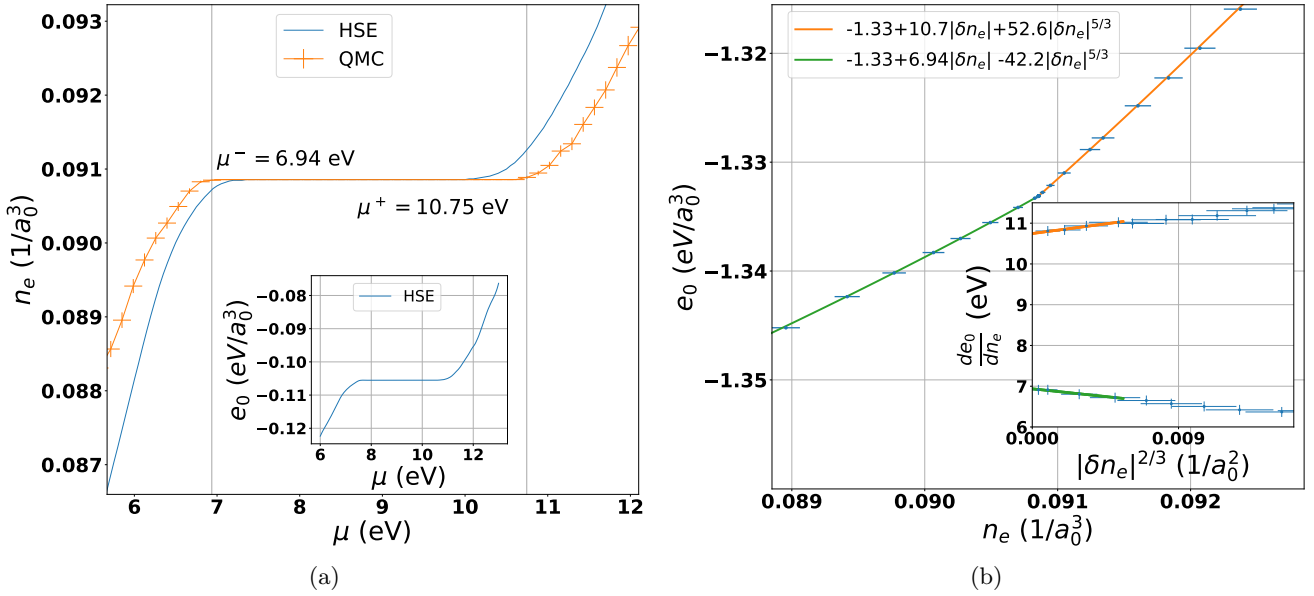


FIG. 1. GCTABC analyses of the C2/c-24 structure of solid hydrogen at $r_s = 1.38$ (234GPa). (a) the electron density n_e as a function of the chemical potential μ obtained from HSE functional in comparison to QMC, the inset illustrates the energy density as a function of μ from HSE functional. (b) energy density e_0 as a function of n_e using QMC, the inset shows the derivative discontinuity where δn_e is the change of the electronic density with respect to the insulating state. Size corrections as discussed in the text are included.

where $\omega_p = 4\pi\hbar^2 e^2 n_e/m$ is the plasma frequency and ϵ_k the static dielectric constant for wavevector k (To simplify the notations, we will suppress the dependence on the wave vector in the following). This inequality is derived by applying the plasmon-pole approximation to the sum rules of the dynamic structure factor $S(k, \omega)$. It implies that the structure factor must vanish quadratically as $k \rightarrow 0$ [31]. Equality will be obtained if $S(k, \omega)$ reduces to a single delta function at small k . The $1/N_e$ finite-size corrections of the energy per electron is a direct consequence of this behavior of $S_{N_e}(k)$ [28]. However, these leading order corrections are not sufficient for excitation energies, since the energy gap is of the same order as finite size corrections to the total energy.

As we will show below, the key to understanding size effects of energy differences is encoded in the change of $S_{N_e}(k)$ as electrons are added or removed. In particular, the limiting behavior of $S_{N_e \pm 1}(k)$ as $k \rightarrow 0$ will provide the dominant finite size correction.

For concreteness, we will assume a Slater-Jastrow form for the ground state wave function $\Psi_0 \propto D \exp[-U]$. The determinant, D , is built out of Bloch orbitals, $\phi_{\mathbf{q}n}(\mathbf{r})$ with \mathbf{q} inside the first Brillouin zone, n is the band index, and U is a general, symmetric n -body correlation factor [32]. For simplicity we assume it is two body: $U = \sum_{i < j} u(r_i, r_j)$. Let us consider the action of $e^{i\mathbf{k} \cdot \mathbf{r}_j}$ on a single particle orbital $\phi_{\mathbf{q}n}(\mathbf{r}_j)$ in the Slater determinant of the ground state. In the limit of small \mathbf{k} , this can be approximately written as $\phi_{\mathbf{q}+\mathbf{k}n}(\mathbf{r}_j)$. Expanding the determinant in terms of its cofactors $\frac{\delta D}{\delta \phi_{\mathbf{q}n}(\mathbf{r}_j)}$ and making

the excitation we have

$$\rho_{\mathbf{k}} \Psi_0 \propto \sum_j \sum_{\mathbf{q}, n} \frac{\delta D}{\delta \phi_{\mathbf{q}n}(\mathbf{r}_j)} e^{i\mathbf{k} \cdot \mathbf{r}_j} \phi_{\mathbf{q}n}(\mathbf{r}_j) e^{-U}. \quad (8)$$

and the resulting determinant after summation over j vanishes for small k if the Bloch orbital $(\mathbf{q} + \mathbf{k}, n)$ is already occupied in the ground state determinant. Considering $N_e \pm 1$ electron wave functions, $\Psi_0(N_e \pm 1; \pm \mathbf{q}, m)$ where N_e corresponds to the insulating state with fully occupied bands in the Slater determinant, and $\mathbf{q}m$ denotes the additional particle/ hole orbital, we get

$$\lim_{k \rightarrow 0} \rho_{\mathbf{k}} \Psi_0(N_e \pm 1; \mathbf{q}, m) \sim \pm \Psi_0(N_e \pm 1; \mathbf{q} + \mathbf{k}, m) \quad (9)$$

for $k \neq 0$ where different sign for particle or hole excitations on the r.h.s. is chosen to match the most common sign convention, e.g. of Ref. [33]. The limit $k \rightarrow 0$ is discontinuous since $\rho_{\mathbf{k}=0} \Psi_0(N_e \pm 1; \mathbf{q}, m) \equiv (N_e \pm 1) \Psi_0(N_e \pm 1; \mathbf{q}, m)$.

Kohn [33, 34] has pointed out that in the insulating state the matrix elements

$$\lim_{\mathbf{q}' \rightarrow \mathbf{q}} \langle \Psi_0(N_e \pm 1; \mathbf{q}, m) | \rho_{\mathbf{q}-\mathbf{q}'} | \Psi_0(N_e \pm 1; \mathbf{q}', m) \rangle = \pm \frac{1}{\epsilon} \quad (10)$$

approach the inverse dielectric constant, ϵ^{-1} , up to a sign.

Substituting Eq. (9) into Eq. (10), suggests the following finite size behavior of the static structure factor of insulators

$$\lim_{k \rightarrow 0} S_k^\pm = \alpha_\pm + \mathcal{O}(k^2), \quad (11)$$

$$S_k^\pm \equiv (N_e \pm 1) S_{N_e \pm 1}(k) - N_e S_{N_e}(k), \quad (12)$$

where α_{\pm} is proportional to ϵ^{-1} . However, α_{\pm} in general differs from ϵ^{-1} unless Eq. (9) is an exact equality.

Figure 2 shows the behavior of S_k^{\pm} for carbon and silicon crystals. Note that these functions extrapolate to a nonzero value as $k \rightarrow 0$.

The long wavelength behavior of the structure factor, Eq. (11), then gives rise to size corrections to excitation energies through the potential energy term

$$\left[\int \frac{d^3k}{(2\pi)^3} - \frac{1}{V} \sum_{\mathbf{k} \neq 0} \right] \frac{v_k}{2} S_k^{\pm} \simeq \alpha_{\pm} \frac{|v_M|}{2}, \quad (13)$$

where we have defined the Madelung constant as

$$v_M = \left[\frac{1}{V} \sum_{\mathbf{k} \neq 0} - \int \frac{d^3k}{(2\pi)^3} \right] v_k \sim L^{-1} \sim N_e^{-1/3}. \quad (14)$$

For the Coulomb potential, v_M is proportional to L^{-1} , the inverse linear extension of the simulation cell. The negative proportionality constant depends on the boundary conditions, e.g. cell geometry, and can be calculated by the Ewald image technique [35].

B. Kinetic energy

Following Ref. [29], we now discuss the kinetic energy contribution $\hbar^2 [\nabla U]^2 / 2m$ which arises from electron correlation. For a two-body Jastrow $U = \sum_{\mathbf{k}} u_{\mathbf{k}} \rho_{\mathbf{k}} \rho_{-\mathbf{k}} / 2V$, and we are only interested in the long-wave length limit, $k \rightarrow 0$, of the electron-electron correlation, with wave vectors smaller than the reciprocal lattice vectors of the crystal, \mathbf{G} . Isolating the singular contributions involving $\rho_{k=0} \equiv N_e$ in the spirit of the rotating (random) phase approximation (RPA) we have

$$\begin{aligned} \langle [\nabla U]^2 \rangle &= -\frac{1}{V^2} \sum_{\mathbf{k} \neq 0, \mathbf{k}' \neq 0} (\mathbf{k} \cdot \mathbf{k}') u_{\mathbf{k}} u_{\mathbf{k}'} \langle \rho_{\mathbf{k}+\mathbf{k}'} \rho_{-\mathbf{k}-\mathbf{k}'} \rangle \\ &\simeq \frac{1}{V^2} \sum_{\mathbf{k} \neq 0} N_e k^2 u_{\mathbf{k}}^2 \langle \rho_{\mathbf{k}} \rho_{-\mathbf{k}} \rangle. \end{aligned} \quad (15)$$

Therefore, for systems with explicit long-range correlations $u_{\mathbf{k}} \sim k^{-2}$, the kinetic energy will contribute also to the leading order size corrections with

$$\left[\int \frac{d^3k}{(2\pi)^3} - \frac{1}{V} \sum_{\mathbf{k} \neq 0} \right] \frac{n_e \hbar^2 k^2 u_{\mathbf{k}}^2}{2m} S_k^{\pm} \simeq \alpha_{\pm} c \frac{|v_M|}{2}, \quad (16)$$

where $c = \lim_{k \rightarrow 0} n_e \hbar^2 k^2 u_{\mathbf{k}}^2 / (mv_k)$ is approximately given by the ratio of the $1/N_e$ finite-size corrections of the kinetic to potential energy of the ground state energy per particle due to two-body correlations [29].

C. Total gap corrections from Coulomb singularity

Up to now, we have shown how the long range behavior of the structure factor and Jastrow factor can give rise to

a $1/L$ correction to the excitation gap with a proportionality factor determined by the structure factor changes. In the following, we will further demonstrate that, given the trial wave functions coincide with the exact ground state wave function for N_e and $N_e \pm 1$ electrons, this proportionality factor is indeed given by the dielectric constant

$$\Delta_{\infty} - \Delta_V = \frac{|v_M|}{\epsilon} + \mathcal{O}\left(\frac{1}{V}\right), \quad (17)$$

as phenomenologically assumed in previous work [14, 25].

We prove this by an independent argument based on commutation relations. Let us denote the exact insulating ground state of the N_e electron system as $|\Psi_0^{N_e}\rangle$, its energy as $E_0^{N_e}$, and the exact excited state of the $N_e \pm 1$ electron system as $|\Psi_{\mathbf{k}}^{N_e \pm 1}\rangle$ with energy $E_{\mathbf{k}}^{N_e \pm 1}$; \mathbf{k} indicates that the additional/subtracted electron adds/subtracts the crystal momentum \mathbf{k} . We have

$$E_{\mathbf{k}}^{N_e+1} - E_0^{N_e} = \frac{\langle \Psi_{\mathbf{k}}^{N_e+1} | [H, a_{\mathbf{k}}^\dagger] | \Psi_0^{N_e} \rangle}{\langle \Psi_{\mathbf{k}}^{N_e+1} | a_{\mathbf{k}}^\dagger | \Psi_0^{N_e} \rangle} \quad (18)$$

for particle and

$$E_{\mathbf{k}}^{N_e-1} - E_0^{N_e} = \frac{\langle \Psi_{\mathbf{k}}^{N_e-1} | [H, a_{\mathbf{k}}] | \Psi_0^{N_e} \rangle}{\langle \Psi_{\mathbf{k}}^{N_e-1} | a_{\mathbf{k}} | \Psi_0^{N_e} \rangle} \quad (19)$$

for hole excitations. In second quantization, the Hamiltonian, $H = T + V_{ee}$, is given by

$$T = \sum_{\mathbf{k}} \left[\frac{\hbar^2 k^2}{2m} a_{\mathbf{k}}^\dagger a_{\mathbf{k}} + \sum_{\mathbf{G}} u(\mathbf{G}) a_{\mathbf{k}+\mathbf{G}}^\dagger a_{\mathbf{k}} \right], \quad (20)$$

$$V_{ee} = \frac{1}{2V} \sum_{\mathbf{q} \neq 0} v_q [\rho_{\mathbf{q}} \rho_{-\mathbf{q}} - N_e], \quad (21)$$

where $a_{\mathbf{k}}$ is the annihilation operator for plane wave states of wave vector \mathbf{k} , $u(\mathbf{G})$ the periodic crystal potential, and v_q is the Coulomb potential between electrons, $\rho_{\mathbf{q}} = \sum_{\mathbf{k}} a_{\mathbf{k}+\mathbf{q}}^\dagger a_{\mathbf{k}}$, and $N_e = \sum_{\mathbf{k}} a_{\mathbf{k}}^\dagger a_{\mathbf{k}}$.

The commutator involving the single-particle energy term is

$$[T, a_{\mathbf{k}}^\dagger] = \frac{\hbar^2 k^2}{2m} a_{\mathbf{k}}^\dagger + \sum_{\mathbf{G}} u(\mathbf{G}) a_{\mathbf{G}+\mathbf{k}}^\dagger. \quad (22)$$

There are corresponding terms for hole excitations, but none of these terms involve singular contributions responsible for anomalous size effects, so that these terms do not contribute at leading order. However,

$$[V_{ee}, a_{\mathbf{k}}^\dagger] = \frac{1}{V} \sum_{\mathbf{q} \neq 0} v_q [\rho_{\mathbf{q}} a_{\mathbf{k}-\mathbf{q}}^\dagger - 1] \quad (23)$$

and

$$[V_{ee}, a_{\mathbf{k}}] = -\frac{1}{V} \sum_{\mathbf{q} \neq 0} v_q \rho_{\mathbf{q}} a_{\mathbf{k}+\mathbf{q}} \quad (24)$$

involve terms approaching the Coulomb singularity, $v_q \sim q^{-2} \rightarrow \infty$ for $q \rightarrow 0$.

From these terms we get the leading order size corrections by noting that

$$\lim_{\mathbf{k}, \mathbf{q} \rightarrow 0} \frac{\langle \Psi_{\mathbf{k}}^{N_e+1} | \rho_{\mathbf{q}} a_{\mathbf{k}-\mathbf{q}}^\dagger | \Psi_0^{N_e} \rangle}{\langle \Psi_{\mathbf{k}}^{N_e+1} | a_{\mathbf{k}}^\dagger | \Psi_0^{N_e} \rangle} = \frac{1}{2} \left[\frac{1}{\epsilon} + 1 \right] \quad (25)$$

and

$$\lim_{\mathbf{k}, \mathbf{q} \rightarrow 0} \frac{\langle \Psi_{\mathbf{k}}^{N_e-1} | \rho_{\mathbf{q}} a_{\mathbf{k}+\mathbf{q}} | \Psi_0^{N_e} \rangle}{\langle \Psi_{\mathbf{k}}^{N_e-1} | a_{\mathbf{k}} | \Psi_0^{N_e} \rangle} = -\frac{1}{2} \left[1 + \frac{1}{\epsilon} \right]. \quad (26)$$

Both relations can be obtained [36] by extending Kohn's diagrammatic approach [33]. Integrating around the v_q singularity for small q in Eq. (23), we obtain the leading order finite size corrections. As before, this involves the Madelung constant, Eq (14). In the particle channel we get $\frac{|v_M|}{2} (\frac{1}{\epsilon} - 1)$ and in the hole channel, $\frac{|v_M|}{2} (\frac{1}{\epsilon} + 1)$. The corrections independent of ϵ correspond to the change in the background charge which cancel for the fundamental gap and we obtain Eq. (17).

Previous, heuristic approaches [25] have suggested that one can use experimental or DFT values of the dielectric constant for finite-size extrapolation. Our approach further suggests that this value can be determined from the QMC structure factor extrapolated to zero wave vector

$$\frac{2}{\epsilon} \equiv (1+c) \lim_{N_e \rightarrow \infty} \lim_{k \rightarrow 0} [S_k^+ + S_k^-], \quad (27)$$

with the singular behavior of the Jastrow factor determining c . We emphasize that the order of the limits involved above is crucial.

An independent estimate is based on the inequality of Eq. (7). We can bound and estimate the value of dielectric constant using the structure factor of the insulating ground state. By extrapolating $1 - \Gamma_k^2$ vs. k to $k = 0$ we obtain an upper bound to the inverse dielectric constant, where $\Gamma_k \equiv 2m\omega_p S_{N_e}(k)/\hbar k^2$. This involves only the extensive part of the density-density correlations, thus, it is less sensitive to noise and has much smaller statistical uncertainty. In Fig. 3, we show that for C and Si, this inequality gives accurate values of the dielectric constant.

D. Twist correction of two particle correlations

The above size effects explain the leading order $1/L$ correction to the single particle gap. However, as we will see in our results, the asymptotic region, where this law can be reliably applied, may still be difficult to reach for currently used system sizes and next-to-leading order effects are important. Here, we show that an important part can be corrected for, by further restoring the full symmetry properties in the contribution of the direct Coulomb interaction.

For inhomogeneous systems, it is convenient to separate the mean density from its fluctuating components in the

static structure factor [29], i.e.

$$S_{N_e}(\mathbf{k}) = \frac{1}{N_e} \langle \rho_{\mathbf{k}} \rangle \langle \rho_{-\mathbf{k}} \rangle + \delta S_{N_e}(\mathbf{k}) \quad (28)$$

$$\delta S_{N_e}(k) = \frac{1}{N_e} \langle (\rho_{\mathbf{k}} - \langle \rho_{\mathbf{k}} \rangle) (\rho_{-\mathbf{k}} - \langle \rho_{-\mathbf{k}} \rangle) \rangle \quad (29)$$

For crystals with periodic density distributions, the Fourier components of the mean density, $\langle \rho_{\mathbf{k}} \rangle$, only contribute for reciprocal lattice vectors, $\mathbf{k} \in \mathbf{G}$. The long wave length behavior of the structure factor is entirely due to the fluctuating part $\delta S_{N_e}(k)$, which therefore contains the leading order size effects [29]. However, the mean single particle density, $\langle \rho(\mathbf{r}) \rangle = V^{-1} \sum_{\mathbf{k}} \langle \rho_{\mathbf{k}} \rangle e^{i\mathbf{k}\cdot\mathbf{r}}$, of the finite system may significantly differ from the infinite one, particularly in cases where the supercell is not compatible with the full symmetry group of the crystal.

Averaging over twisted boundary conditions is designed to restore the symmetry of the crystal and thus accelerate the convergence of single particle densities to the thermodynamic limit. In the following, we denote the twist averaged expectation value by

$$\overline{\mathcal{O}} \equiv \frac{1}{M_\theta} \sum_\theta \langle \mathcal{O} \rangle_{N_e, \theta} \quad (30)$$

where we have explicitly indicated the N_e and θ dependence on the expectation value on the r.h.s. For any single particle theory, $\rho(\mathbf{r})$ approaches its thermodynamic limit for calculations at fixed N_e by averaging over a dense grid of twist angles ($M_\theta \rightarrow \infty$). Within many-body calculations, twist-averaging [30] takes over large part of this property to any observable *linear* in the density. Here, we extend this approach to correct also the quadratic expression entering the two-body contributions of the total energy.

For the potential energy, this correction to the twist converged QMC calculation is

$$\begin{aligned} \delta V_{N_e}^s &= \frac{1}{2V} \sum_{\mathbf{k}} v_k \delta C(\mathbf{k}) \\ \delta C(\mathbf{k}) &= \overline{\rho_{\mathbf{k}}} \overline{\rho_{-\mathbf{k}}} - \overline{\rho_{\mathbf{k}} \rho_{-\mathbf{k}}}. \end{aligned} \quad (31)$$

For the ground state energies, this correction provides only a small improvement over our previous correction [28, 29].

For the gap, many terms entering Eq. (31) cancel and the expression can be simplified. Let us consider the case of adding/removing one electron at twist ϕ to the insulating ground state, denoting $\Pi_{\mathbf{k}}^\pm$ the difference of the respective densities

$$\Pi_{\mathbf{k}}^\pm \equiv \langle \rho_{\mathbf{k}} \rangle_{N_e \pm 1, \phi} - \langle \rho_{\mathbf{k}} \rangle_{N_e, \phi} \quad (32)$$

In the thermodynamic limit, the density of the ground state system with N_e electrons coincides with the twist averaged ground state density $\overline{\rho_{\mathbf{k}}}$, whereas we obtain $\overline{\rho_{\mathbf{k}}} + \Pi_{\mathbf{k}}^\pm$ for the density of the $N_e \pm 1$ electron system. Inserting into Eq. (31), we obtain the correction for the difference

between the two states

$$\delta V_{N_e \pm 1, \phi}^s - \delta V_{N_e}^s = \frac{1}{V} \sum_{\mathbf{k} \in \mathbf{G}} v_k \operatorname{Re} [(\bar{\rho}_{\mathbf{k}} - \langle \rho_{\mathbf{k}} \rangle_{N_e, \phi}) \Pi_{-\mathbf{k}}^{\pm}] \quad (33)$$

where only wave vectors of the reciprocal crystal lattice contribute to the sum. The corresponding finite size correction for the gap, denoted by $\delta\Delta_s$ in the following, is order $1/N_e$ or smaller, mainly determined by the changes of the ground state densities at the first Bragg-peaks due to twist averaging.

Equation (33) can be understood quite intuitively: it corrects the direct Coulomb interaction between the electron/hole in the excited state (Π^{\pm}) with the unexcited electrons. The density of those electrons is expected to change by $\bar{\rho}_{\mathbf{k}} - \langle \rho_{\mathbf{k}} \rangle_{N_e, \phi}$ in the thermodynamic limit.

Converged ground state densities are naturally calculated within GCTABC. It is straightforward to apply the correction Eq. (33) to all excitation energies. Alternatively, the corresponding DFT densities may be used. This removes the stochastic error at the cost of introducing a small bias in the next-to-leading order size correction.

IV. COMPUTATIONAL METHODS

We have performed electronic QMC calculations on three insulating solids: molecular hydrogen at high pressure, and carbon and silicon in the diamond structure at zero pressure. Since we are interested in the charge gap, we used an equal number of spin up and spin down electrons. We used a Slater-Jastrow trial wave function with backflow corrections [37, 38]. The Jastrow and backflow functions were fully optimized within Variational Monte Carlo including the long-range (reciprocal lattice) contributions. The orbitals in the Slater determinant were taken from DFT calculations using Quantum Espresso [39, 40]. The carbon and silicon orbitals were generated using the LDA functional, whereas the hydrogen orbitals were generated using the PBE functional, which has been shown to provide a good trial QMC wave function [41, 42].

Molecular hydrogen was placed in the C2/c-24 structure [43] at two different densities ($r_s = 1.38$ and $r_s = 1.34$), roughly corresponding to pressures of 234GPa and 285 GPa, respectively. Energies and structure factors were obtained from Reptation Quantum Monte Carlo calculations using the BOPIMC code [44]. For carbon and silicon, Diffusion Monte Carlo calculations have been performed with the QCMPACK code [45] at the experimentally measured zero pressure valence densities, $r_s = 1.318$ and $r_s = 2.005$, respectively. For hydrogen, the QMC calculations have been done with the bare Coulomb interaction. The PAW pseudopotential has been used for the DFT results shown in Fig. 1. For carbon and silicon, psuedopotentials were used to remove the core electrons: carbon ions modeled by the Burkatzki-Filippi

Dolg (BFD) pseudopotential [46], and silicon ions by the Trail-Needs (TN) pseudopotential [47]. These are considered good pseudopotentials for correlated calculations, but their use within DFT calculations produces slightly different results from the literature even with the same functional. For hydrogen, we used a supercell with $2 \times 2 \times 1$ primitive cells so that the supercell is nearly cubic and contained 96 protons. For carbon, we used two system sizes: the cubic cell containing 8 atoms and a $2 \times 2 \times 2$ supercell containing 64 atoms. For silicon, in addition to these systems, we used a $3 \times 3 \times 3$ supercell containing 216 atoms. For hydrogen, the twist convergence has been achieved using a $8 \times 8 \times 8$ twist grid. For C and Si, the twist grid density decreases with increasing system size. The supplementary material contains the QMC calculated energies and variances of the insulating ground states of the various systems obtained after twist averaging and two-body finite size corrections.

V. RESULTS

For any single-particle theory, such as Kohn-Sham DFT, the densities and energies, $n_e(\mu)$ and $e_0(\mu)$, are obtained by occupying all single particle states below the chemical potential μ . By construction, the gap, as determined from the incompressible region of $n_e(\mu)$ or from the discontinuity in the derivative of de_0/dn_e (see Fig.1), then coincides with the one obtained from the band structure.

To illustrate the equivalence of the two ways of computing the gap with LDA calculations. The LDA band gaps of carbon and silicon in the diamond structure, are indirect, and lie along the ΓX direction where Γ is the origin of the Brillouin zone and X the Brillouin boundary in the (100) direction. By looking directly at the HOMO and LUMO states with LDA it is found that the carbon gap is 3.89 eV and the silicon gap is 0.34 eV. The bands immediately above and below the gap can be fit to a quadratic form which implies $e_0(\mu) = \mu^{\pm} n_e(\mu) + b^{\pm} n_e(\mu)^{5/3}$. Therefore, the derivative $de_0/dn_e = \mu^{\pm} + \frac{5b^{\pm}}{3} n_e^{2/3}$ has a discontinuity at $n_e = 0$ and behaves as $n_e^{2/3}$ above and below the gap. Applying our GCTABC procedure to a single-particle theory, all states with energies below the chemical potential are occupied. Varying the chemical potential thus scans the underlying density of states. The band gap is then determined by locating the band edges, μ^{\pm} , disregarding the location in the Brillouin zone [48]. Figure 5 illustrates the density of states obtained from GCTABC giving an LDA gap of 3.95 eV for the carbon gap and 0.38 eV for the silicon gap. The small differences (~ 0.05 eV) from the values obtained before are due to the finite resolution of the twist grid, and can be controlled by using denser grids.

As can be seen in the same figure, the effective band edge densities of states from GCTABC-DMC have a similar functional form, but with a larger gap than the DFT

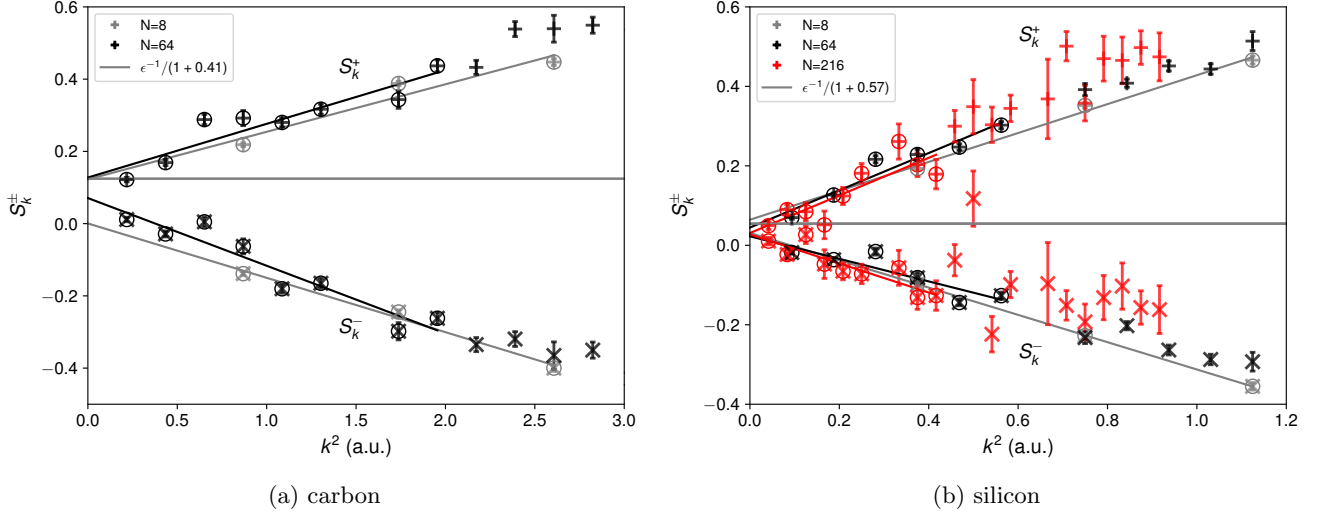


FIG. 2. Change in the static structure factor as an electron (upper curves) or a hole (lower curves) is added to the insulating system with N atoms. The lines are fits to the data points. The horizontal lines show the expected $k \rightarrow 0$ limit based on the experimental dielectric constants. We have used $c = 0.40$ for C and $c = 0.57$ for Si.

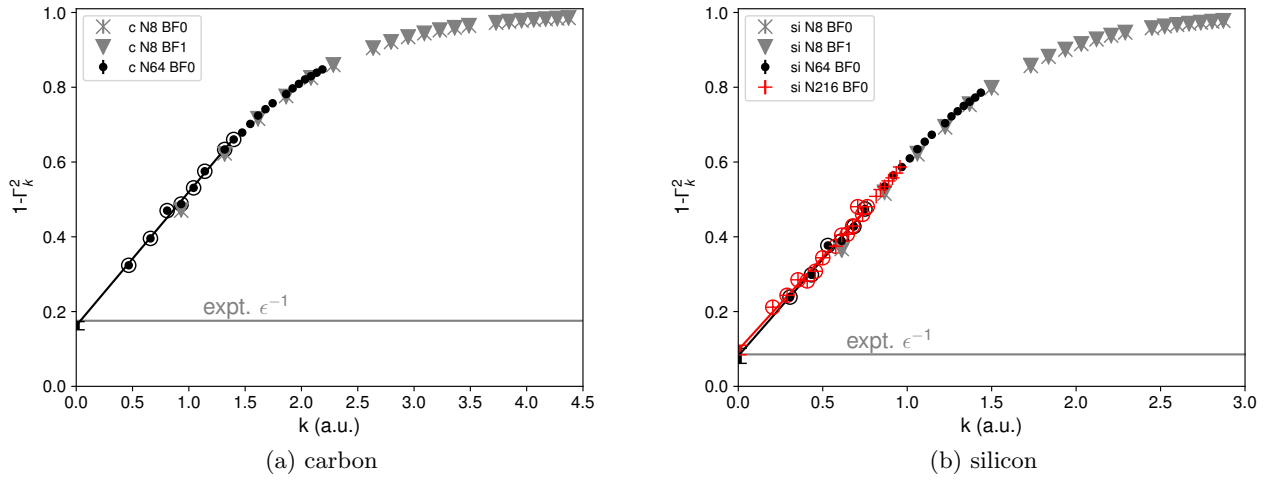


FIG. 3. Upper bound to the inverse dielectric constant eq. (7), where $\Gamma_k \equiv \frac{2m\omega_p S_{N_e}(k)}{\hbar k^2}$. Lines are fits to the low- k data. The horizontal lines mark experimental inverse dielectric constants.

ones. The QMC computed gaps for the different sizes of the supercell are summarized in table I. The results from different supercells clearly show the important bias on gap introduced by the finite size of the supercell. In Figure 4, we show the bare gap, Δ_N , the Madelung-corrected one, $\Delta_N + |v_M|/\epsilon$, and our best correction, $\Delta_\infty = \Delta_N + |v_M|/\epsilon + \delta\Delta_s$, for both systems against the linear size of the supercell where N is the number of atoms in the supercell. We see that the next-to-leading-order corrections are comparable to the leading-order one, in particular for the 8-atom supercell of Si, whereas they rapidly decay for the larger sizes.

The finite size corrected values, Δ_∞ , of all different sizes C and Si supercells agree with each other within

the statistical uncertainty, yielding the DMC-SJ values $\Delta_\infty = 6.8(1)$ and $\Delta_\infty = 1.8(1)$ for the C and Si gap, respectively. We further note, that these values also agree with a numerical $N^{-1/3}$ extrapolation of the gap values corrected by $\delta\Delta_s$. For any numerical $N^{-1/3}$ extrapolation, it is very important to reduce any bias due to higher order corrections as much as possible, since the outcome of a fit is sensitive to the smallest system sizes since they have the smallest statistical uncertainty. For Si, a $N^{-1/3}$ extrapolation of the bare Δ_N values yields an overestimation of 0.3 eV compared to Δ_∞ .

Since our finite-size corrected gaps show size-convergence for the smallest system size, it is now feasible to address the systematic error due to the fixed node ap-

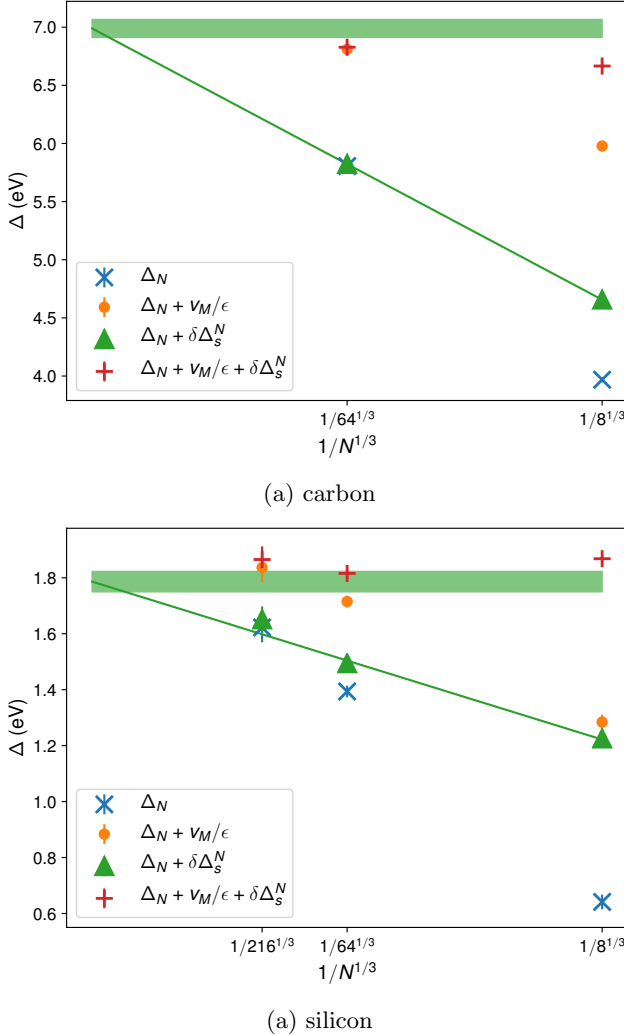


FIG. 4. Fundamental gap before and after finite-size corrections. Δ_N is the DMC gap from a simulation with N atoms in the supercell without any finite-size correction, $\delta\Delta_s^N$ is the leading-order Madelung correction using the experimental value of ϵ^{-1} , Δ_s^N is the next-to-leading-order density correction, which is related to the static part of the structure factor. The line is a fit to Δ_s^N .

proximation. In order to reduce this bias we have added backflow (BF) correlations in the Slater orbitals. Our backflow correlations lower the SJ gap by 0.1 eV for both, C and Si. Previous BF calculations [25] on Si have reported a 0.2 eV lowering compared to SJ. The difference might be due to a different functional form or optimization procedure. A systematic study on the bias of the fixed-node approximation such as done with more general backflow correlations [49, 50] or multi-determinant trial wave functions [51], possible for small supercells, could be done in the future.

So far, in our analysis of C and Si, we have imposed the experimentally known dielectric constant in the leading order Madelung correction. As described in Sec. III, there is no need for any external knowledge to perform

TABLE I. Energy gaps obtained from GCTAB QMC calculations in eV. The bare gap, Δ_N , was calculated from Eq. (1) for a finite supercell containing N atoms. The leading-order finite-size corrections are given by the screened Madelung constants $|v_M|/\epsilon$, the next-to-leading order by the twist correction of two particle density correlations, $\delta\Delta_s$. We used the experimental value of ϵ for C and Si (5.7 and 11.7, respectively) and 18.8 for H₂ extracted from S(k). Finite size corrections were applied also to the band edges, μ_{∞}^{\pm} . The estimate of the gap in the thermodynamic limit is $\Delta_{\infty} = \Delta_N + |v_M|/\epsilon + \delta\Delta_s$. From our LDA analysis, we estimate a systematic bias of ~ 0.1 eV from the finite twist grid. This bias is larger than the statistical error. SJ indicates Slater-Jastrow trial wave function, BF backflow.

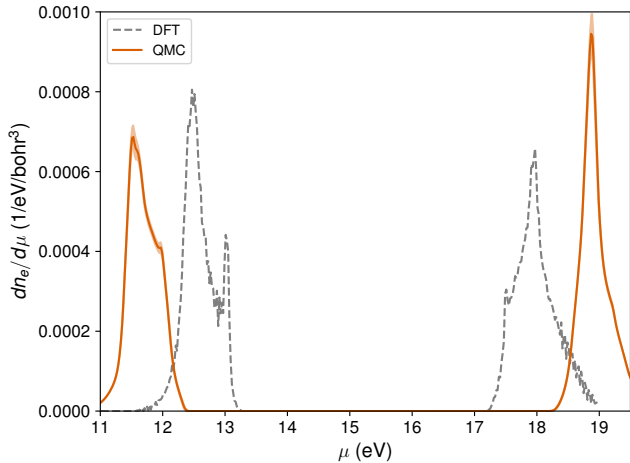
	r_s	N	Δ_N	$ v_M /\epsilon$	$\delta\Delta_s$	μ_{∞}^-	μ_{∞}^+	Δ_{∞}
H ₂ (BF)	1.38	96	3.3(1)	0.40	0.020	6.9(1)	10.7(1)	3.8(1)
	1.34	96	2.4(1)	0.20	0.018	8.6(1)	11.2(1)	2.6(1)
C (BF)	1.318	8	3.9(1)	2.01	0.69	11.5(1)	18.1(1)	6.6(1)
C (SJ)	1.318	8	4.0(1)	2.01	0.69	11.5(1)	18.2(1)	6.7(1)
	64	5.8(1)	1.00	0.02	11.9(1)	18.7(1)	6.8(1)	
Si (BF)	2.005	8	0.6(1)	0.64	0.55	5.2(1)	6.9(1)	1.7(1)
	2.005	8	0.6(1)	0.64	0.58	5.2(1)	7.0(1)	1.9(1)
Si (SJ)	2.005	8	1.4(1)	0.32	0.08	5.5(1)	7.3(1)	1.8(1)
	216	1.6(1)	0.21	0.01	5.6(1)	7.4(1)	1.8(1)	

the size extrapolation as the value of the Madelung correction can be obtained from the behavior of the static structure factor, calculable within the same QMC run, see Figs 2 and 3. However, since the extrapolation involved introduces an additional uncertainty, we have preferred to use the experimental values to benchmark our theory and better distinguish leading from next-to-leading order size effects.

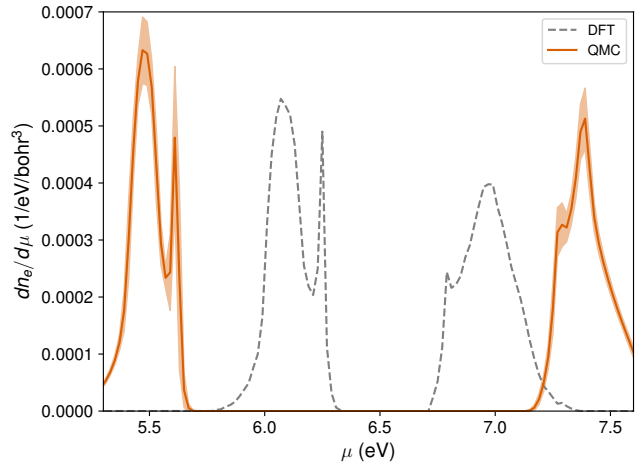
Using the dielectric bound eq. (7) on the ground-state structure factor to determine ϵ , we get $\epsilon_0 = 6.2 \pm 0.4$ for C and $\epsilon_0 = 10.3 \pm 1.3$ for Si, which are compatible with the experimental values of 5.7 and 11.7. The corresponding leading-order finite-size corrections on the gap of the 64-atom system are then 0.92 ± 0.06 eV for C and 0.36 ± 0.14 eV for Si using the *ab initio* ϵ^{-1} , as opposed to 1.00 eV for C and 0.32 eV for Si based on the experimental values of ϵ^{-1} .

As shown in Fig. 2, the asymptotic values of the finite sized structure factors, S_k^{\pm} , are affected by a much larger uncertainty, introducing larger systematic bias when used for *ab initio* size corrections. Still, already the extrapolation to a non-zero value fixes the leading order size corrections to decay as $1/L$. This information alone can be crucial as calculations for only two different supercell sizes will be sufficient to determine size effects, whereas more supercell sizes would be needed if the asymptotic form was not known.

We have also computed the band gap of solid hydrogen using GCTABC in BF-RQMC calculations for one of the possible molecular structures predicted for phase III: C2/c-24 at $r_s = 1.38$ and $r_s = 1.34$ (roughly corresponding to pressures of 234 and 285 GPa respectively). The results, in table I show that the gap and size effects



(a) carbon



(a) silicon

FIG. 5. Density of states for carbon and silicon near the band edge. Each plot shows the derivative of the mean electron density with respect to the chemical potential. This is the electronic density of states (DOS) in DFT, so the gap appears as a depleted region. The calculated DOS is only valid near the band edge because only the two bands closest to the gap are considered within DFT and QMC. The DFT bands (done in a primitive cell) have been folded into the Brillouin zone (BZ) of the 64-atom supercell to allow comparison with QMC.

decrease with increasing pressure. For these calculations, we use calculations for one supercell and use its structure factor to estimate the dielectric constant. From Fig. 1, we see that HSE DFT slightly underestimates the gap, however the deviations from the plateau on both sides are quite similar.

VI. COMPARISON WITH EXPERIMENT

Our best values for the fundamental electronic gap (BF-DMC) significantly overestimate the experimentally measured values for C and Si by 1.1 and 0.5 eV, respectively as shown in Table II. There are two main sources of systematic errors which need to be taken into account: the use of pseudo-potentials and the neglect of electron-phonon coupling.

The QMC values for C and Si presented above are based on pseudo-potentials to replace the core electrons of the atoms. Pseudo-potentials are usually designed for accurate prediction of static structural quantities. Excitation spectra, in particular the single particle excitation gap, may be less well described. This has been found in many-body perturbation theory calculations within the *GW* framework where all-electron calculations have been shown to lower the gap of C and Si by ~ -0.3 eV [52, 53] with respect to pseudo-potentials calculations. Although the actual pseudo-potentials of our QMC simulations differ from those used in the *GW* calculations, we expect that our QMC values will be shifted by a similar amount; we can roughly transfer the all-electron correction of *GW* to our QMC results.

For lighter atoms, electron-phonon coupling leads to a further reduction of the gap values, even at zero temper-

ature, due to the presence of zero point motion of the ions in the crystal. For C, *GW* predicts a significant lowering of the gap by -0.6 eV [54], whereas a smaller shift between -60 meV [55] and -0.1 eV [56] is expected from DFT for Si.

Considering both, the bias due to the pseudo-potential approximation and the neglect of electron-phonon coupling, our BF-DMC for C and Si overestimate the gap by $\sim 0.1 - 0.2$ eV (see table II), larger than our statistical uncertainty. This remaining offset to experiment may either be due to residual bias of the fixed-node approximation, or due to effects in pseudo-potential and e-ph coupling beyond our simple estimations based on *GW* and DFT.

For hydrogen, we do not compare to experiment since electron-phonon coupling is expected to be very large, and the experimental results are not precise. If we do not make size corrections, our results are comparable to the Slater-Jastrow DMC calculations of Ref. [27] where the DFT band structure was corrected by a “scissor operator” based on QMC runs at the Γ point of the supercell. However, no size effects been observed within the statistical error in Ref. [27], so that their extrapolated results differ from ours by $0.3 - 0.8$ eV (3.0 and 2.3 eV for 250 and 300 GPa). Comparison to *GW* values are also not conclusive: whereas Ref. [57] provides smaller values of the gaps (1.8 and 1.0 eV for 250 and 300 GPa), the results of Ref. [58] (3.7 and 2.8 eV for 250 and 313 GPa) are close to our predictions. However, we note that the *GW* calculations were done with slightly different crystal structures. In Ref. [57] PBE functional was used to optimize the lattice structure in contrast to the vdW-DF1 functional of Ref. [58] shown to be the most accurate functional at this density [59]. The smaller gap can then be seen as a

TABLE II. Extrapolated band-gap of Si and C from backflow DMC calculations, Δ_{BF} compared to the experimental values (exp). We tabulated two main corrections: the difference between the gap of an all-electron (AE) and the pseudo-potential (PP) calculation within GW calculations, and the neglect of electron-phonon coupling (e-ph).

	Δ_{BF}	AE - PP	e-ph	exp
C	6.6(2)	-0.26 (G_0W_0) [52]	-0.6 (GW) [54]	5.48 [60]
Si	1.7(1)	-0.25 (G_0W_0) [52]	-0.06 (DFT) [55]	1.17 [60]

consequence of a larger bond length as it was shown that structures optimized with PBE functional have a larger bond length than the ones with vdW-DF1 [58].

VII. CONCLUSIONS

We have introduced a method to calculate the fundamental gap of insulators and semi-conductors using QMC. Using grand-canonical twist averaging, the value of the gap can be determined at any point in the Brillouin zone whether the system has a direct or indirect gap. Although it is possible to map out the whole band structure, we have focused on the minimal, fundamental gap in this paper. We have shown that for charged systems, finite size supercell calculations are necessarily biased by a finite size error decaying as $1/L$, where the prefactor is determined by the absolute value of the Madelung constant and the inverse dielectric constant. We have pointed out that the $1/L$ functional form is encoded in the long wave length behavior of the finite size structure factor extrapolating to a non-vanishing value at the origin. Next-to-leading order effects can be corrected by proper use of twist-averaging in the two-particle part of the static Coulomb potential.

We have applied this procedure to determine the fundamental gap of molecular Hydrogen at high pressure and carbon and silicon in the diamond structure at zero pressure. Our bare values for carbon and silicon are larger than the experimental ones. We have shown the bias is most likely due to the pseudo-potential approximation and the neglect of electron-phonon coupling.

We note that this procedure is not restricted to QMC calculations, but can be applied within any method which calculates the many-body wave functions and ground state energies, e.g. for coupled cluster methods [8]. Our results for C and Si demonstrate that the bias due to the finite size supercell can be corrected for, so that precise values in thermodynamic limit can be obtained for small supercells without need for numerical extrapolation.

The procedure here has been developed for perfect crystals but can be generalized to systems with disorder, either due to thermal or quantum effects. Furthermore, the procedure provides a starting point to address optical –i. e. charge neutral – excitations. Although neutral excitations are expected to be less sensitive to finite size effects, recent calculations [24, 25] have observed the same slow $1/L$ decay for the optical gap. Since it is often not practical to perform calculations for more than two significantly different supercell sizes, our method suggests that the asymptotic behavior of the structure factor provides the needed insight to whether $1/L$ or $1/L^3$ should be used as functional form for the size extrapolation.

ACKNOWLEDGMENTS

DMC and MH thank CCQ at the Flatiron Institute for support during the writing of this paper and the Fondation NanoSciences (Grenoble) for support. The Flatiron Institute is a division of the Simons Foundation. DMC and YY were supported by DOE Grant NA DE-NA0001789. V.G. and C.P. were supported by the Agence Nationale de la Recherche (ANR) France, under the program “Accueil de Chercheurs de Haut Niveau 2015” project: HyLightExtreme. Computer time was provided by the PRACE Project 2016143296, ISCRAF the high-performance computer resources from Grand Equipement National de Calcul Intensif (GENCI) Allocations 2018-A0030910282 and by an allocation of the Blue Waters sustained petascale computing project, supported by the National Science Foundation (Award OCI 07- 25070) and the State of Illinois, and by GRICAD infrastructure (Grenoble) within the Equip@Meso project, ANR-10-EQPX-29-01.

-
- [1] R.M. Martin, L. Reining, and D. M. Ceperley, *Interacting Electrons*, Cambridge University Press, Cambridge (2016).
- [2] J.P. Perdew, Int. J. Quantum Chem. Symp. **19**, 497 (1986).
- [3] W. M. C. Foulkes, L. Mitas, R. J. Needs, and G. Rajagopal, Rev. Mod. Phys. **73**, 33 (2001).
- [4] J. Kolorenč and L. Mitas, Rep. Prog. Phys. **74**, 026502 (2011).
- [5] L. K. Wagner and D. M. Ceperley, Rep. Prog. Phys. **79**, 094501 (2016).
- [6] M. Ruggeri, P. López Ríos, and A. Alavi, Phys. Rev. B **98**, 161105(R) (2018).
- [7] J.J. Shepherd and A. Grüneis, Phys. Rev. Lett. **110**, 226401 (2013).
- [8] T. Gruber, K. Liao, T. Tsatsoulis, F. Hummel, and A. Grüneis, Phys. Rev. X **8**, 021043 (2018).
- [9] P.R.C. Kent, R.Q. Hood, M.D. Towler, R.J. Needs, and G. Rajagopal, Phys. Rev. B **57**, 15293 (1998).
- [10] P.R.C. Kent, R.Q. Hood, A.J. Williamson, and R.J. Needs, Phys. Rev. B **59**, 1917 (1999).
- [11] C. Mitra, J. T. Krogel, J. A. Santana, and F. A. Reboredo

- doa, J. Chem. Phys. **143**, 164710 (2015).
- [12] J. McMinis, M. A. Morales, D. M. Ceperley, and J. Kim, J. Chem. Phys. **143**, 194703 (2015).
- [13] G. Makov and M.C. Payne, Phys. Rev. B **51**, 4014 (1995).
- [14] G.E. Engel, Y. Kwon, and R.M. Martin, Phys. Rev. B **51**, 13538 (1995).
- [15] A.J. Williamson, R.Q. Hood, R.J. Needs, and G. Rajagopal, Phys. Rev. B **57**, 12140 (1998).
- [16] L. Mitas and R.M. Martin, Phys. Rev. Lett. **72**, 2438 (1994).
- [17] M. D. Towler, R. Q. Hood, and R. J. Needs, Phys. Rev. B **62**, 2330 (2000).
- [18] D. M. Ceperley and B. J. Alder, Phys. Rev. B **36**, 2092 (1987).
- [19] J. Kolorenč and L. Mitas, Phys. Rev. Lett. **101**, 185502 (2008).
- [20] F. Ma, S. Zhang, and H. Krakauer, New J. Phys. **15**, 093017 (2013).
- [21] L. K. Wagner and P. Abbamonte, Phys. Rev. B **90**, 125129 (2014).
- [22] J. Yu, L. K. Wagner, and E. Ertekin, J. Chem. Phys. **143**, 224707 (2015).
- [23] H. Zheng and L. K. Wagner, Phys. Rev. Lett. **114**, 176401 (2018).
- [24] T. Frank, R. Derian, K. Tokár, L. Mitas, J. Fabian, and I. Štich, Phys. Rev. X **9**, 011018 (2019).
- [25] R.J. Hunt, M. Szyniszewski, G.I. Prayogo, R. Maezono, and N.D. Drummond, Phys. Rev. B **98**, 075122 (2018).
- [26] W.M.C. Foulkes, R.Q. Hood, and R.J. Needs, Phys. Rev. B **60**, 4558 (1999).
- [27] S. Azadi, N. D. Drummond, and W.M.C. Foulkes, Phys. Rev. B **95**, 035142 (2017).
- [28] S. Chiesa, D.M. Ceperley, R.M. Martin, and M. Holzmann, Phys. Rev. Lett. **97**, 076404 (2006).
- [29] M. Holzmann, R.C. Clay III, M. A. Morales, N.M. Tushman, D. M. Ceperley, and C. Pierleoni, Phys. Rev. B **94**, 035126 (2016).
- [30] C. Lin, F.-H. Zong, and D. M. Ceperley, Phys. Rev. E **64**, 016702 (2001).
- [31] D. Pines and P. Nozières, *The Theory of Quantum Liquids*, vol I, Addison-Wesley, Redwood City, CA (1989).
- [32] M. Holzmann, B. Bernu, and D.M. Ceperley, Phys. Rev. B **74**, 104510 (2006).
- [33] W. Kohn, Phys. Rev. **110**, 857 (1958).
- [34] W. Kohn, Phys. Rev. **105**, 509 (1957).
- [35] P.P. Ewald, Ann. Phys. **64**, 253 (1921).
- [36] We can adapt the proof of Kohn [33] by noting that the extra particle (hole) propagator does not interact with the other particles before $t = 0$. The equivalent graphs of class I contribute with ± 1 for particle and hole excitations, the equivalent graphs of class IIA remain, contributing $\pm(1/\epsilon - 1)/2$, whereas graphs of class IIB are absent.
- [37] M. Holzmann, D. M. Ceperley, C. Pierleoni, and K. Esler, Phys. Rev. E **68** 046707 (2003).
- [38] C. Pierleoni, K.T. Delaney, M.A. Morales, D.M. Ceperley, and M. Holzmann, Comp. Phys. Comm. **179**, 89 (2008).
- [39] P. Giannozzi et al., J. Phys.: Condens. Matter **21**, 395502 (2009).
- [40] P. Giannozzi et al., J. Phys.: Condens. Matter **29**, 465901 (2017).
- [41] M.A. Morales, R. Clay, C. Pierleoni, D.M. Ceperley, Entropy, **16**, 287 (2014).
- [42] C. Pierleoni, M.A. Morales, G. Rillo, M. Holzmann, and D.M. Ceperley, Proc. Nat. Acad. Sc. **113**, 4953 (2016).
- [43] C. J. Pickard, R. J. Needs, Nat. Phys. **3**, 473-476 (2007).
- [44] C. Pierleoni and D.M. Ceperley, Lecture Notes in Physics **703**, 641 (2006).
- [45] J. Kim, et al., J. Phys. Condens. Matter, **30** 195901 (2018).
- [46] M. Burkatzki, C. Filippi, and M. Dolg, J. Chem. Phys. **126**, 234105 (2007).
- [47] J. R. Trail, and R. J. Needs, J. Chem. Phys. **122**, 174109 (2005).
- [48] The reciprocal space information is not lost. By keeping track of the Bloch momentum of the states we can determine the locations of the HOMO and LUMO, but that has not been done here.
- [49] M. Ruggeri, S. Moroni, and M. Holzmann, Phys. Rev. Lett. **120**, 205302 (2018).
- [50] M. Holzmann and S. Moroni, Phys. Rev. B **99**, 085121 (2019).
- [51] L. Zhao and E. Neuscamman, Phys. Rev. Lett. **123**, 036402 (2019).
- [52] R. Gómez-Abal, X. Li, M. Sheffler, and C. Ambrosch-Draxl, Phys. Rev. Lett. **101**, 106404 (2008).
- [53] W. Ku and A. G. Eguiluz, Phys. Rev. Lett. **89**, 126401 (2002).
- [54] F. Giustino, S.G. Louie, and M.L. Cohen, Phys. Rev. Lett. **105**, 265501 (2010).
- [55] B. Monserrat and R.J. Needs, Phys. Rev. B **89**, 214304 (2014).
- [56] P. Lautenschlager, P.B. Allen, and M. Cardona, Phys. Rev. B **31**, 2163 (1985).
- [57] S. Lebegue, C. M. Araujo, D. Y. Kim, M. Ramzan, H. Mao, and R. Ahuja, Proc. Nat. Acad. Sc. **109** 9766, (2012).
- [58] J. McMinis, R. C. Clay, D. Lee, and M. A. Morales, Phys. Rev. Letts. **114**, 105305 (2015).
- [59] R. C. Clay, III, J. McMinis, J. M. McMahon, C. Pierleoni, D. M. Ceperley, and M. A. Morales, Phys. Rev. B **89**, 184106 (2014).
- [60] O. Madelung, M. Schulz, and H. Weiss, Intrinsic Properties of Group IV Elements and III-V, II-VI and I-VII Compounds, Landolt-Bornstein, New Series, Group III/22A (Springer-Verlag, New York, 1987).

Electronic band gaps from Quantum Monte Carlo methods (Supplemental Materials)

Yubo Yang,¹ Vitaly Gorelov,² Carlo Pierleoni,^{2,3} David M. Ceperley,¹ and Markus Holzmann^{4,5}

¹*Department of Physics, University of Illinois Urbana-Champaign, Urbana, Illinois 61801, USA*

²*Maison de la Simulation, CEA, CNRS, Univ. Paris-Sud,
UVSQ, Université Paris-Saclay, 91191 Gif-sur-Yvette, France*

³*Department of Physical and Chemical Sciences,
University of L'Aquila, Via Vetoio 10, I-67010 L'Aquila, Italy*

⁴*Univ. Grenoble Alpes, CNRS, LPMMC, 3800 Grenoble, France*

⁵*Institut Laue Langevin, BP 156, F-38042 Grenoble Cedex 9, France*

A. Diagrammatic proof of the asymptotic behavior of the matrix elements

In Ref. [1], W. Kohn proved that the static dielectric constant is given by the matrix elements, Eq.(10) in the main paper,

$$\lim_{\mathbf{q}', \mathbf{q} \rightarrow 0, \mathbf{q}' \neq \mathbf{q}} \langle \Psi_0(N_e \pm 1; \mathbf{q}) | \rho_{\mathbf{q}-\mathbf{q}'} | \Psi_0(N_e \pm 1; \mathbf{q}') \rangle = \pm \frac{1}{\epsilon_0} \quad (1)$$

based on diagrammatic perturbation theory where $\Psi_0(N_e \pm 1; \mathbf{q})$ denotes the fully insulating N_e electron state with one electron added/ removed in the particle/ hole orbital \mathbf{q} . Here, we show how to adapt the diagrammatic proof of Ref. [1] to obtain the following matrix elements needed for the dominant size corrections of the band gap:

$$\lim_{\mathbf{K}, \mathbf{q} \rightarrow 0} \frac{\langle \Psi_{\mathbf{K}}^{N+1} | \rho_{\mathbf{q}} a_{\mathbf{K}-\mathbf{q}}^\dagger | \Psi_0^N \rangle}{\langle \Psi_{\mathbf{K}}^{N+1} | a_{\mathbf{K}}^\dagger | \Psi_0^N \rangle} = \frac{1}{2} \left[\frac{1}{\epsilon_0} + 1 \right], \quad (2)$$

and

$$\lim_{\mathbf{K}, \mathbf{q} \rightarrow 0} \frac{\langle \Psi_{\mathbf{K}}^{N-1} | \rho_{\mathbf{q}} a_{\mathbf{K}+\mathbf{q}} | \Psi_0^N \rangle}{\langle \Psi_{\mathbf{K}}^{N-1} | a_{\mathbf{K}} | \Psi_0^N \rangle} = -\frac{1}{2} \left[1 + \frac{1}{\epsilon_0} \right]. \quad (3)$$

Both relations can be obtained directly from Kohn's approach by noting that the extra particle (hole) propagator does not interact with the other particles before $t = 0$. In the following, we sketch the argument for a particle excitation.

In figure 1, we show a typical graph of the perturbation series contributing to the particle propagator in the denominator of eq. (2), $\langle \Psi_{\mathbf{K}}^{N+1} | a_{\mathbf{K}}^\dagger | \Psi_0^N \rangle$. Interband transitions are suppressed in the limit of vanishing momenta, so we need to consider only diagrams where the particle excitation is in the conduction band. Diagrams contributing to the numerator $\langle \Psi_{\mathbf{K}}^{N+1} | \rho_{\mathbf{q}} a_{\mathbf{K}-\mathbf{q}}^\dagger | \Psi_0^N \rangle$ fall into two classes. In Class I, we simply attach the external density operator $\rho_{\mathbf{K}'-\mathbf{K}}$ to split a propagator line at $t = 0$. This is represented by the external dashed line $\mathbf{K}' - \mathbf{K}$, which ends at X in Figure 2. Insertion at V_1 contains intraband transitions for the matrix elements of $\rho_{\mathbf{K}'-\mathbf{K}}$, giving 1 in the limit $\mathbf{K}' \rightarrow \mathbf{K}$, and the remaining term contributes exactly the same as the equivalent diagram in the denominator. Insertion at V_2 cancels the contribution from an insertion at V_3 in the limit of vanishing momenta, because they differ by only a minus sign due to the difference in the number of hole propagators involved. Therefore, all diagrams of class I contribute exactly 1 to the l.h.s. of Eq. (2).

Diagrams of class II create an additional particle-hole pair at $t = 0$, playing a similar role as one side of the Coulomb interaction vertex. A typical graph is shown in Figure 3. In the limit of vanishing external momenta, these diagrams separate into a normalization diagram and a graph involved in the static density response function, e.g. a simple electron-hole bubble attached at point V in Figure 3. These diagrams exactly coincide with those of class IIA of Ref. [1], whereas class IIB diagrams of Ref. [1] do not occur in our calculation because they are built out of dielectric graphs attached at points V with $t < 0$. Following the line of argument presented in Ref. [1], we see that class II diagrams contribute with $\frac{1}{2} \left(\frac{1}{\epsilon_0} - 1 \right)$ to the l.h.s. of Eq. (2).

Since class I and II diagrams are the only non-vanishing graphs, we obtain Eq. (2). The same argument can be applied to the hole excitation diagrams, differing by only a global sign due to the additional hole propagator involved, giving Eq. (3).

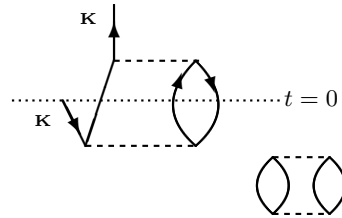


FIG. 1: A graph occurring in the perturbation expansion of the normalization $\langle \Psi_{\mathbf{K}}^{N+1} | a_{\mathbf{K}}^\dagger | \Psi_0^N \rangle$. The disconnected part contains only ground state diagrams.

B. Simulation cell

For hydrogen, we studied the C2/c-24 structure of molecular solid hydrogen at two different densities $r_s = 1.38$ and $r_s = 1.34$, corresponding to pressures of 234GPa and 285GPa, respectively as estimated with QMC. The crystalline

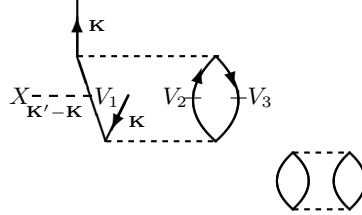


FIG. 2: A graph occurring in class I of the perturbation expansion of the numerator $\langle \Psi_{\mathbf{K}'}^{N+1} | \rho_{\mathbf{K}'-\mathbf{K}} a_{\mathbf{K}}^\dagger | \Psi_0^N \rangle$, where $\rho_{\mathbf{K}'-\mathbf{K}}$ is inserted at the point V_1 at $t = 0$.

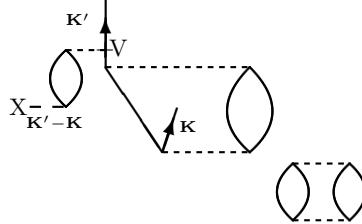


FIG. 3: A graph occurring in class II of the perturbation expansion of the numerator $\langle \Psi_{\mathbf{K}'}^{N+1} | \rho_{\mathbf{K}'-\mathbf{K}} a_{\mathbf{K}}^\dagger | \Psi_0^N \rangle$.

structures have been optimized by variable cell structural relaxation with DFT vdW-DF1 at pressures of 250GPa and 300GPa, respectively. (QMC and DFT-vdW-DF1 pressures differ by \sim 10-20GPa [2, 3]).

For carbon and silicon, we studied the diamond lattice at experimental densities at ambient conditions $r_s = 1.318$ and $r_s = 2.005$, respectively. Then the lattice constant of the conventional unit cell was $L = 6.74065$ bohr and $L = 10.2622$ bohr for carbon and silicon, respectively. The ideal simple cubic Madelung constant for the conventional cell is $v_M \equiv [\sum -f]v_k = -2.837297479/L$ ha/e.

C. Insulating state total energy, structure factor, and finite-size corrections

In Table I, we show total energies and variances of the insulating state of all systems studied. The hydrogen total energies are upper bounds to the exact ground-state energy at the corresponding density and system size because no pseudopotential was used. The carbon and silicon energies and variances are comparable only to calculations that use the same pseudopotentials. More accurate trial wavefunctions have a lower energy and variance as can be seen in the change from SJ to BF wavefunction for carbon and silicon.

TABLE I: RQMC/DMC energies per electron (in Ha), E_0/N_e , for H₂, C and S crystals with Slater-Jastrow (SJ) trial wave functions and backflow transformations (BF). σ_E^2/N_e is the DMC energy variance. The RQMC energy variance depends on projection time and are not shown. $(E_0/N_e)_\infty$ denotes the finite-size corrected results including two-body potential and kinetic energy corrections.

r_s		N_e	E_0/N_e	σ_E^2/N_e	$(E_0/N_e)_\infty$
H ₂	1.38	BF	96	-0.539206(4)	-0.536056(4)
	1.34	BF	96	-0.531888(5)	-0.528548(5)
C	1.318	BF	32	-1.435550(5)	0.016676(8)
	SJ	32	-1.434641(6)	0.022406(8)	-1.424061(6)
		256	-1.425975(1)	0.026937(3)	-1.424635(1)
Si	2.005	BF	32	-0.989922(4)	0.005179(4)
	SJ	32	-0.989240(7)	0.008349(4)	-0.982740(7)
		256	-0.983847(1)	0.008709(2)	-0.983017(1)
		864	-0.983296(1)	0.009115(2)	-0.983046(1)

The fluctuating part of the static structure factors $S(k)$ from our simulations are shown in Fig. 4 and 5. The small-k region of $S(k)$ is fit to the one-parameter model $(1 - \exp(-\alpha k^2))$ at the largest system size available for each

structure. As shown in the bottom panels in Fig. 5, the fit residue is small and flat as $k \rightarrow 0$. Further, the same fit matches the data from all sizes rather well. We therefore use one $S(k)$ for each element to correct the potential energy finite-size errors at all system sizes. Also shown in Fig. 5 are the Jastrow pair potential for carbon and silicon $U(k)$. The $1/k^2$ divergence of $U(k)$ is used to estimate the kinetic energy correction. Similar to $S(k)$, we fit the small- k region of $U(k)$ to the one-parameter model $4\pi a \left(\frac{1}{k^2} + \frac{1}{k^2+1/a} \right)$. We correct both $S(k)$ and $U(k)$ for mixed-estimator bias to calculate unbiased finite-size corrections for fixed-node potential and kinetic energies. In Fig. 5, the fixed-node static structure factor is approximated by linear extrapolation $S(k) = 2S_{DMC} - S_{VMC}$. The fixed-node Jastrow pair potential $U(k) = U_T(k) + \frac{S_{DMC}^{-1}(k) - S_{VMC}^{-1}(k)}{n}$, where n is the electron density. The Jastrow potentials of the hydrogen structures are not shown, because the asymptotic behavior of the analytical trial wavefunction for hydrogen is exactly known [4]. Further, RQMC has no mixed-estimator error, so these corrections do not apply. If the RPA is exact, then $u_k = \frac{4\pi}{\omega_p k^2}$, where the plasmon frequency in 3D $\omega_p = \sqrt{\frac{3}{r_s^3}}$. This implies that for hydrogen $a = \frac{1}{\omega_p}$. Assuming $\lim_{k \rightarrow 0} u_k = \frac{4\pi a}{k^2}$, the c variable defined after eq. (14) in the main text can be shown to be $c = (a\omega_p)^2 = 1$.

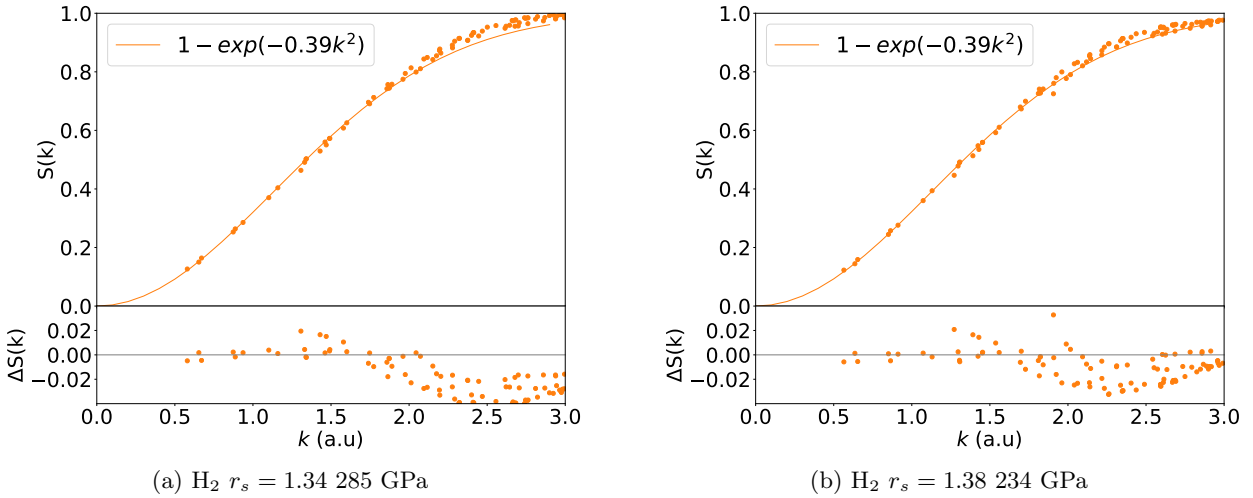


FIG. 4: Structure factor $S(k)$ of molecular hydrogen. The dots are RQMC data. The lines are fits to $1 - e^{-\alpha k^2}$. The bottom panels show the fit residues.

TABLE II: Fit parameters of $S(k) = 1 - e^{-\alpha k^2}$ and $U(k) = 4\pi a \left(\frac{1}{k^2} + \frac{1}{k^2+1/a} \right)$, $c = 3a^2/r_s^3$ and total energy finite-size correction calculated from $\rho(k)$ (δV_N^s), $S(k)$ (δV_N^f), and $u(k)$ (δT_N) as compared to that from $1/N$ extrapolation. All energies are in units of mha/e.

	wf	N_e	α	a	δV_N^f	δV_N^s	δT_N^f	c	δT_N^{BF}	δE_N	$\delta E_N^{extrap.}$
H_2	1.38	BF	96	0.386	0.936	2.59	-0.047	2.59	1	-1.98	3.15
	1.34	BF	96	0.390	0.896	2.74	-0.056	2.74	1	-2.08	3.34
C	BF	32	0.365	0.572	7.47	-0.08	3.10	0.428			
	SJ	32	0.370	0.544	7.46	-0.08	2.81	0.388	0	10.27	9.904(6)
	SJ	256	0.357	0.555	0.92	-0.00	0.37	0.403	0	1.29	1.234(2)
Si	BF	32	0.74	1.25	4.32	-0.10	2.46	0.581			
	SJ	32	0.75	1.07	4.34	-0.10	1.80	0.427	0	6.04	6.176(7)
	SJ	256	0.73	1.00	0.53	-0.00	0.19	0.372	0	0.72	0.783(2)
	SJ	864	0.72	1.25	0.16	-0.00	0.09	0.577	0	0.25	0.232(2)

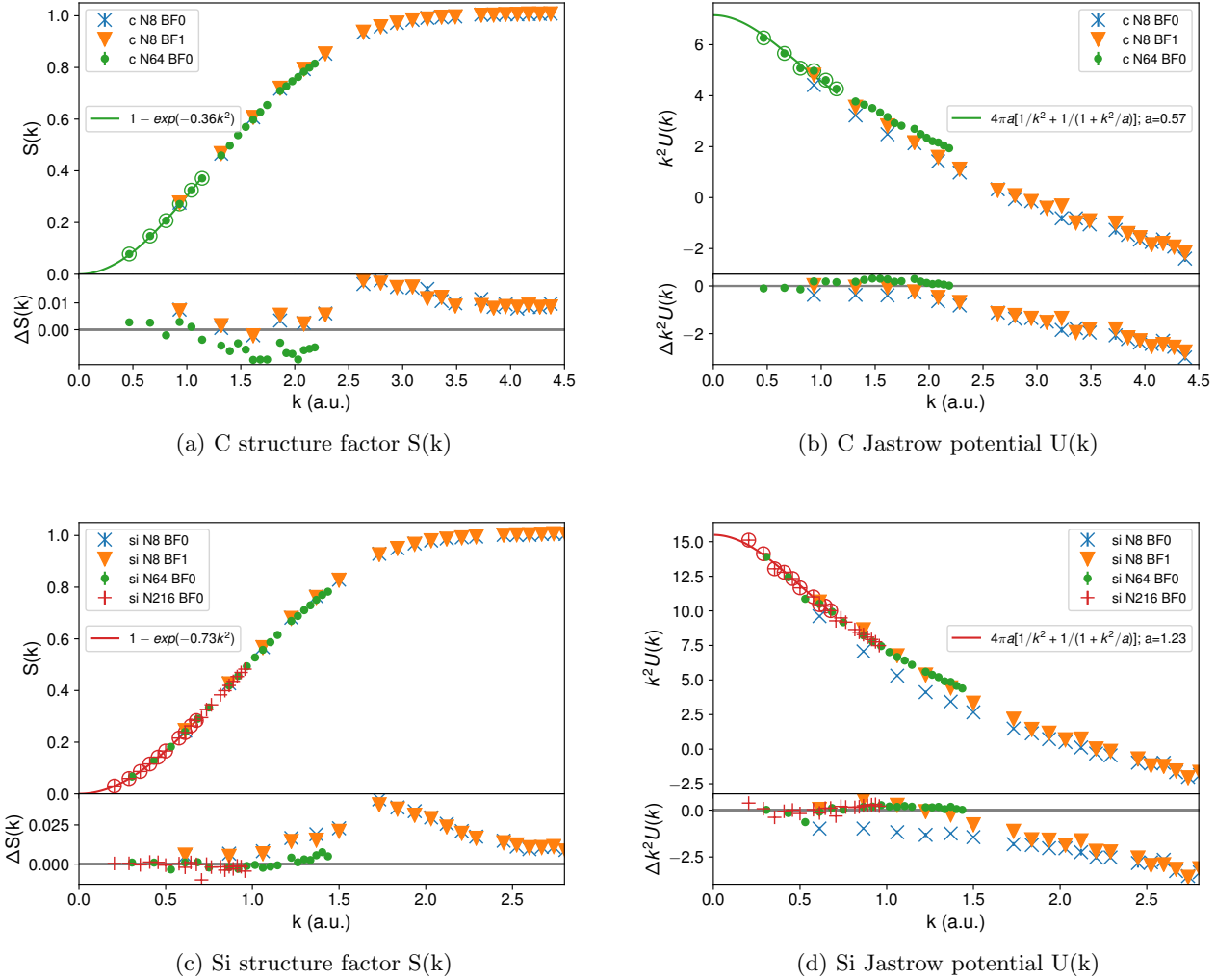


FIG. 5: Structure factor $S(k)$ and Jastrow pair potential $U(k)$ for carbon and silicon. The markers in the $S(k)$ plot are QMC data linearly extrapolated to remove mixed-estimator error. The markers in the $U(k)$ plot are approximations to the fixed-node Jastrow pair potential $U(k) = U_T(k) + \frac{S_{DMC}^{-1}(k) - S_{VBM}^{-1}(k)}{n}$, where n is the electron density. The lines in the upper panels show $S(k)$ and $U(k)$ models fit to data from the largest system (circled points of the same color).

D. Extract dielectric constant from structure factor

For hydrogen, it is difficult to access experimental information on the static dielectric constant. Therefore, we use the asymptotic values of the structure factors S_k^\pm (Fig. 7) as *ab-initio* size corrections of the excitation energies. From Fig. 7 it can be noticed that the size effects are decreasing with increasing pressure. Fig. 8 shows the upper bound on the inverse dielectric constant based on Eq. (6) of the main text. We see that for hydrogen the above inequality holds for both densities, however the values of inverse dielectric constants determined from the asymptotic behavior of S_k^\pm are considerably lower than the bound. As the S_k^\pm explicitly contain information on the excitation energies, we used it to correct the gap values. The equivalent of Fig. 7 and 8 for carbon and silicon are shown in Fig. 2 and 3 in the main article.

E. GCTA vs. CBM-VBM approaches to the gap

In Fig. 9 and 10, we compare the GCTA approach to the traditional CBM-VBM approach to the gap. The right panels show de_0/dn_e from the GCTA approach, similar to the inset of Fig. 1b in the main text. The discontinuity

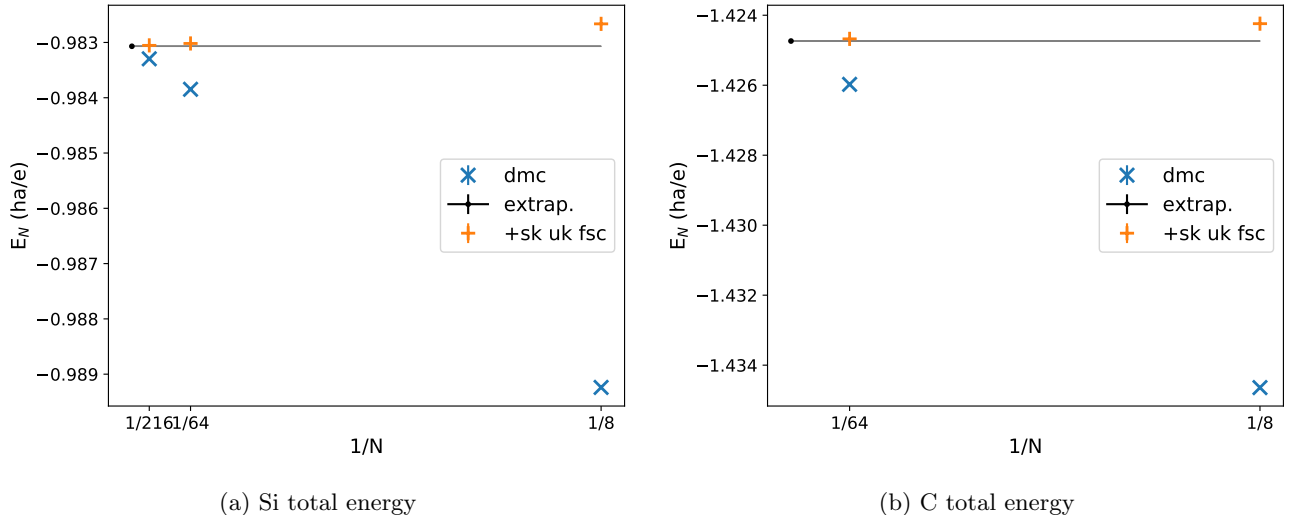


FIG. 6: Total energy finite-size correction

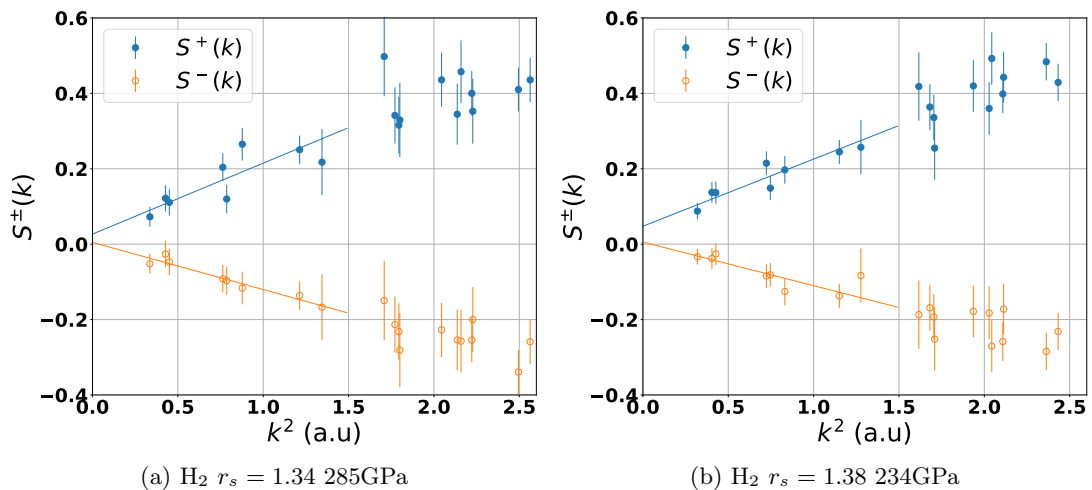


FIG. 7: Change to static structure factor as an electron (blue filled circle) or a hole (orange open circle) is added to the neutral system. The lines are the fits to obtain asymptotic values at $k \rightarrow 0$.

at zero is the GCTA estimate of the gap. The left panels show the CBM and VBM values on the grid of electron addition and removal energies ($\mu^{+/-}$). The two methods give the same results within 0.1 eV at all sizes for carbon and silicon. Therefore, we have assigned 0.1 eV as the systematic error in our estimates of the gap in Table I of the main article.

F. Electron addition/removal energy tables

Table III and IV summarizes information on conduction-band minimum (CBM) and valence-band maximum (VBM) only for those k -vectors that give the fundamental gap. It is clear that the gap for both densities is indirect. More detailed information for all k -vectors for both densities is presented in tables XII - XIX. From these tables one can notice that the energy corrections from static charge density are largest around the Γ point (first entries of tables XII and XVI).

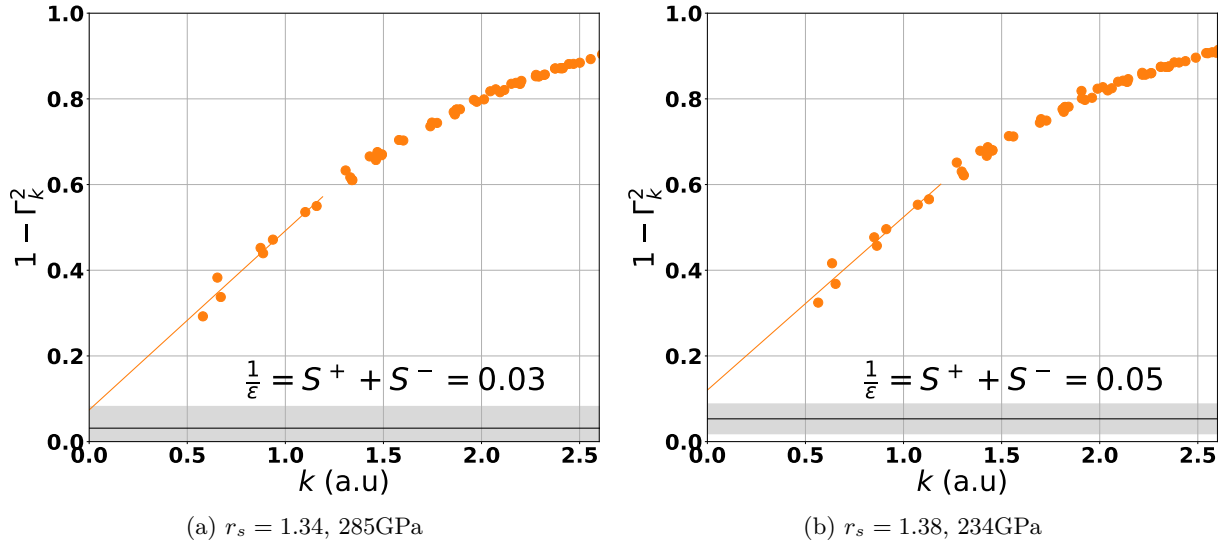


FIG. 8: Inverse dielectric constant upper bound for solid H_2 , where $\Gamma_k \equiv \frac{2m\omega_p S_{N_e}(k)}{\hbar k^2}$. The line is the fit to obtain asymptotic values at $k \rightarrow 0$. Black line indicates the inverse dielectric constant extracted from asymptotic behavior of S_k^\pm (Fig. 7) and considering constant $c = 1$ (see table II). Gray shaded area is the error of the fit of S_k^\pm .

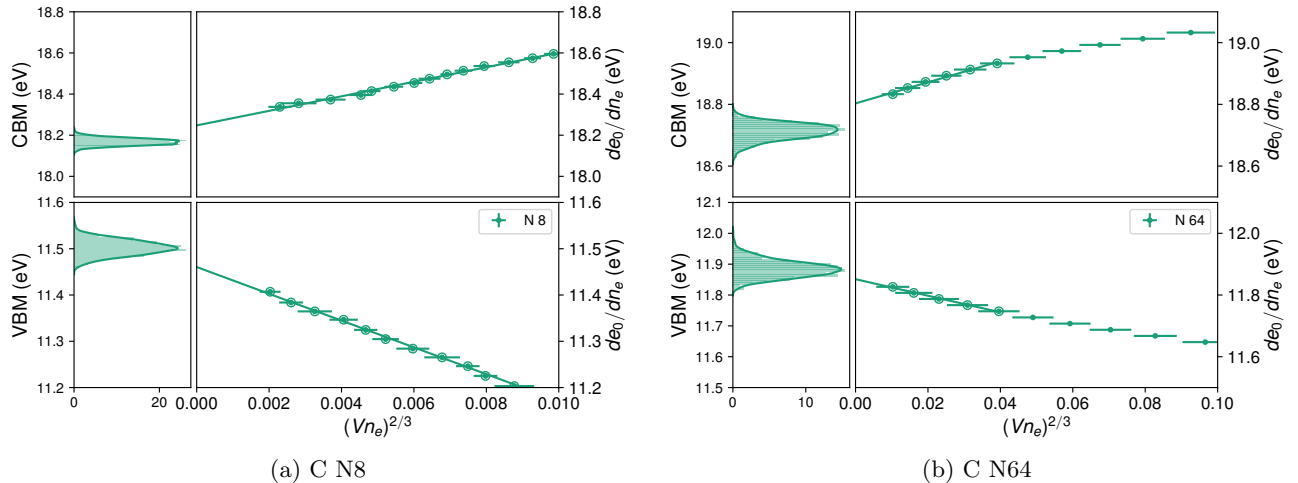


FIG. 9: Finite-size corrected gap of carbon from conduction band minimum (CBM), valence band maximum (VBM) and grand-canonical twist average (GCTA) discontinuity of $d\epsilon_0/dn_e$. We linearly interpolate μ^{+-} on a $64 \times 64 \times 64$ uniform grid in the Brillouin zone of the simulation cell. The left panels show the CBM and VBM of the interpolated grid. The right panels show $d\epsilon_0/dn_e$ calculated on the interpolated grid. The statistical errors of DMC data are propagated using 1024 bootstrap samples.

TABLE III: Removal and addition energies (μ^\pm) and corrections static charge density (μ_s^\pm) for hydrogen. Shown only for those twists that give CBM-VBM gap (bold). Quantities with an overline are twist-average corrected. Δ_k is the vertical gap at twist value k . K-vectors of CBM and VBM are in units of $2\pi/a$.

	r_s	k_x	k_y	k_z	μ^+	μ^-	$\delta\mu_s^+$	$\delta\mu_s^-$	$\overline{\mu}^+$	$\overline{\mu}^-$	Δ_k	$\overline{\Delta}_k$
H_2	1.38	0.062	-0.062	0.062	10.64(12)	6.35(16)	0.015	0.066	10.65(12)	6.41(16)	4.29(20)	4.24(20)
	1.38	0.437	-0.188	0.312	11.65(11)	6.97(16)	0.009	0.006	11.66(11)	6.97(16)	4.68(19)	4.69(19)
	1.34	0.063	-0.062	0.063	11.23(14)	7.79(19)	0.005	0.045	11.23(14)	7.83(19)	3.44(24)	3.40(24)
	1.34	0.063	-0.062	0.437	11.52(14)	8.51(20)	0.006	0.013	11.53(14)	8.53(20)	3.01(24)	3.00(24)

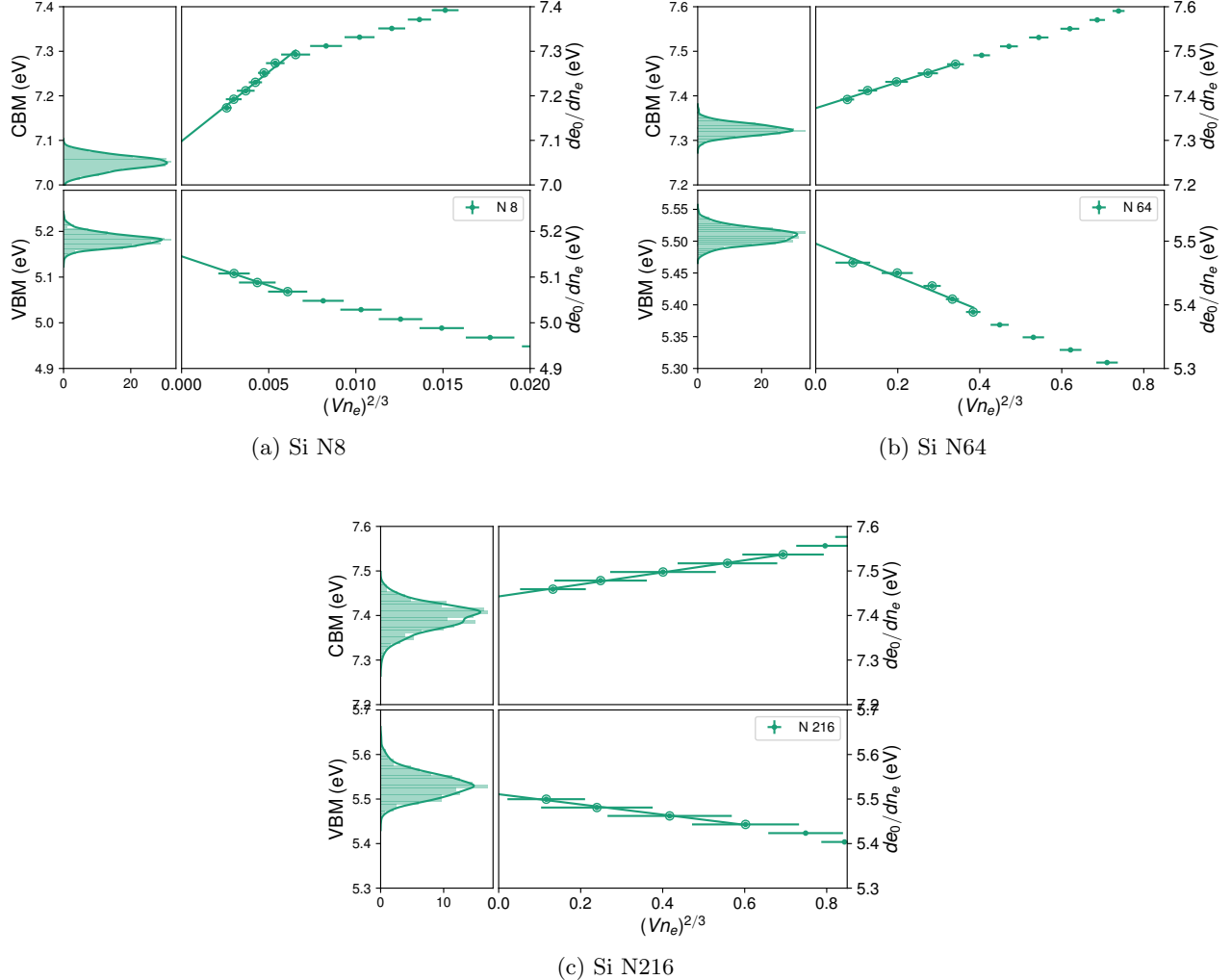


FIG. 10: Finite-size corrected gap of silicon. Similar to Fig. 9.

TABLE IV: Removal and addition energies (μ^\pm) and corrections static charge density (μ_s^\pm) for carbon and silicon. Shown only for those twists that give CBM-VBM gap (**bold**). Quantities with an overline are twist-average corrected. Δ_k is the vertical gap at twist value k . K-vectors of CBM and VBM are fractional units.

N	k_x	k_y	k_z	μ^+	μ^-	$\delta\mu_s^+$	$\delta\mu_s^-$	$\bar{\mu}^+$	$\bar{\mu}^-$	Δ_k	$\overline{\Delta}_k$	
Si	8	0.000	0.000	0.000	7.09(2)	6.03(2)	0.03	-0.54	7.12(2)	5.49(2)	1.06(3)	1.63(3)
	8	0.000	0.000	0.250	6.68(2)	5.01(2)	0.06	-0.12	6.75(2)	4.89(2)	1.67(3)	1.86(3)
	64	0.0	0.0	0.0	7.41(2)	5.74(2)	0.01	-0.10	7.42(2)	5.64(2)	1.67(3)	1.77(3)
	64	0.0	0.0	0.2	7.14(2)	5.63(2)	0.01	-0.05	7.15(2)	5.57(2)	1.51(2)	1.57(2)
	216	0.0	0.0	0.0	7.71(4)	5.39(4)	0.0	-0.02	7.71(4)	5.37(4)	2.32(6)	2.34(6)
	216	0.0	0.0	0.2	7.27(5)	5.64(6)	0.0	-0.01	7.27(5)	5.63(6)	1.63(7)	1.65(7)
C	8	0.000	0.000	0.000	17.94(2)	13.17(2)	-0.05	-0.67	17.89(2)	12.51(2)	4.77(2)	5.38(2)
	8	0.000	0.000	0.250	17.14(3)	11.39(3)	0.02	-0.09	17.16(3)	11.30(3)	5.75(4)	5.86(4)
	64	0.00	0.00	0.00	18.81(5)	12.27(4)	-0.03	-0.07	18.78(5)	12.19(4)	6.54(6)	6.59(6)
	64	0.00	0.00	-0.50	18.25(2)	10.69(2)	0.01	0.02	18.26(2)	10.71(2)	7.57(3)	7.55(3)

TABLE V: C SJ N8 gap. Conduction-band minimum (CBM) $\min(\mu^+)=17.14(3)$ eV at twist 2. Valence-band maximum (VBM) $\max(\mu^-)=13.17(2)$ eV at twist 0. CBM-VBM gap $\Delta=3.97(4)$ eV.

	kx	ky	kz	μ^+	μ^-	$\delta\mu_s^+$	$\delta\mu_s^-$	$\bar{\mu}^+$	$\bar{\mu}^-$	Δ_v	$\bar{\Delta}_v$
0	0.000	0.000	0.000	17.94(2)	13.17(2)	-0.05	-0.67	17.89(2)	12.51(2)	4.77(2)	5.38(2)
1	0.000	0.000	0.125	17.35(2)	12.69(2)	-0.06	-0.46	17.30(2)	12.23(2)	4.67(2)	5.07(2)
2	0.000	0.000	0.250	17.14(3)	11.39(3)	0.02	-0.09	17.16(3)	11.30(3)	5.75(4)	5.86(4)
3	0.000	0.000	0.375	17.25(1)	9.69(2)	0.10	0.13	17.35(1)	9.82(2)	7.56(2)	7.54(2)
4	0.000	0.000	-0.500	17.63(2)	8.04(2)	0.15	0.04	17.78(2)	8.07(2)	9.59(3)	9.71(3)
5	0.000	0.125	0.125	18.13(2)	12.74(2)	-0.06	-0.37	18.07(2)	12.36(2)	5.40(2)	5.71(2)
6	0.000	0.125	0.250	17.82(2)	11.92(2)	0.00	-0.11	17.82(2)	11.81(2)	5.90(2)	6.00(2)
7	0.000	0.125	0.375	17.90(2)	10.52(2)	0.08	0.10	17.98(2)	10.62(2)	7.38(2)	7.36(2)
8	0.000	0.125	-0.500	18.30(2)	8.96(2)	0.13	0.14	18.43(2)	9.10(2)	9.33(3)	9.33(3)
9	0.000	0.250	0.250	18.80(2)	11.89(2)	0.07	-0.03	18.87(2)	11.86(2)	6.91(3)	7.01(3)
10	0.000	0.250	0.375	19.71(1)	11.00(2)	0.07	0.10	19.78(1)	11.10(2)	8.71(2)	8.68(2)
11	0.000	0.250	-0.500	20.00(2)	9.63(2)	0.10	0.15	20.10(2)	9.79(2)	10.37(3)	10.32(3)
12	0.000	0.375	0.375	20.01(2)	10.84(2)	0.11	0.08	20.12(2)	10.92(2)	9.18(2)	9.21(2)
13	0.000	0.375	-0.500	21.17(1)	9.90(2)	0.10	0.07	21.27(1)	9.97(2)	11.27(2)	11.30(2)
14	0.000	-0.500	-0.500	21.43(2)	9.38(2)	0.13	0.01	21.56(2)	9.39(2)	12.05(3)	12.17(3)
15	0.125	0.125	0.125	18.22(1)	12.19(1)	-0.01	-0.28	18.22(1)	11.91(1)	6.03(2)	6.31(2)
16	0.125	0.125	0.250	18.13(2)	11.69(1)	0.03	-0.09	18.16(2)	11.60(1)	6.44(2)	6.56(2)
17	0.125	0.125	0.375	18.31(2)	10.46(2)	0.09	0.10	18.39(2)	10.56(2)	7.84(2)	7.83(2)
18	0.125	0.125	-0.500	18.77(1)	8.89(2)	0.13	0.14	18.91(1)	9.03(2)	9.88(2)	9.87(2)
19	0.125	0.250	0.250	18.91(2)	11.62(2)	0.08	-0.04	19.00(2)	11.58(2)	7.29(3)	7.41(3)
20	0.125	0.250	0.375	19.60(2)	10.87(2)	0.08	0.07	19.68(2)	10.93(2)	8.73(3)	8.75(3)
21	0.125	0.250	-0.500	20.18(2)	9.55(1)	0.10	0.11	20.27(2)	9.66(1)	10.63(3)	10.61(3)
22	0.125	0.375	0.375	20.19(2)	10.77(2)	0.09	0.03	20.28(2)	10.80(2)	9.42(2)	9.48(2)
23	0.125	0.375	-0.500	21.31(2)	9.91(2)	0.07	0.02	21.37(2)	9.93(2)	11.40(2)	11.45(2)
24	0.125	-0.500	-0.500	21.58(2)	9.47(2)	0.09	-0.04	21.67(2)	9.43(2)	12.11(2)	12.24(2)
25	0.250	0.250	0.250	19.52(2)	10.88(1)	0.12	-0.09	19.64(2)	10.79(1)	8.64(2)	8.85(2)
26	0.250	0.250	0.375	19.83(1)	10.55(2)	0.10	-0.04	19.94(1)	10.51(2)	9.28(2)	9.42(2)
27	0.250	0.250	-0.500	20.74(2)	9.34(2)	0.08	-0.00	20.82(2)	9.34(2)	11.40(2)	11.48(2)
28	0.250	0.375	0.375	20.60(2)	10.61(2)	0.04	-0.10	20.64(2)	10.50(2)	9.99(2)	10.14(2)
29	0.250	0.375	-0.500	21.92(2)	9.88(2)	-0.05	-0.12	21.87(2)	9.76(2)	12.04(3)	12.11(3)
30	0.250	-0.500	-0.500	21.96(1)	9.61(1)	-0.02	-0.19	21.94(1)	9.43(1)	12.35(2)	12.51(2)
31	0.375	0.375	0.375	21.46(2)	10.29(1)	-0.03	-0.26	21.42(2)	10.04(1)	11.16(2)	11.39(2)
32	0.375	0.375	-0.500	22.19(2)	9.83(1)	-0.15	-0.29	22.04(2)	9.54(1)	12.36(2)	12.50(2)
33	0.375	-0.500	-0.500	22.41(1)	9.81(2)	-0.19	-0.36	22.22(1)	9.45(2)	12.60(2)	12.77(2)
34	-0.500	-0.500	-0.500	22.71(2)	9.92(2)	-0.27	-0.47	22.44(2)	9.45(2)	12.79(3)	12.99(3)

TABLE VI: C SJ N64 gap. Conduction-band minimum (CBM) $\min(\mu^+)=18.25(2)$ eV at twist 2. Valence-band maximum (VBM) $\max(\mu^-)=12.27(4)$ eV at twist 0. CBM-VBM gap $\Delta=5.98(4)$ eV.

	kx	ky	kz	μ^+	μ^-	$\delta\mu_s^+$	$\delta\mu_s^-$	$\bar{\mu}^+$	$\bar{\mu}^-$	Δ_v	$\bar{\Delta}_v$
0	0.00	0.00	0.00	18.81(5)	12.27(4)	-0.03	-0.07	18.78(5)	12.19(4)	6.54(6)	6.59(6)
1	0.00	0.00	0.25	18.27(2)	12.06(2)	-0.00	-0.02	18.27(2)	12.04(2)	6.22(2)	6.24(2)
2	0.00	0.00	-0.50	18.25(2)	10.69(2)	0.01	0.02	18.26(2)	10.71(2)	7.57(3)	7.55(3)
3	0.00	0.25	0.25	18.91(1)	12.30(1)	-0.01	-0.01	18.91(1)	12.29(1)	6.61(2)	6.62(2)
4	0.00	0.25	-0.50	18.78(1)	11.58(1)	0.01	0.02	18.79(1)	11.59(1)	7.21(2)	7.20(2)
5	0.00	-0.50	-0.50	19.88(3)	11.44(2)	0.01	0.01	19.89(3)	11.45(2)	8.44(4)	8.44(4)
6	0.25	0.25	0.25	18.95(2)	11.75(2)	0.02	-0.00	18.97(2)	11.74(2)	7.20(2)	7.23(2)
7	0.25	0.25	-0.50	19.03(1)	11.42(1)	0.01	0.00	19.04(1)	11.42(1)	7.61(2)	7.62(2)
8	0.25	-0.50	-0.50	19.89(2)	11.30(2)	0.00	-0.01	19.89(2)	11.29(2)	8.59(2)	8.60(2)
9	-0.50	-0.50	-0.50	20.54(5)	10.23(6)	-0.01	-0.03	20.53(5)	10.20(6)	10.31(7)	10.33(7)

TABLE VII: C BF N8 gap. Conduction-band minimum (CBM) $\min(\mu^+)=17.06(2)$ eV at twist 2. Valence-band maximum (VBM) $\max(\mu^-)=13.13(1)$ eV at twist 0. CBM-VBM gap $\Delta=3.92(2)$ eV.

	kx	ky	kz	μ^+	μ^-	$\delta\mu_s^+$	$\delta\mu_s^-$	$\bar{\mu}^+$	$\bar{\mu}^-$	Δ_v	$\overline{\Delta}_v$
0	0.000	0.000	0.000	17.76(1)	13.13(1)	-0.05	-0.67	17.71(1)	12.47(1)	4.63(2)	5.25(2)
1	0.000	0.000	0.125	17.25(1)	12.66(2)	-0.06	-0.46	17.19(1)	12.20(2)	4.59(3)	4.99(3)
2	0.000	0.000	0.250	17.06(2)	11.38(2)	0.02	-0.09	17.08(2)	11.28(2)	5.68(2)	5.79(2)
3	0.000	0.000	0.375	17.19(1)	9.67(2)	0.10	0.13	17.30(1)	9.80(2)	7.52(2)	7.50(2)
4	0.000	0.000	-0.500	17.54(1)	8.20(2)	0.15	0.04	17.69(1)	8.24(2)	9.34(2)	9.46(2)
5	0.000	0.125	0.125	17.92(2)	12.69(2)	-0.06	-0.37	17.87(2)	12.32(2)	5.23(2)	5.54(2)
6	0.000	0.125	0.250	17.73(1)	11.90(1)	0.00	-0.11	17.73(1)	11.79(1)	5.82(2)	5.93(2)
7	0.000	0.125	0.375	17.81(2)	10.52(2)	0.08	0.10	17.89(2)	10.61(2)	7.30(3)	7.28(3)
8	0.000	0.125	-0.500	18.19(1)	8.92(2)	0.13	0.14	18.33(1)	9.06(2)	9.27(2)	9.27(2)
9	0.000	0.250	0.250	18.74(2)	11.86(2)	0.07	-0.03	18.81(2)	11.83(2)	6.88(3)	6.98(3)
10	0.000	0.250	0.375	19.60(1)	10.99(2)	0.07	0.10	19.68(1)	11.10(2)	8.61(2)	8.58(2)
11	0.000	0.250	-0.500	19.89(2)	9.61(2)	0.10	0.15	19.99(2)	9.77(2)	10.28(2)	10.22(2)
12	0.000	0.375	0.375	19.93(1)	10.80(1)	0.11	0.08	20.04(1)	10.88(1)	9.13(2)	9.15(2)
13	0.000	0.375	-0.500	21.14(1)	9.86(1)	0.10	0.07	21.24(1)	9.93(1)	11.29(2)	11.31(2)
14	0.000	-0.500	-0.500	21.41(2)	9.49(2)	0.13	0.01	21.54(2)	9.50(2)	11.92(2)	12.04(2)
15	0.125	0.125	0.125	18.00(1)	12.16(2)	-0.01	-0.28	17.99(1)	11.88(2)	5.84(2)	6.11(2)
16	0.125	0.125	0.250	17.99(2)	11.66(2)	0.03	-0.09	18.02(2)	11.57(2)	6.33(2)	6.45(2)
17	0.125	0.125	0.375	18.24(1)	10.43(1)	0.09	0.10	18.33(1)	10.53(1)	7.81(2)	7.80(2)
18	0.125	0.125	-0.500	18.64(2)	8.86(1)	0.13	0.14	18.77(2)	9.01(1)	9.78(2)	9.76(2)
19	0.125	0.250	0.250	18.84(1)	11.61(1)	0.08	-0.04	18.92(1)	11.57(1)	7.23(2)	7.35(2)
20	0.125	0.250	0.375	19.47(1)	10.87(1)	0.08	0.07	19.56(1)	10.94(1)	8.61(2)	8.62(2)
21	0.125	0.250	-0.500	19.96(2)	9.50(2)	0.10	0.11	20.06(2)	9.61(2)	10.46(2)	10.45(2)
22	0.125	0.375	0.375	20.09(1)	10.75(1)	0.09	0.03	20.18(1)	10.78(1)	9.33(2)	9.39(2)
23	0.125	0.375	-0.500	21.26(2)	9.88(2)	0.07	0.02	21.32(2)	9.90(2)	11.38(2)	11.43(2)
24	0.125	-0.500	-0.500	21.52(2)	9.60(2)	0.09	-0.04	21.61(2)	9.56(2)	11.92(3)	12.05(3)
25	0.250	0.250	0.250	19.20(1)	10.86(2)	0.12	-0.09	19.32(1)	10.78(2)	8.34(2)	8.55(2)
26	0.250	0.250	0.375	19.76(1)	10.56(1)	0.10	-0.04	19.86(1)	10.53(1)	9.20(2)	9.34(2)
27	0.250	0.250	-0.500	20.39(1)	9.37(2)	0.08	-0.00	20.47(1)	9.36(2)	11.02(2)	11.11(2)
28	0.250	0.375	0.375	20.48(1)	10.58(1)	0.04	-0.10	20.52(1)	10.48(1)	9.89(2)	10.04(2)
29	0.250	0.375	-0.500	21.61(1)	9.91(1)	-0.05	-0.12	21.56(1)	9.79(1)	11.70(2)	11.77(2)
30	0.250	-0.500	-0.500	21.85(2)	9.81(2)	-0.02	-0.19	21.83(2)	9.63(2)	12.04(2)	12.21(2)
31	0.375	0.375	0.375	21.12(1)	10.29(1)	-0.03	-0.26	21.08(1)	10.03(1)	10.82(2)	11.05(2)
32	0.375	0.375	-0.500	21.85(2)	9.87(2)	-0.15	-0.29	21.70(2)	9.58(2)	11.99(3)	12.12(3)
33	0.375	-0.500	-0.500	22.32(1)	10.07(2)	-0.19	-0.36	22.12(1)	9.71(2)	12.25(2)	12.42(2)
34	-0.500	-0.500	-0.500	22.48(1)	10.15(1)	-0.27	-0.47	22.21(1)	9.68(1)	12.33(2)	12.53(2)

TABLE VIII: Si SJ N8 gap. $\delta\mu_s^\pm$ is finite-size correction of electron addition/removal energy from static charge density. Quantities with an overline are twist-average corrected. Conduction-band minimum (CBM) $\min(\mu^+) = 6.68(2)$ eV at twist 2, valence-band maximum (VBM) $\max(\mu^-) = 6.03(2)$ eV at twist 0, CBM-VBM gap $\Delta = 0.65(3)$ eV.

kx	ky	kz	μ^+	μ^-	$\delta\mu_s^+$	$\delta\mu_s^-$	$\overline{\mu}^+$	$\overline{\mu}^-$	Δ_v	$\overline{\Delta}_v$	
0	0.000	0.000	0.000	7.09(2)	6.03(2)	0.03	-0.54	7.12(2)	5.49(2)	1.06(3)	1.63(3)
1	0.000	0.000	0.125	6.69(2)	5.68(2)	0.04	-0.35	6.73(2)	5.33(2)	1.01(3)	1.40(3)
2	0.000	0.000	0.250	6.68(2)	5.01(2)	0.06	-0.12	6.75(2)	4.89(2)	1.67(3)	1.86(3)
3	0.000	0.000	0.375	6.89(2)	4.33(2)	0.09	-0.02	6.97(2)	4.31(2)	2.55(3)	2.66(3)
4	0.000	0.000	-0.500	7.18(2)	3.74(2)	0.10	0.00	7.28(2)	3.74(2)	3.44(3)	3.55(3)
5	0.000	0.125	0.125	7.07(2)	5.81(2)	0.01	-0.31	7.09(2)	5.50(2)	1.26(3)	1.59(3)
6	0.000	0.125	0.250	7.12(2)	5.36(2)	0.01	-0.08	7.13(2)	5.27(2)	1.76(3)	1.86(3)
7	0.000	0.125	0.375	7.27(3)	4.65(3)	0.05	0.05	7.32(3)	4.70(3)	2.62(4)	2.62(4)
8	0.000	0.125	-0.500	7.64(2)	4.03(2)	0.07	0.07	7.71(2)	4.10(2)	3.60(3)	3.61(3)
9	0.000	0.250	0.250	7.42(2)	5.46(3)	0.08	-0.04	7.49(2)	5.42(3)	1.95(4)	2.07(4)
10	0.000	0.250	0.375	8.00(2)	5.00(2)	0.04	0.08	8.05(2)	5.09(2)	3.00(3)	2.96(3)
11	0.000	0.250	-0.500	8.66(2)	4.34(2)	0.05	0.12	8.71(2)	4.46(2)	4.32(3)	4.26(3)
12	0.000	0.375	0.375	8.06(2)	4.99(2)	0.10	0.04	8.16(2)	5.03(2)	3.07(3)	3.13(3)
13	0.000	0.375	-0.500	8.71(1)	4.55(2)	0.08	0.04	8.79(1)	4.58(2)	4.16(2)	4.21(2)
14	0.000	-0.500	-0.500	8.99(2)	4.24(2)	0.19	-0.04	9.18(2)	4.20(2)	4.75(3)	4.97(3)
15	0.125	0.125	0.125	7.13(2)	5.58(2)	0.06	-0.20	7.19(2)	5.38(2)	1.55(3)	1.81(3)
16	0.125	0.125	0.250	7.18(2)	5.22(2)	0.05	-0.06	7.23(2)	5.16(2)	1.96(3)	2.07(3)
17	0.125	0.125	0.375	7.41(2)	4.47(2)	0.06	0.07	7.47(2)	4.54(2)	2.94(3)	2.94(3)
18	0.125	0.125	-0.500	7.93(2)	3.67(2)	0.08	0.07	8.01(2)	3.74(2)	4.25(2)	4.27(2)
19	0.125	0.250	0.250	7.50(2)	5.35(3)	0.09	-0.05	7.59(2)	5.30(3)	2.15(4)	2.29(4)
20	0.125	0.250	0.375	8.14(2)	4.91(1)	0.04	0.06	8.18(2)	4.97(1)	3.23(2)	3.21(2)
21	0.125	0.250	-0.500	8.61(3)	4.27(2)	0.06	0.09	8.67(3)	4.36(2)	4.34(4)	4.31(4)
22	0.125	0.375	0.375	8.13(2)	4.99(2)	0.10	0.00	8.22(2)	5.00(2)	3.13(2)	3.23(2)
23	0.125	0.375	-0.500	8.77(2)	4.59(2)	0.07	0.01	8.84(2)	4.60(2)	4.19(3)	4.25(3)
24	0.125	-0.500	-0.500	9.05(2)	4.27(2)	0.17	-0.07	9.22(2)	4.21(2)	4.78(3)	5.02(3)
25	0.250	0.250	0.250	7.82(2)	5.01(3)	0.12	-0.06	7.93(2)	4.95(3)	2.81(4)	2.99(4)
26	0.250	0.250	0.375	8.08(2)	4.72(2)	0.08	-0.00	8.16(2)	4.72(2)	3.36(3)	3.44(3)
27	0.250	0.250	-0.500	8.69(2)	3.92(3)	0.07	-0.00	8.76(2)	3.92(3)	4.77(4)	4.84(4)
28	0.250	0.375	0.375	8.29(3)	4.93(2)	0.06	-0.09	8.36(3)	4.84(2)	3.36(4)	3.52(4)
29	0.250	0.375	-0.500	8.90(2)	4.55(2)	-0.02	-0.08	8.87(2)	4.46(2)	4.35(3)	4.41(3)
30	0.250	-0.500	-0.500	9.03(2)	4.37(2)	0.08	-0.15	9.11(2)	4.22(2)	4.66(2)	4.89(2)
31	0.375	0.375	0.375	8.13(3)	4.75(2)	0.03	-0.19	8.16(3)	4.56(2)	3.38(3)	3.60(3)
32	0.375	0.375	-0.500	8.45(2)	4.29(2)	-0.09	-0.24	8.35(2)	4.05(2)	4.16(3)	4.31(3)
33	0.375	-0.500	-0.500	8.46(2)	4.45(2)	-0.12	-0.29	8.35(2)	4.16(2)	4.01(2)	4.18(2)
34	-0.500	-0.500	-0.500	8.01(2)	4.55(2)	-0.18	-0.41	7.83(2)	4.14(2)	3.47(3)	3.69(3)

TABLE IX: Si SJ N64 gap. Conduction-band minimum (CBM) $\min(\mu^+) = 7.14(2)$ eV at twist 1, valence-band maximum (VBM) $\max(\mu^-) = 5.74(2)$ eV at twist 0, CBM-VBM gap $\Delta = 1.40(2)$ eV.

kx	ky	kz	μ^+	μ^-	$\delta\mu_s^+$	$\delta\mu_s^-$	$\overline{\mu}^+$	$\overline{\mu}^-$	Δ_v	$\overline{\Delta}_v$	
0	0.0	0.0	0.0	7.41(2)	5.74(2)	0.01	-0.10	7.42(2)	5.64(2)	1.67(3)	1.77(3)
1	0.0	0.0	0.2	7.14(2)	5.63(2)	0.01	-0.05	7.15(2)	5.57(2)	1.51(2)	1.57(2)
2	0.0	0.0	0.4	7.20(2)	5.07(2)	0.02	-0.00	7.22(2)	5.07(2)	2.13(3)	2.15(3)
3	0.0	0.2	0.2	7.34(2)	5.70(2)	0.01	-0.03	7.35(2)	5.68(2)	1.64(3)	1.67(3)
4	0.0	0.2	0.4	7.39(2)	5.46(2)	0.01	0.02	7.39(2)	5.47(2)	1.93(3)	1.92(3)
5	0.0	0.4	0.4	7.64(1)	5.54(1)	0.01	0.02	7.65(1)	5.55(1)	2.10(2)	2.09(2)
6	0.2	0.2	0.2	7.37(1)	5.53(1)	0.01	-0.02	7.39(1)	5.51(1)	1.84(2)	1.88(2)
7	0.2	0.2	0.4	7.41(2)	5.39(2)	0.01	0.01	7.43(2)	5.40(2)	2.03(2)	2.03(2)
8	0.2	0.4	0.4	7.66(2)	5.47(2)	0.01	-0.00	7.66(2)	5.47(2)	2.18(2)	2.19(2)
9	0.4	0.4	0.4	7.87(2)	5.11(2)	0.00	-0.04	7.87(2)	5.07(2)	2.76(2)	2.80(2)

TABLE X: Si SJ N216 gap. Conduction-band minimum (CBM) $\min(\mu^+) = 7.27(5)$ eV at twist 1, valence-band maximum (VBM) $\max(\mu^-) = 5.64(2)$ eV at twist 1, CBM-VBM gap $\Delta = 1.63(7)$ eV.

kx	ky	kz	μ^+	μ^-	$\delta\mu_s^+$	$\delta\mu_s^-$	$\bar{\mu}^+$	$\bar{\mu}^-$	Δ_v	$\bar{\Delta}_v$	
0	0.0	0.0	0.0	7.71(4)	5.39(4)	0.0	-0.02	7.71(4)	5.37(4)	2.32(6)	2.34(6)
1	0.0	0.0	0.2	7.27(5)	5.64(6)	0.0	-0.01	7.27(5)	5.63(6)	1.63(7)	1.65(7)
2	0.0	0.0	0.4	7.41(4)	5.20(4)	0.0	-0.00	7.41(4)	5.20(4)	2.21(5)	2.21(5)
3	0.0	0.2	0.2	7.50(5)	5.60(5)	0.0	-0.01	7.50(5)	5.59(5)	1.90(7)	1.90(7)
4	0.0	0.2	0.4	7.37(3)	5.53(4)	0.0	0.00	7.37(3)	5.53(4)	1.84(5)	1.84(5)
5	0.0	0.4	0.4	7.62(4)	5.47(4)	-0.0	0.00	7.62(4)	5.48(4)	2.15(6)	2.14(6)
6	0.2	0.2	0.2	7.40(5)	5.56(4)	0.0	-0.00	7.40(5)	5.55(4)	1.84(6)	1.85(6)
7	0.2	0.2	0.4	7.32(4)	5.62(4)	0.0	0.00	7.32(4)	5.62(4)	1.70(5)	1.70(5)
8	0.2	0.4	0.4	7.59(5)	5.48(4)	-0.0	0.00	7.59(5)	5.48(4)	2.11(7)	2.11(7)
9	0.4	0.4	0.4	7.72(4)	5.27(5)	-0.0	-0.01	7.72(4)	5.27(5)	2.44(6)	2.45(6)

TABLE XI: Si BF N8 gap. $\delta\mu_s^\pm$ is finite-size correction of electron addition/removal energy from static charge density. Quantities with an overline are twist-average corrected. Conduction-band minimum (CBM) $\min(\mu^+) = 6.60(2)$ eV at twist 2, valence-band maximum (VBM) $\max(\mu^-) = 6.03(1)$ eV at twist 0, CBM-VBM gap $\Delta = 0.56(2)$ eV.

kx	ky	kz	μ^+	μ^-	$\delta\mu_s^+$	$\delta\mu_s^-$	$\bar{\mu}^+$	$\bar{\mu}^-$	Δ_v	$\bar{\Delta}_v$	
0	0.000	0.000	0.000	6.87(1)	6.03(1)	0.03	-0.54	6.90(1)	5.49(1)	0.83(2)	1.41(2)
1	0.000	0.000	0.125	6.60(2)	5.65(1)	0.04	-0.35	6.64(2)	5.30(1)	0.94(2)	1.34(2)
2	0.000	0.000	0.250	6.60(1)	4.99(1)	0.06	-0.12	6.67(1)	4.87(1)	1.62(1)	1.80(1)
3	0.000	0.000	0.375	6.80(1)	4.36(2)	0.09	-0.02	6.88(1)	4.34(2)	2.43(2)	2.54(2)
4	0.000	0.000	-0.500	7.15(1)	3.82(2)	0.10	0.00	7.26(1)	3.82(2)	3.34(2)	3.44(2)
5	0.000	0.125	0.125	6.94(1)	5.84(1)	0.01	-0.31	6.95(1)	5.53(1)	1.10(2)	1.43(2)
6	0.000	0.125	0.250	7.01(1)	5.35(1)	0.01	-0.08	7.03(1)	5.27(1)	1.66(2)	1.76(2)
7	0.000	0.125	0.375	7.19(2)	4.65(2)	0.05	0.05	7.24(2)	4.70(2)	2.54(3)	2.54(3)
8	0.000	0.125	-0.500	7.56(1)	4.02(2)	0.07	0.07	7.63(1)	4.08(2)	3.54(2)	3.55(2)
9	0.000	0.250	0.250	7.35(1)	5.44(1)	0.08	-0.04	7.42(1)	5.40(1)	1.90(2)	2.02(2)
10	0.000	0.250	0.375	7.944(10)	5.00(1)	0.04	0.08	7.986(10)	5.08(1)	2.95(2)	2.91(2)
11	0.000	0.250	-0.500	8.53(1)	4.31(1)	0.05	0.12	8.58(1)	4.43(1)	4.22(2)	4.15(2)
12	0.000	0.375	0.375	7.96(1)	5.01(1)	0.10	0.04	8.07(1)	5.05(1)	2.95(2)	3.02(2)
13	0.000	0.375	-0.500	8.68(1)	4.53(1)	0.08	0.04	8.76(1)	4.57(1)	4.15(2)	4.19(2)
14	0.000	-0.500	-0.500	8.77(1)	4.44(1)	0.19	-0.04	8.96(1)	4.40(1)	4.33(2)	4.56(2)
15	0.125	0.125	0.125	6.99(1)	5.62(1)	0.06	-0.20	7.05(1)	5.42(1)	1.37(2)	1.63(2)
16	0.125	0.125	0.250	7.13(1)	5.20(1)	0.05	-0.06	7.18(1)	5.15(1)	1.93(2)	2.04(2)
17	0.125	0.125	0.375	7.39(1)	4.426(10)	0.06	0.07	7.46(1)	4.495(10)	2.97(1)	2.96(1)
18	0.125	0.125	-0.500	7.80(1)	3.87(1)	0.08	0.07	7.88(1)	3.94(1)	3.93(2)	3.94(2)
19	0.125	0.250	0.250	7.42(1)	5.34(1)	0.09	-0.05	7.51(1)	5.28(1)	2.08(2)	2.22(2)
20	0.125	0.250	0.375	8.02(1)	4.93(1)	0.04	0.06	8.06(1)	4.99(1)	3.09(2)	3.08(2)
21	0.125	0.250	-0.500	8.44(1)	4.25(1)	0.06	0.09	8.50(1)	4.34(1)	4.19(2)	4.17(2)
22	0.125	0.375	0.375	8.03(1)	4.98(1)	0.10	0.00	8.13(1)	4.99(1)	3.05(2)	3.14(2)
23	0.125	0.375	-0.500	8.73(1)	4.55(1)	0.07	0.01	8.80(1)	4.56(1)	4.18(2)	4.24(2)
24	0.125	-0.500	-0.500	8.78(1)	4.50(1)	0.17	-0.07	8.95(1)	4.43(1)	4.28(2)	4.52(2)
25	0.250	0.250	0.250	7.65(2)	5.06(2)	0.12	-0.06	7.77(2)	5.00(2)	2.59(2)	2.77(2)
26	0.250	0.250	0.375	8.03(1)	4.71(1)	0.08	-0.00	8.11(1)	4.71(1)	3.32(2)	3.40(2)
27	0.250	0.250	-0.500	8.433(10)	4.14(1)	0.07	-0.00	8.504(10)	4.14(1)	4.29(2)	4.36(2)
28	0.250	0.375	0.375	8.25(1)	4.93(1)	0.06	-0.09	8.31(1)	4.84(1)	3.31(2)	3.47(2)
29	0.250	0.375	-0.500	8.75(1)	4.56(1)	-0.02	-0.08	8.73(1)	4.48(1)	4.19(2)	4.25(2)
30	0.250	-0.500	-0.500	8.75(1)	4.59(1)	0.08	-0.15	8.83(1)	4.44(1)	4.16(2)	4.39(2)
31	0.375	0.375	0.375	8.03(1)	4.82(1)	0.03	-0.19	8.06(1)	4.63(1)	3.21(2)	3.43(2)
32	0.375	0.375	-0.500	8.37(1)	4.55(2)	-0.09	-0.24	8.27(1)	4.31(2)	3.82(2)	3.96(2)
33	0.375	-0.500	-0.500	8.34(1)	4.74(1)	-0.12	-0.29	8.22(1)	4.45(1)	3.60(2)	3.77(2)
34	-0.500	-0.500	-0.500	8.00(1)	4.83(1)	-0.18	-0.41	7.82(1)	4.42(1)	3.18(2)	3.41(2)

TABLE XII: H₂ r_s = 1.38. Removal and addition energies corrections (μ_s^\pm) from static charge density for 8 × 8 × 8 k-grid shifted to exclude the Γ point. Part I.

k_x	k_y	k_z	μ^+	μ^-	$\delta\mu_s^+$	$\delta\mu_s^-$	$\bar{\mu}^+$	$\bar{\mu}^-$	Δ_k	$\bar{\Delta}_k$
0.062	0.062	0.062	11.17(12)	6.07(16)	0.024	0.103	11.19(12)	6.17(16)	5.10(20)	5.02(20)
0.062	0.062	0.187	11.19(11)	5.86(16)	0.008	0.041	11.20(11)	5.91(16)	5.32(20)	5.29(20)
0.062	0.062	0.312	11.54(11)	6.42(16)	0.005	0.032	11.54(11)	6.46(16)	5.12(20)	5.09(20)
0.062	0.062	0.437	10.81(12)	6.76(16)	0.002	0.015	10.81(12)	6.78(16)	4.05(20)	4.04(20)
0.062	0.062	-0.437	11.09(11)	6.52(16)	0.008	0.025	11.10(11)	6.54(16)	4.58(19)	4.56(19)
0.062	0.062	-0.312	11.66(11)	6.23(16)	0.009	0.021	11.67(11)	6.25(16)	5.42(19)	5.41(19)
0.062	0.062	-0.187	11.24(11)	5.86(16)	0.008	0.050	11.24(11)	5.91(16)	5.38(20)	5.33(20)
0.062	0.062	-0.062	11.00(12)	6.30(16)	-0.005	0.069	11.00(12)	6.37(16)	4.70(20)	4.63(20)
0.062	0.188	0.062	11.24(12)	5.71(16)	0.000	0.034	11.24(12)	5.74(16)	5.53(20)	5.50(20)
0.062	0.188	0.187	11.45(11)	5.69(15)	0.014	0.037	11.46(11)	5.72(15)	5.76(19)	5.74(19)
0.062	0.188	0.312	11.41(11)	6.13(16)	-0.000	-0.000	11.41(11)	6.13(16)	5.28(19)	5.28(19)
0.062	0.188	0.437	11.12(11)	6.52(16)	0.005	-0.005	11.12(11)	6.52(16)	4.60(20)	4.61(20)
0.062	0.188	-0.437	11.17(11)	6.59(16)	-0.001	-0.003	11.17(11)	6.59(16)	4.58(19)	4.58(19)
0.062	0.188	-0.312	11.19(12)	6.27(16)	0.007	-0.002	11.20(12)	6.27(16)	4.92(20)	4.93(20)
0.062	0.188	-0.187	11.63(11)	5.43(15)	0.002	0.014	11.63(11)	5.44(15)	6.20(19)	6.19(19)
0.062	0.188	-0.062	11.32(12)	5.63(16)	0.015	0.050	11.34(12)	5.68(16)	5.69(20)	5.66(20)
0.062	0.312	0.062	11.87(11)	5.25(16)	0.005	0.029	11.88(11)	5.28(16)	6.62(19)	6.60(19)
0.062	0.312	0.187	11.90(11)	5.82(15)	0.002	0.001	11.90(11)	5.82(15)	6.08(19)	6.08(19)
0.062	0.312	0.312	11.42(11)	6.29(16)	0.007	-0.006	11.42(11)	6.29(16)	5.12(19)	5.14(19)
0.062	0.312	0.437	11.37(12)	6.52(16)	0.024	-0.030	11.39(12)	6.49(16)	4.84(20)	4.90(20)
0.062	0.312	-0.437	11.51(11)	6.58(15)	0.013	-0.025	11.53(11)	6.55(15)	4.94(19)	4.97(19)
0.062	0.312	-0.312	11.34(11)	6.30(16)	0.006	-0.011	11.35(11)	6.29(16)	5.04(19)	5.06(19)
0.062	0.312	-0.187	11.99(11)	5.68(16)	0.003	-0.001	11.99(11)	5.68(16)	6.30(19)	6.31(19)
0.062	0.312	-0.062	11.61(12)	5.45(16)	0.002	0.006	11.61(12)	5.46(16)	6.15(20)	6.15(20)
0.062	0.438	0.062	11.83(12)	5.37(16)	0.004	0.008	11.84(12)	5.37(16)	6.47(20)	6.47(20)
0.062	0.438	0.187	12.08(11)	5.92(15)	0.016	-0.004	12.10(11)	5.92(15)	6.16(19)	6.18(19)
0.062	0.438	0.312	11.97(11)	5.96(16)	0.008	-0.032	11.98(11)	5.92(16)	6.01(19)	6.05(19)
0.062	0.438	0.437	12.68(12)	5.90(16)	0.010	-0.052	12.69(12)	5.85(16)	6.78(20)	6.84(20)
0.062	0.438	-0.437	12.49(12)	5.88(16)	0.008	-0.061	12.50(12)	5.82(16)	6.62(20)	6.69(20)
0.062	0.438	-0.312	12.07(11)	6.02(16)	0.015	-0.023	12.08(11)	5.99(16)	6.05(19)	6.09(19)
0.062	0.438	-0.187	12.09(11)	5.95(16)	0.011	-0.015	12.10(11)	5.93(16)	6.14(19)	6.17(19)
0.062	0.438	-0.062	11.94(12)	5.37(16)	0.014	-0.004	11.95(12)	5.36(16)	6.57(20)	6.59(20)
0.062	-0.438	0.062	12.01(12)	5.31(16)	0.005	0.007	12.02(12)	5.32(16)	6.70(20)	6.70(20)
0.062	-0.438	0.187	12.22(11)	5.94(16)	-0.000	-0.013	12.22(11)	5.93(16)	6.28(19)	6.29(19)
0.062	-0.438	0.312	11.61(11)	6.13(16)	0.009	-0.025	11.62(11)	6.10(16)	5.48(19)	5.51(19)
0.062	-0.438	0.437	12.13(12)	6.22(16)	0.016	-0.037	12.15(12)	6.18(16)	5.92(20)	5.97(20)
0.062	-0.438	-0.437	12.37(11)	5.92(16)	-0.005	-0.037	12.37(11)	5.88(16)	6.45(19)	6.49(19)
0.062	-0.438	-0.312	11.77(11)	6.05(16)	0.006	-0.015	11.78(11)	6.04(16)	5.72(20)	5.74(20)
0.062	-0.438	-0.187	12.18(11)	6.09(16)	0.011	-0.007	12.19(11)	6.08(16)	6.10(19)	6.12(19)
0.062	-0.438	-0.062	11.87(12)	5.43(16)	0.004	0.009	11.87(12)	5.44(16)	6.44(20)	6.43(20)
0.062	-0.312	0.062	11.74(12)	5.58(16)	0.007	0.039	11.74(12)	5.62(16)	6.16(20)	6.13(20)
0.062	-0.312	0.187	11.61(11)	5.86(16)	0.004	0.003	11.62(11)	5.86(16)	5.75(19)	5.76(19)
0.062	-0.312	0.312	11.50(11)	6.05(16)	0.003	-0.011	11.50(11)	6.04(16)	5.45(19)	5.46(19)
0.062	-0.312	0.437	11.36(11)	6.34(16)	0.017	-0.018	11.38(11)	6.32(16)	5.02(19)	5.06(19)
0.062	-0.312	-0.437	11.32(11)	6.50(16)	0.017	-0.022	11.34(11)	6.48(16)	4.82(19)	4.85(19)
0.062	-0.312	-0.312	11.31(11)	6.16(16)	0.008	-0.013	11.32(11)	6.15(16)	5.16(19)	5.18(19)
0.062	-0.312	-0.187	11.41(11)	6.01(16)	0.005	0.004	11.42(11)	6.02(16)	5.40(19)	5.40(19)
0.062	-0.312	-0.062	11.60(11)	5.49(16)	0.008	0.031	11.61(11)	5.52(16)	6.10(19)	6.08(19)
0.062	-0.188	0.062	10.76(11)	5.87(16)	0.014	0.032	10.77(11)	5.90(16)	4.89(20)	4.87(20)
0.062	-0.188	0.187	11.16(11)	5.41(16)	0.014	0.013	11.17(11)	5.42(16)	5.75(19)	5.75(19)
0.062	-0.188	0.312	11.31(12)	6.32(16)	0.002	0.002	11.31(12)	6.32(16)	4.99(20)	4.99(20)
0.062	-0.188	0.437	10.94(11)	6.68(16)	0.002	-0.008	10.95(11)	6.67(16)	4.26(20)	4.27(20)
0.062	-0.188	-0.437	10.69(11)	6.78(15)	0.007	-0.012	10.70(11)	6.77(15)	3.91(19)	3.93(19)
0.062	-0.188	-0.312	11.39(12)	6.01(16)	0.010	0.013	11.40(12)	6.02(16)	5.38(20)	5.38(20)
0.062	-0.188	-0.187	10.91(11)	5.52(16)	0.010	0.015	10.92(11)	5.54(16)	5.39(19)	5.38(19)
0.062	-0.188	-0.062	10.80(12)	5.58(16)	-0.002	0.036	10.80(12)	5.61(16)	5.22(20)	5.18(20)
0.062	-0.062	0.062	10.64(12)	6.35(16)	0.015	0.066	10.65(12)	6.41(16)	4.29(20)	4.24(20)
0.062	-0.062	0.187	11.02(11)	5.76(15)	0.023	0.066	11.04(11)	5.83(15)	5.25(19)	5.21(19)
0.062	-0.062	0.312	11.39(12)	6.30(16)	0.011	0.013	11.40(12)	6.31(16)	5.09(20)	5.09(20)
0.062	-0.062	0.437	11.12(11)	6.56(16)	0.001	0.012	11.12(11)	6.58(16)	4.55(19)	4.54(19)
0.062	-0.062	-0.437	10.84(12)	6.86(16)	-0.000	0.019	10.84(12)	6.88(16)	3.98(20)	3.96(20)
0.062	-0.062	-0.312	11.21(12)	6.50(16)	0.014	0.031	11.23(12)	6.53(16)	4.72(20)	4.70(20)
0.062	-0.062	-0.187	11.02(11)	5.87(16)	0.003	0.031	11.02(11)	5.90(16)	5.15(19)	5.12(19)
0.062	-0.062	-0.062	10.75(12)	6.12(16)	0.011	0.093	10.76(12)	6.21(16)	4.63(20)	4.55(20)

TABLE XIII: H_2 $r_s = 1.38$. Part II.

k_x	k_y	k_z	μ^+	μ^-	$\delta\mu_s^+$	$\delta\mu_s^-$	$\bar{\mu}^+$	$\bar{\mu}^-$	Δ_k	$\bar{\Delta}_k$
0.188	0.062	0.062	12.06(11)	6.16(16)	-0.011	0.040	12.05(11)	6.20(16)	5.90(20)	5.85(20)
0.188	0.062	0.187	12.28(11)	6.50(16)	-0.001	0.027	12.28(11)	6.53(16)	5.78(20)	5.75(20)
0.188	0.062	0.312	11.48(11)	6.40(16)	-0.002	0.013	11.47(11)	6.41(16)	5.08(19)	5.06(19)
0.188	0.062	0.437	10.95(11)	6.76(16)	-0.003	-0.000	10.95(11)	6.76(16)	4.18(19)	4.18(19)
0.188	0.062	-0.437	11.29(11)	6.68(15)	0.003	0.001	11.30(11)	6.68(15)	4.62(19)	4.62(19)
0.188	0.062	-0.312	11.30(11)	6.46(16)	0.005	0.011	11.31(11)	6.47(16)	4.85(19)	4.84(19)
0.188	0.062	-0.187	12.51(11)	6.53(16)	0.004	0.031	12.52(11)	6.56(16)	5.98(19)	5.95(19)
0.188	0.062	-0.062	12.06(12)	6.47(16)	-0.000	0.048	12.06(12)	6.51(16)	5.59(20)	5.54(20)
0.188	0.188	0.062	11.69(12)	5.91(16)	0.002	0.033	11.69(12)	5.95(16)	5.77(20)	5.74(20)
0.188	0.188	0.187	11.94(11)	5.91(16)	0.004	0.022	11.94(11)	5.93(16)	6.02(19)	6.00(19)
0.188	0.188	0.312	11.48(11)	5.84(16)	0.001	-0.003	11.49(11)	5.84(16)	5.64(19)	5.64(19)
0.188	0.188	0.437	11.42(11)	6.28(16)	0.003	-0.014	11.42(11)	6.26(16)	5.14(19)	5.15(19)
0.188	0.188	-0.437	11.62(11)	6.03(16)	0.022	0.011	11.64(11)	6.04(16)	5.59(19)	5.60(19)
0.188	0.188	-0.312	11.38(11)	5.85(16)	0.001	-0.005	11.38(11)	5.84(16)	5.54(20)	5.54(20)
0.188	0.188	-0.187	11.99(11)	5.95(16)	0.015	0.032	12.01(11)	5.98(16)	6.04(19)	6.03(19)
0.188	0.188	-0.062	11.66(12)	6.08(16)	0.019	0.039	11.68(12)	6.12(16)	5.58(19)	5.56(19)
0.188	0.312	0.062	11.74(11)	5.62(16)	0.004	0.018	11.74(11)	5.64(16)	6.12(19)	6.11(19)
0.188	0.312	0.187	11.95(11)	5.82(16)	0.014	-0.007	11.96(11)	5.81(16)	6.13(19)	6.15(19)
0.188	0.312	0.312	11.94(12)	5.68(16)	-0.001	-0.001	11.94(12)	5.67(16)	6.27(20)	6.27(20)
0.188	0.312	0.437	11.56(11)	5.90(16)	0.015	-0.021	11.58(11)	5.88(16)	5.67(19)	5.70(19)
0.188	0.312	-0.437	11.62(11)	5.91(16)	0.011	-0.020	11.63(11)	5.89(16)	5.71(20)	5.74(20)
0.188	0.312	-0.312	11.58(11)	5.76(15)	0.003	-0.005	11.59(11)	5.75(15)	5.82(19)	5.83(19)
0.188	0.312	-0.187	11.75(12)	5.61(16)	0.013	0.005	11.76(12)	5.62(16)	6.13(19)	6.14(19)
0.188	0.312	-0.062	11.57(12)	5.77(16)	0.008	0.011	11.58(12)	5.78(16)	5.80(20)	5.80(20)
0.188	0.438	0.062	11.97(11)	5.82(16)	0.013	0.008	11.98(11)	5.83(16)	6.15(19)	6.15(19)
0.188	0.438	0.187	12.25(11)	5.76(16)	0.010	-0.005	12.26(11)	5.75(16)	6.50(19)	6.51(19)
0.188	0.438	0.312	12.17(11)	5.88(16)	0.008	-0.022	12.18(11)	5.86(16)	6.29(19)	6.32(19)
0.188	0.438	0.437	12.24(11)	5.69(16)	0.024	-0.026	12.26(11)	5.67(16)	6.54(19)	6.59(19)
0.188	0.438	-0.437	12.09(12)	5.81(16)	0.016	-0.008	12.11(12)	5.80(16)	6.29(20)	6.31(20)
0.188	0.438	-0.312	11.93(11)	5.85(16)	0.023	-0.013	11.95(11)	5.84(16)	6.07(19)	6.11(19)
0.188	0.438	-0.187	12.31(11)	5.85(16)	0.014	-0.008	12.33(11)	5.84(16)	6.46(19)	6.49(19)
0.188	0.438	-0.062	12.13(12)	5.91(16)	0.012	0.017	12.14(12)	5.93(16)	6.22(20)	6.21(20)
0.188	-0.438	0.062	11.81(11)	5.85(16)	0.008	0.006	11.82(11)	5.85(16)	5.96(19)	5.96(19)
0.188	-0.438	0.187	12.05(11)	5.91(16)	0.012	-0.010	12.06(11)	5.90(16)	6.14(19)	6.16(19)
0.188	-0.438	0.312	12.00(11)	5.67(15)	0.015	-0.012	12.01(11)	5.65(15)	6.33(19)	6.36(19)
0.188	-0.438	0.437	12.06(11)	5.65(16)	0.016	-0.037	12.07(11)	5.62(16)	6.40(19)	6.46(19)
0.188	-0.438	-0.437	12.18(11)	5.70(16)	0.007	-0.029	12.19(11)	5.68(16)	6.48(19)	6.52(19)
0.188	-0.438	-0.312	11.92(11)	5.73(16)	0.017	-0.021	11.94(11)	5.71(16)	6.19(19)	6.23(19)
0.188	-0.438	-0.187	11.89(11)	6.09(16)	0.006	-0.013	11.90(11)	6.08(16)	5.80(19)	5.82(19)
0.188	-0.438	-0.062	11.88(11)	5.78(16)	0.012	0.013	11.90(11)	5.79(16)	6.10(19)	6.10(19)
0.188	-0.312	0.062	11.20(11)	5.88(16)	0.007	0.013	11.20(11)	5.89(16)	5.32(19)	5.31(19)
0.188	-0.312	0.187	11.42(11)	5.82(16)	0.016	0.003	11.44(11)	5.82(16)	5.60(19)	5.62(19)
0.188	-0.312	0.312	11.50(11)	5.66(16)	0.010	-0.005	11.51(11)	5.66(16)	5.83(19)	5.85(19)
0.188	-0.312	0.437	11.26(11)	6.17(16)	0.006	-0.019	11.26(11)	6.15(16)	5.09(20)	5.11(20)
0.188	-0.312	-0.437	11.27(11)	6.07(15)	0.021	-0.003	11.29(11)	6.06(15)	5.21(19)	5.23(19)
0.188	-0.312	-0.312	11.52(11)	5.67(16)	0.018	-0.009	11.54(11)	5.66(16)	5.85(19)	5.88(19)
0.188	-0.312	-0.187	11.27(12)	6.10(16)	0.015	0.007	11.29(12)	6.11(16)	5.17(19)	5.18(19)
0.188	-0.312	-0.062	11.12(11)	6.09(16)	0.007	0.011	11.13(11)	6.10(16)	5.03(19)	5.03(19)
0.188	-0.188	0.062	11.29(11)	6.08(16)	0.011	0.041	11.30(11)	6.12(16)	5.21(19)	5.18(19)
0.188	-0.188	0.187	11.28(11)	5.91(15)	0.013	0.036	11.29(11)	5.95(15)	5.37(19)	5.35(19)
0.188	-0.188	0.312	11.35(11)	6.19(16)	0.007	-0.004	11.36(11)	6.19(16)	5.16(19)	5.17(19)
0.188	-0.188	0.437	10.97(11)	6.50(16)	0.011	-0.007	10.98(11)	6.49(16)	4.47(20)	4.48(20)
0.188	-0.188	-0.437	10.96(11)	6.69(15)	0.009	-0.002	10.97(11)	6.69(15)	4.27(19)	4.29(19)
0.188	-0.188	-0.312	11.37(11)	6.16(15)	-0.000	-0.007	11.37(11)	6.15(15)	5.21(19)	5.22(19)
0.188	-0.188	-0.187	11.42(11)	5.82(16)	0.009	0.016	11.42(11)	5.84(16)	5.59(19)	5.59(19)
0.188	-0.188	-0.062	11.07(11)	6.27(15)	0.019	0.035	11.09(11)	6.31(15)	4.80(19)	4.78(19)
0.188	-0.062	0.062	11.64(12)	6.42(16)	-0.005	0.036	11.63(12)	6.46(16)	5.22(20)	5.18(20)
0.188	-0.062	0.187	11.79(11)	6.31(16)	-0.002	0.036	11.79(11)	6.34(16)	5.49(20)	5.45(20)
0.188	-0.062	0.312	11.48(12)	6.54(16)	0.002	0.021	11.49(12)	6.56(16)	4.95(20)	4.93(20)
0.188	-0.062	0.437	11.20(11)	6.55(16)	0.005	0.007	11.20(11)	6.55(16)	4.65(19)	4.65(19)
0.188	-0.062	-0.437	10.82(11)	6.65(16)	-0.001	0.010	10.82(11)	6.66(16)	4.17(19)	4.16(19)
0.188	-0.062	-0.312	11.41(12)	6.68(16)	0.012	0.026	11.42(12)	6.70(16)	4.73(20)	4.72(20)
0.188	-0.062	-0.187	11.71(11)	6.42(16)	0.013	0.049	11.72(11)	6.47(16)	5.29(19)	5.25(19)
0.188	-0.062	-0.062	11.48(11)	6.49(15)	0.007	0.057	11.48(11)	6.55(15)	4.98(19)	4.93(19)

TABLE XIV: H_2 $r_s = 1.38$. Part III.

k_x	k_y	k_z	μ^+	μ^-	$\delta\mu_s^+$	$\delta\mu_s^-$	$\bar{\mu}^+$	$\bar{\mu}^-$	Δ_k	$\bar{\Delta}_k$
0.312	0.062	0.062	13.15(12)	6.38(16)	-0.009	0.045	13.14(12)	6.43(16)	6.76(20)	6.71(20)
0.312	0.062	0.187	12.44(11)	6.47(16)	-0.006	0.026	12.44(11)	6.50(16)	5.97(19)	5.94(19)
0.312	0.062	0.312	11.70(11)	6.48(16)	-0.000	0.015	11.70(11)	6.49(16)	5.22(19)	5.21(19)
0.312	0.062	0.437	11.78(11)	6.19(16)	-0.001	0.021	11.78(11)	6.21(16)	5.59(19)	5.57(19)
0.312	0.062	-0.437	11.89(11)	6.27(16)	0.004	0.009	11.89(11)	6.28(16)	5.61(20)	5.61(20)
0.312	0.062	-0.312	11.64(11)	6.36(16)	0.003	0.023	11.64(11)	6.38(16)	5.28(19)	5.26(19)
0.312	0.062	-0.187	12.56(11)	6.62(16)	-0.001	0.018	12.56(11)	6.63(16)	5.95(19)	5.93(19)
0.312	0.062	-0.062	12.95(12)	6.40(16)	-0.002	0.048	12.95(12)	6.45(16)	6.55(20)	6.50(20)
0.312	0.188	0.062	12.47(11)	6.22(16)	0.003	0.021	12.47(11)	6.24(16)	6.25(19)	6.23(19)
0.312	0.188	0.187	12.09(11)	6.69(16)	0.000	0.012	12.09(11)	6.70(16)	5.40(19)	5.39(19)
0.312	0.188	0.312	11.92(11)	6.24(16)	0.000	0.004	11.92(11)	6.25(16)	5.68(19)	5.68(19)
0.312	0.188	0.437	11.72(11)	6.08(16)	0.008	-0.004	11.73(11)	6.07(16)	5.64(19)	5.66(19)
0.312	0.188	-0.437	12.14(11)	5.84(16)	-0.004	-0.013	12.14(11)	5.83(16)	6.30(19)	6.31(19)
0.312	0.188	-0.312	11.82(11)	6.51(15)	0.004	-0.002	11.82(11)	6.51(15)	5.31(19)	5.32(19)
0.312	0.188	-0.187	12.27(11)	6.41(16)	0.007	0.020	12.28(11)	6.43(16)	5.87(19)	5.85(19)
0.312	0.188	-0.062	12.76(11)	6.14(16)	0.005	0.009	12.76(11)	6.15(16)	6.62(19)	6.61(19)
0.312	0.312	0.062	12.15(11)	6.19(16)	0.005	0.008	12.15(11)	6.20(16)	5.95(19)	5.95(19)
0.312	0.312	0.187	12.32(11)	6.58(16)	0.000	0.017	12.32(11)	6.60(16)	5.74(19)	5.72(19)
0.312	0.312	0.312	12.40(11)	6.28(15)	-0.003	-0.004	12.40(11)	6.28(15)	6.12(19)	6.12(19)
0.312	0.312	0.437	11.88(11)	5.76(16)	0.018	0.001	11.90(11)	5.76(16)	6.13(19)	6.14(19)
0.312	0.312	-0.437	11.93(11)	5.76(16)	0.015	-0.014	11.94(11)	5.74(16)	6.17(19)	6.20(19)
0.312	0.312	-0.312	12.48(11)	6.17(15)	0.002	-0.007	12.49(11)	6.16(15)	6.31(19)	6.32(19)
0.312	0.312	-0.187	12.21(11)	6.47(15)	-0.001	-0.003	12.21(11)	6.47(15)	5.74(19)	5.74(19)
0.312	0.312	-0.062	12.33(11)	6.19(16)	0.009	0.013	12.34(11)	6.20(16)	6.15(19)	6.14(19)
0.312	0.438	0.062	12.32(12)	6.15(16)	0.001	-0.001	12.32(12)	6.15(16)	6.17(20)	6.17(20)
0.312	0.438	0.187	12.37(11)	6.25(16)	0.011	-0.003	12.38(11)	6.24(16)	6.12(19)	6.13(19)
0.312	0.438	0.312	12.66(11)	5.97(15)	0.021	-0.004	12.69(11)	5.97(15)	6.69(19)	6.72(19)
0.312	0.438	0.437	12.24(11)	5.32(16)	0.011	-0.016	12.25(11)	5.31(16)	6.91(19)	6.94(19)
0.312	0.438	-0.437	12.32(11)	5.41(16)	0.012	-0.002	12.33(11)	5.41(16)	6.91(19)	6.92(19)
0.312	0.438	-0.312	12.42(11)	5.98(15)	0.019	-0.012	12.44(11)	5.97(15)	6.44(19)	6.47(19)
0.312	0.438	-0.187	12.42(11)	6.43(15)	0.009	-0.008	12.43(11)	6.42(15)	5.99(19)	6.01(19)
0.312	0.438	-0.062	12.30(11)	6.21(16)	0.015	0.007	12.32(11)	6.22(16)	6.09(19)	6.10(19)
0.312	-0.438	0.062	12.08(11)	5.99(16)	0.010	0.007	12.09(11)	5.99(16)	6.10(19)	6.10(19)
0.312	-0.438	0.187	12.11(11)	6.23(16)	0.013	-0.009	12.12(11)	6.22(16)	5.87(19)	5.89(19)
0.312	-0.438	0.312	12.18(11)	5.82(16)	0.020	-0.009	12.20(11)	5.81(16)	6.37(19)	6.39(19)
0.312	-0.438	0.437	12.08(11)	5.28(16)	0.022	0.001	12.10(11)	5.28(16)	6.80(19)	6.82(19)
0.312	-0.438	-0.437	11.90(11)	5.44(16)	0.032	-0.005	11.94(11)	5.43(16)	6.47(19)	6.50(19)
0.312	-0.438	-0.312	12.56(11)	5.88(15)	0.015	-0.003	12.58(11)	5.88(15)	6.69(19)	6.70(19)
0.312	-0.438	-0.187	12.29(11)	6.15(16)	0.014	0.003	12.31(11)	6.15(16)	6.15(19)	6.16(19)
0.312	-0.438	-0.062	12.05(11)	5.99(16)	0.003	0.004	12.06(11)	6.00(16)	6.06(19)	6.06(19)
0.312	-0.312	0.062	12.01(11)	6.03(16)	0.007	0.001	12.02(11)	6.03(16)	5.98(19)	5.99(19)
0.312	-0.312	0.187	12.09(11)	6.41(16)	0.020	0.004	12.11(11)	6.41(16)	5.68(19)	5.70(19)
0.312	-0.312	0.312	12.14(11)	6.06(15)	0.005	-0.011	12.14(11)	6.05(15)	6.08(19)	6.09(19)
0.312	-0.312	0.437	11.58(11)	5.70(16)	0.009	-0.003	11.59(11)	5.70(16)	5.88(19)	5.89(19)
0.312	-0.312	-0.437	11.47(11)	5.79(15)	0.011	-0.004	11.48(11)	5.78(15)	5.68(19)	5.70(19)
0.312	-0.312	-0.312	11.97(11)	6.06(16)	-0.004	-0.008	11.96(11)	6.05(16)	5.91(19)	5.91(19)
0.312	-0.312	-0.187	12.26(11)	6.43(16)	0.004	0.010	12.26(11)	6.44(16)	5.83(19)	5.82(19)
0.312	-0.312	-0.062	11.89(11)	6.09(16)	0.004	0.016	11.89(11)	6.10(16)	5.80(19)	5.79(19)
0.312	-0.188	0.062	12.54(11)	6.26(16)	-0.002	0.024	12.54(11)	6.28(16)	6.28(19)	6.25(19)
0.312	-0.188	0.187	12.21(11)	6.59(16)	0.005	0.024	12.21(11)	6.62(16)	5.62(19)	5.60(19)
0.312	-0.188	0.312	11.82(11)	6.26(15)	-0.000	0.023	11.82(11)	6.28(15)	5.56(19)	5.53(19)
0.312	-0.188	0.437	11.38(11)	6.05(16)	0.011	-0.003	11.39(11)	6.04(16)	5.34(19)	5.35(19)
0.312	-0.188	-0.437	11.32(11)	6.08(16)	0.011	0.003	11.33(11)	6.08(16)	5.24(19)	5.25(19)
0.312	-0.188	-0.312	11.54(11)	6.36(16)	0.000	0.007	11.54(11)	6.37(16)	5.18(19)	5.18(19)
0.312	-0.188	-0.187	12.42(11)	6.36(16)	0.000	0.026	12.42(11)	6.39(16)	6.06(19)	6.03(19)
0.312	-0.188	-0.062	12.82(11)	6.19(16)	0.009	0.036	12.83(11)	6.23(16)	6.63(19)	6.60(19)
0.312	-0.062	0.062	12.94(11)	6.44(16)	0.002	0.022	12.94(11)	6.46(16)	6.50(20)	6.48(20)
0.312	-0.062	0.187	12.64(11)	6.73(16)	-0.005	0.034	12.63(11)	6.76(16)	5.91(20)	5.87(20)
0.312	-0.062	0.312	11.46(11)	6.44(16)	0.002	0.019	11.47(11)	6.46(16)	5.03(20)	5.01(20)
0.312	-0.062	0.437	11.38(11)	6.32(16)	-0.001	-0.005	11.38(11)	6.31(16)	5.06(19)	5.07(19)
0.312	-0.062	-0.437	11.24(12)	6.39(16)	-0.001	0.013	11.23(12)	6.40(16)	4.84(20)	4.83(20)
0.312	-0.062	-0.312	11.45(11)	6.57(15)	0.008	0.013	11.46(11)	6.59(15)	4.87(19)	4.87(19)
0.312	-0.062	-0.187	12.66(11)	6.65(16)	-0.004	0.033	12.65(11)	6.68(16)	6.01(19)	5.97(19)
0.312	-0.062	-0.062	13.05(12)	6.22(16)	-0.003	0.027	13.05(12)	6.25(16)	6.83(20)	6.80(20)

TABLE XV: H_2 $r_s = 1.38$. Part IV.

k_x	k_y	k_z	μ^+	μ^-	$\delta\mu_s^+$	$\delta\mu_s^-$	$\bar{\mu}^+$	$\bar{\mu}^-$	Δ_k	$\bar{\Delta}_k$
0.437	0.062	0.062	13.60(11)	6.22(16)	-0.003	0.014	13.59(11)	6.23(16)	7.38(20)	7.36(20)
0.437	0.062	0.187	12.57(11)	6.80(16)	-0.004	0.023	12.57(11)	6.82(16)	5.77(19)	5.75(19)
0.437	0.062	0.312	12.03(11)	6.95(16)	0.001	0.013	12.03(11)	6.96(16)	5.08(19)	5.07(19)
0.437	0.062	0.437	12.81(12)	6.57(16)	0.002	0.006	12.82(12)	6.57(16)	6.25(20)	6.24(20)
0.437	0.062	-0.437	12.70(12)	6.65(16)	0.004	0.009	12.70(12)	6.66(16)	6.05(20)	6.05(20)
0.437	0.062	-0.312	12.11(12)	6.89(16)	-0.006	0.011	12.10(12)	6.90(16)	5.22(20)	5.20(20)
0.437	0.062	-0.187	12.47(11)	6.84(15)	-0.004	0.031	12.46(11)	6.87(15)	5.63(19)	5.60(19)
0.437	0.062	-0.062	13.79(12)	6.23(16)	0.036	0.064	13.83(12)	6.29(16)	7.56(20)	7.54(20)
0.437	0.188	0.062	13.44(12)	6.19(16)	0.007	0.011	13.45(12)	6.20(16)	7.26(20)	7.25(20)
0.437	0.188	0.187	12.40(11)	6.93(16)	0.003	0.020	12.40(11)	6.95(16)	5.47(19)	5.46(19)
0.437	0.188	0.312	12.25(11)	6.78(15)	-0.000	0.004	12.25(11)	6.79(15)	5.47(19)	5.46(19)
0.437	0.188	0.437	12.39(11)	6.61(16)	0.005	-0.007	12.39(11)	6.61(16)	5.77(19)	5.79(19)
0.437	0.188	-0.437	12.49(11)	6.34(16)	0.002	-0.005	12.49(11)	6.33(16)	6.15(19)	6.16(19)
0.437	0.188	-0.312	12.24(11)	6.72(16)	0.016	0.001	12.25(11)	6.72(16)	5.52(19)	5.53(19)
0.437	0.188	-0.187	12.59(11)	6.84(15)	-0.003	0.004	12.59(11)	6.84(15)	5.75(19)	5.75(19)
0.437	0.188	-0.062	13.34(11)	6.23(16)	0.003	0.009	13.35(11)	6.24(16)	7.11(19)	7.11(19)
0.437	0.312	0.062	13.40(12)	6.15(16)	0.003	0.000	13.40(12)	6.15(16)	7.24(19)	7.25(19)
0.437	0.312	0.187	13.04(11)	6.62(16)	0.000	0.003	13.04(11)	6.62(16)	6.41(19)	6.41(19)
0.437	0.312	0.312	12.70(11)	6.40(15)	0.002	-0.005	12.70(11)	6.40(15)	6.30(19)	6.30(19)
0.437	0.312	0.437	12.52(11)	6.03(16)	0.018	-0.003	12.54(11)	6.02(16)	6.49(19)	6.51(19)
0.437	0.312	-0.437	12.47(11)	6.11(16)	0.006	0.001	12.47(11)	6.11(16)	6.35(19)	6.36(19)
0.437	0.312	-0.312	12.57(11)	6.56(16)	0.017	0.010	12.58(11)	6.57(16)	6.00(19)	6.01(19)
0.437	0.312	-0.187	12.68(11)	6.59(16)	0.002	-0.002	12.68(11)	6.59(16)	6.09(19)	6.09(19)
0.437	0.312	-0.062	13.36(11)	6.13(16)	0.007	0.012	13.37(11)	6.14(16)	7.23(19)	7.23(19)
0.437	0.438	0.062	13.32(11)	6.17(16)	0.001	0.003	13.32(11)	6.17(16)	7.15(20)	7.14(20)
0.437	0.438	0.187	13.32(11)	6.30(16)	0.010	-0.014	13.33(11)	6.28(16)	7.02(20)	7.04(20)
0.437	0.438	0.312	13.15(11)	6.29(16)	0.007	-0.009	13.15(11)	6.28(16)	6.85(19)	6.87(19)
0.437	0.438	0.437	12.71(11)	5.15(16)	0.007	0.003	12.72(11)	5.15(16)	7.56(20)	7.56(20)
0.437	0.438	-0.437	12.77(11)	5.34(16)	0.017	-0.002	12.79(11)	5.34(16)	7.43(20)	7.45(20)
0.437	0.438	-0.312	13.20(11)	5.94(15)	0.003	-0.015	13.20(11)	5.93(15)	7.26(19)	7.28(19)
0.437	0.438	-0.187	13.30(11)	6.13(16)	0.000	-0.005	13.30(11)	6.12(16)	7.17(19)	7.18(19)
0.437	0.438	-0.062	13.16(11)	6.15(16)	0.006	0.012	13.16(11)	6.16(16)	7.01(20)	7.01(20)
0.437	-0.438	0.062	13.37(12)	5.75(16)	0.000	0.014	13.37(12)	5.76(16)	7.62(20)	7.60(20)
0.437	-0.438	0.187	13.13(11)	6.04(16)	0.019	-0.018	13.15(11)	6.03(16)	7.09(19)	7.13(19)
0.437	-0.438	0.312	13.53(11)	5.33(15)	0.005	-0.012	13.54(11)	5.32(15)	8.21(19)	8.22(19)
0.437	-0.438	0.437	12.21(11)	4.96(16)	0.018	-0.005	12.23(11)	4.96(16)	7.25(19)	7.27(19)
0.437	-0.438	-0.437	12.41(11)	4.98(16)	0.003	-0.006	12.41(11)	4.97(16)	7.43(19)	7.44(19)
0.437	-0.438	-0.312	13.34(11)	5.74(15)	0.015	-0.019	13.35(11)	5.72(15)	7.60(19)	7.63(19)
0.437	-0.438	-0.187	13.34(11)	6.02(16)	0.002	-0.005	13.34(11)	6.01(16)	7.32(19)	7.33(19)
0.437	-0.438	-0.062	13.50(11)	5.79(16)	0.001	0.009	13.51(11)	5.79(16)	7.72(19)	7.71(19)
0.437	-0.312	0.062	13.50(11)	5.94(16)	0.003	0.001	13.50(11)	5.94(16)	7.55(20)	7.55(20)
0.437	-0.312	0.187	12.72(11)	6.30(16)	0.004	-0.003	12.72(11)	6.30(16)	6.42(20)	6.42(20)
0.437	-0.312	0.312	12.25(11)	6.21(16)	0.003	-0.002	12.25(11)	6.21(16)	6.04(19)	6.05(19)
0.437	-0.312	0.437	11.80(11)	5.76(16)	0.011	-0.005	11.81(11)	5.76(16)	6.04(19)	6.06(19)
0.437	-0.312	-0.437	11.88(11)	5.61(16)	0.015	0.001	11.90(11)	5.61(16)	6.28(19)	6.29(19)
0.437	-0.312	-0.312	12.28(11)	6.36(15)	0.030	-0.005	12.31(11)	6.36(15)	5.92(19)	5.95(19)
0.437	-0.312	-0.187	12.73(12)	6.29(16)	0.005	0.006	12.73(12)	6.30(16)	6.44(20)	6.43(20)
0.437	-0.312	-0.062	13.46(11)	5.90(16)	0.007	0.006	13.46(11)	5.91(16)	7.56(19)	7.56(19)
0.437	-0.188	0.062	13.69(11)	6.16(16)	0.006	0.007	13.70(11)	6.17(16)	7.53(19)	7.52(19)
0.437	-0.188	0.187	12.48(11)	6.72(16)	-0.001	0.009	12.48(11)	6.73(16)	5.76(19)	5.75(19)
0.437	-0.188	0.312	11.65(11)	6.97(16)	0.009	0.006	11.66(11)	6.97(16)	4.68(19)	4.69(19)
0.437	-0.188	0.437	11.81(12)	6.52(16)	0.008	-0.001	11.82(12)	6.52(16)	5.29(20)	5.30(20)
0.437	-0.188	-0.437	11.79(11)	6.29(16)	0.031	-0.003	11.82(11)	6.29(16)	5.49(19)	5.53(19)
0.437	-0.188	-0.312	11.67(11)	6.79(15)	0.003	0.011	11.67(11)	6.80(15)	4.88(19)	4.87(19)
0.437	-0.188	-0.187	12.40(11)	6.79(16)	0.005	0.013	12.41(11)	6.81(16)	5.61(19)	5.60(19)
0.437	-0.188	-0.062	13.61(11)	6.12(15)	0.009	0.016	13.62(11)	6.13(15)	7.49(19)	7.49(19)
0.437	-0.062	0.062	13.71(12)	6.37(16)	0.008	0.032	13.72(12)	6.41(16)	7.34(20)	7.31(20)
0.437	-0.062	0.187	12.60(11)	6.86(16)	-0.003	0.015	12.60(11)	6.87(16)	5.75(19)	5.73(19)
0.437	-0.062	0.312	11.70(11)	6.77(16)	0.000	0.017	11.70(11)	6.79(16)	4.93(20)	4.92(20)
0.437	-0.062	0.437	12.29(12)	6.48(16)	0.007	0.007	12.30(12)	6.49(16)	5.81(20)	5.81(20)
0.437	-0.062	-0.437	12.25(12)	6.92(16)	-0.002	0.011	12.25(12)	6.93(16)	5.33(20)	5.31(20)
0.437	-0.062	-0.312	11.73(12)	6.95(16)	-0.004	0.015	11.73(12)	6.96(16)	4.79(20)	4.77(20)
0.437	-0.062	-0.187	12.54(11)	6.79(16)	0.005	0.026	12.54(11)	6.82(16)	5.74(19)	5.72(19)

TABLE XVI: H₂ r_s = 1.34. Removal and addition energies corrections (μ_s^\pm) from static charge density for 8 × 8 × 8 k-grid shifted to exclude the Γ point. Part I.

k_x	k_y	k_z	μ^+	μ^-	$\delta\mu_s^+$	$\delta\mu_s^-$	$\bar{\mu}^+$	$\bar{\mu}^-$	Δ_k	$\bar{\Delta}_k$
0.063	0.062	0.063	11.80(14)	7.77(20)	0.023	0.064	11.82(14)	7.83(20)	4.02(24)	3.98(24)
0.063	0.062	0.187	11.82(14)	7.48(18)	0.009	0.039	11.83(14)	7.52(18)	4.34(23)	4.31(23)
0.063	0.062	0.313	12.33(14)	7.72(19)	0.019	0.024	12.35(14)	7.75(19)	4.61(23)	4.60(23)
0.063	0.062	0.437	11.56(14)	8.06(19)	-0.002	0.011	11.56(14)	8.07(19)	3.50(24)	3.49(24)
0.063	0.062	-0.437	11.51(14)	8.24(20)	0.009	0.016	11.52(14)	8.26(20)	3.26(24)	3.26(24)
0.063	0.062	-0.313	12.24(14)	7.91(19)	0.006	0.022	12.24(14)	7.93(19)	4.33(24)	4.31(24)
0.063	0.062	-0.187	11.77(14)	7.27(19)	0.002	0.039	11.78(14)	7.31(19)	4.50(24)	4.46(24)
0.063	0.062	-0.063	11.73(14)	7.58(19)	0.021	0.053	11.75(14)	7.63(19)	4.15(24)	4.12(24)
0.063	0.187	0.063	12.19(14)	6.88(20)	0.002	0.048	12.19(14)	6.92(20)	5.31(24)	5.27(24)
0.063	0.187	0.187	12.21(14)	7.10(19)	0.002	0.013	12.21(14)	7.11(19)	5.11(24)	5.10(24)
0.063	0.187	0.313	11.98(14)	7.75(19)	0.011	-0.001	11.99(14)	7.75(19)	4.22(24)	4.24(24)
0.063	0.187	0.437	11.81(14)	8.16(19)	0.010	-0.005	11.82(14)	8.15(19)	3.66(23)	3.67(23)
0.063	0.187	-0.437	11.88(14)	8.19(19)	-0.002	-0.007	11.88(14)	8.18(19)	3.69(24)	3.70(24)
0.063	0.187	-0.313	11.83(14)	7.75(19)	0.010	-0.002	11.84(14)	7.75(19)	4.08(23)	4.09(23)
0.063	0.187	-0.187	12.20(14)	7.03(19)	0.009	0.012	12.20(14)	7.04(19)	5.16(24)	5.16(24)
0.063	0.187	-0.063	11.82(14)	7.29(19)	-0.011	0.023	11.81(14)	7.31(19)	4.53(24)	4.49(24)
0.063	0.312	0.063	12.27(14)	6.72(19)	0.013	0.022	12.29(14)	6.74(19)	5.56(24)	5.55(24)
0.063	0.312	0.187	12.60(14)	7.38(19)	0.013	0.014	12.62(14)	7.39(19)	5.23(24)	5.23(24)
0.063	0.312	0.313	12.14(14)	7.79(19)	0.032	-0.005	12.17(14)	7.79(19)	4.35(24)	4.39(24)
0.063	0.312	0.437	12.35(14)	7.94(19)	0.015	-0.022	12.37(14)	7.92(19)	4.41(24)	4.44(24)
0.063	0.312	-0.437	12.43(14)	7.88(19)	0.007	-0.028	12.44(14)	7.85(19)	4.55(23)	4.58(23)
0.063	0.312	-0.313	12.09(14)	7.92(19)	0.012	-0.003	12.10(14)	7.92(19)	4.17(24)	4.18(24)
0.063	0.312	-0.187	12.88(14)	7.29(19)	0.009	0.012	12.89(14)	7.30(19)	5.59(23)	5.58(23)
0.063	0.312	-0.063	12.34(14)	6.76(20)	0.004	0.016	12.35(14)	6.77(20)	5.59(24)	5.57(24)
0.063	0.437	0.063	12.56(14)	6.78(20)	0.006	0.013	12.57(14)	6.79(20)	5.79(24)	5.78(24)
0.063	0.437	0.187	12.95(14)	7.54(19)	0.006	-0.008	12.96(14)	7.53(19)	5.41(23)	5.42(23)
0.063	0.437	0.313	12.96(14)	7.83(19)	0.003	-0.029	12.96(14)	7.60(19)	5.33(24)	5.37(24)
0.063	0.437	0.437	13.24(14)	7.48(20)	-0.006	-0.040	13.24(14)	7.44(20)	5.77(24)	5.80(24)
0.063	0.437	-0.437	13.21(15)	7.58(20)	0.040	-0.040	13.25(15)	7.54(20)	5.63(25)	5.71(25)
0.063	0.437	-0.313	12.89(14)	7.59(19)	0.011	-0.039	12.90(14)	7.55(19)	5.30(23)	5.35(23)
0.063	0.437	-0.187	12.86(14)	7.37(19)	0.004	-0.001	12.86(14)	7.37(19)	5.49(23)	5.49(23)
0.063	0.437	-0.063	12.59(14)	6.94(19)	0.006	0.005	12.60(14)	6.95(19)	5.65(24)	5.65(24)
0.063	-0.437	0.063	12.39(14)	7.10(19)	0.007	0.017	12.39(14)	7.12(19)	5.29(24)	5.28(24)
0.063	-0.437	0.187	12.92(14)	7.57(19)	0.009	-0.003	12.93(14)	7.56(19)	5.35(23)	5.36(23)
0.063	-0.437	0.313	12.44(14)	7.74(19)	0.020	-0.028	12.46(14)	7.71(19)	4.70(23)	4.75(23)
0.063	-0.437	0.437	13.14(15)	7.47(20)	0.016	-0.046	13.16(15)	7.43(20)	5.67(25)	5.73(25)
0.063	-0.437	-0.437	13.27(14)	7.48(20)	0.004	-0.036	13.27(14)	7.44(20)	5.78(24)	5.83(24)
0.063	-0.437	-0.313	12.44(14)	7.73(19)	0.016	-0.024	12.45(14)	7.71(19)	4.70(24)	4.74(24)
0.063	-0.437	-0.187	13.08(13)	7.30(19)	0.002	-0.007	13.08(13)	7.29(19)	5.78(23)	5.79(23)
0.063	-0.437	-0.063	12.54(14)	6.81(20)	0.003	0.004	12.54(14)	6.82(20)	5.73(25)	5.73(25)
0.063	-0.312	0.063	12.12(14)	7.04(19)	-0.002	0.019	12.12(14)	7.06(19)	5.08(24)	5.06(24)
0.063	-0.312	0.187	12.43(14)	7.37(19)	0.013	-0.002	12.45(14)	7.37(19)	5.06(23)	5.07(23)
0.063	-0.312	0.313	11.88(14)	7.80(19)	0.015	0.005	11.89(14)	7.80(19)	4.08(23)	4.09(23)
0.063	-0.312	0.437	12.17(14)	7.82(19)	0.005	-0.026	12.17(14)	7.80(19)	4.35(24)	4.38(24)
0.063	-0.312	-0.437	12.12(14)	8.17(19)	0.020	-0.030	12.14(14)	8.14(19)	3.95(23)	4.00(23)
0.063	-0.312	-0.313	12.17(14)	7.71(19)	0.018	-0.007	12.18(14)	7.70(19)	4.46(24)	4.48(24)
0.063	-0.312	-0.187	12.49(14)	7.11(19)	0.011	0.012	12.50(14)	7.12(19)	5.38(23)	5.38(23)
0.063	-0.312	-0.063	12.10(14)	6.98(19)	0.005	0.024	12.11(14)	7.01(19)	5.12(24)	5.10(24)
0.063	-0.187	0.063	11.34(14)	7.37(20)	0.044	0.067	11.39(14)	7.44(20)	3.97(24)	3.95(24)
0.063	-0.187	0.187	11.58(14)	6.89(19)	0.026	0.054	11.61(14)	6.94(19)	4.69(24)	4.66(24)
0.063	-0.187	0.313	12.05(14)	7.71(19)	0.013	0.014	12.06(14)	7.73(19)	4.34(23)	4.34(23)
0.063	-0.187	0.437	11.61(14)	8.13(19)	0.020	0.007	11.63(14)	8.14(19)	3.48(24)	3.50(24)
0.063	-0.187	-0.437	11.70(14)	8.15(19)	0.003	-0.004	11.70(14)	8.14(19)	3.55(24)	3.56(24)
0.063	-0.187	-0.313	11.77(14)	7.89(19)	0.016	0.011	11.79(14)	7.90(19)	3.89(24)	3.89(24)
0.063	-0.187	-0.187	11.49(14)	7.18(19)	0.015	0.029	11.51(14)	7.21(19)	4.31(23)	4.29(23)
0.063	-0.187	-0.063	11.29(14)	7.43(20)	0.007	0.033	11.29(14)	7.46(20)	3.86(24)	3.83(24)
0.063	-0.062	0.063	11.23(14)	7.79(19)	0.005	0.045	11.23(14)	7.83(19)	3.44(24)	3.40(24)
0.063	-0.062	0.187	11.44(14)	7.33(20)	0.003	0.030	11.44(14)	7.36(20)	4.11(25)	4.08(25)
0.063	-0.062	0.313	11.72(14)	7.84(19)	0.014	0.010	11.73(14)	7.85(19)	3.88(24)	3.88(24)
0.063	-0.062	0.437	11.52(14)	8.51(20)	0.006	0.013	11.53(14)	8.53(20)	3.01(24)	3.00(24)
0.063	-0.062	-0.437	11.33(14)	8.46(19)	-0.002	0.004	11.33(14)	8.46(19)	2.87(24)	2.87(24)
0.063	-0.062	-0.313	11.79(14)	7.83(19)	0.006	0.016	11.79(14)	7.85(19)	3.95(24)	3.94(24)
0.063	-0.062	-0.187	11.62(14)	7.52(19)	0.021	0.058	11.64(14)	7.58(19)	4.10(24)	4.06(24)
0.063	-0.062	-0.063	11.49(14)	7.58(19)	0.014	0.053	11.51(14)	7.63(19)	3.92(24)	3.88(24)

TABLE XVII: H₂ r_s = 1.34. Part II.

k_x	k_y	k_z	μ^+	μ^-	$\delta\mu_s^+$	$\delta\mu_s^-$	$\bar{\mu}^+$	$\bar{\mu}^-$	Δ_k	$\bar{\Delta}_k$
0.187	0.062	0.063	12.53(14)	7.84(19)	-0.003	0.040	12.52(14)	7.88(19)	4.69(24)	4.64(24)
0.187	0.062	0.187	13.36(14)	7.99(19)	0.004	0.039	13.37(14)	8.02(19)	5.38(24)	5.34(24)
0.187	0.062	0.313	12.16(14)	7.64(19)	0.001	0.017	12.16(14)	7.65(19)	4.52(24)	4.51(24)
0.187	0.062	0.437	11.98(14)	7.98(19)	-0.005	0.002	11.97(14)	7.98(19)	4.00(24)	3.99(24)
0.187	0.062	-0.437	11.94(14)	8.11(19)	0.003	0.013	11.95(14)	8.12(19)	3.84(24)	3.83(24)
0.187	0.062	-0.313	12.08(14)	7.84(19)	0.010	0.007	12.09(14)	7.85(19)	4.24(24)	4.24(24)
0.187	0.062	-0.187	13.32(14)	7.81(19)	0.011	0.044	13.34(14)	7.85(19)	5.52(24)	5.49(24)
0.187	0.062	-0.063	12.35(15)	7.93(20)	0.004	0.073	12.36(15)	8.00(20)	4.42(25)	4.35(25)
0.187	0.187	0.063	12.42(14)	7.48(19)	0.008	0.027	12.43(14)	7.51(19)	4.94(24)	4.92(24)
0.187	0.187	0.187	12.63(14)	7.37(20)	0.013	0.014	12.65(14)	7.39(20)	5.26(24)	5.26(24)
0.187	0.187	0.313	11.94(14)	7.51(19)	0.005	0.003	11.94(14)	7.51(19)	4.43(23)	4.43(23)
0.187	0.187	0.437	12.14(14)	7.85(19)	0.013	-0.001	12.16(14)	7.85(19)	4.29(24)	4.31(24)
0.187	0.187	-0.437	12.17(14)	7.64(19)	0.004	-0.007	12.18(14)	7.63(19)	4.54(23)	4.55(23)
0.187	0.187	-0.313	11.94(13)	7.23(19)	0.007	-0.003	11.95(13)	7.23(19)	4.71(23)	4.72(23)
0.187	0.187	-0.187	12.66(14)	7.48(19)	0.015	0.036	12.68(14)	7.51(19)	5.19(24)	5.17(24)
0.187	0.187	-0.063	12.24(14)	7.56(20)	-0.001	0.029	12.24(14)	7.59(20)	4.68(24)	4.65(24)
0.187	0.312	0.063	12.48(14)	6.88(19)	0.013	0.013	12.50(14)	6.90(19)	5.60(24)	5.60(24)
0.187	0.312	0.187	12.41(14)	7.31(19)	0.020	-0.005	12.43(14)	7.30(19)	5.10(24)	5.13(24)
0.187	0.312	0.313	12.49(14)	7.08(20)	0.004	-0.009	12.49(14)	7.07(20)	5.41(24)	5.42(24)
0.187	0.312	0.437	12.31(14)	7.42(19)	0.023	-0.015	12.33(14)	7.41(19)	4.88(24)	4.92(24)
0.187	0.312	-0.437	12.19(14)	7.51(19)	0.031	-0.009	12.22(14)	7.50(19)	4.68(24)	4.72(24)
0.187	0.312	-0.313	12.54(14)	7.31(19)	0.000	-0.013	12.54(14)	7.30(19)	5.23(23)	5.25(23)
0.187	0.312	-0.187	12.27(14)	7.24(18)	0.001	-0.001	12.27(14)	7.24(18)	5.03(23)	5.03(23)
0.187	0.312	-0.063	12.23(14)	7.17(19)	0.007	0.016	12.24(14)	7.18(19)	5.07(24)	5.06(24)
0.187	0.437	0.063	12.83(14)	7.36(19)	0.009	-0.004	12.84(14)	7.36(19)	5.47(23)	5.49(23)
0.187	0.437	0.187	12.93(14)	7.34(19)	0.011	-0.011	12.94(14)	7.33(19)	5.60(23)	5.62(23)
0.187	0.437	0.313	12.68(14)	7.46(19)	0.034	-0.017	12.72(14)	7.44(19)	5.23(23)	5.28(23)
0.187	0.437	0.437	12.98(14)	7.17(19)	0.026	-0.023	13.01(14)	7.15(19)	5.81(24)	5.85(24)
0.187	0.437	-0.437	12.84(14)	7.23(19)	0.023	-0.030	12.86(14)	7.19(19)	5.61(24)	5.66(24)
0.187	0.437	-0.313	12.84(14)	7.13(19)	0.011	-0.013	12.85(14)	7.12(19)	5.71(23)	5.73(23)
0.187	0.437	-0.187	12.93(14)	7.54(19)	0.024	0.004	12.95(14)	7.54(19)	5.39(23)	5.41(23)
0.187	0.437	-0.063	12.81(14)	7.36(19)	0.011	0.009	12.82(14)	7.37(19)	5.45(24)	5.45(24)
0.187	-0.437	0.063	12.39(14)	7.49(20)	0.009	0.011	12.40(14)	7.50(20)	4.90(24)	4.90(24)
0.187	-0.437	0.187	12.50(14)	7.57(19)	0.012	-0.010	12.51(14)	7.56(19)	4.93(24)	4.95(24)
0.187	-0.437	0.313	12.60(14)	7.36(19)	0.013	-0.019	12.61(14)	7.34(19)	5.24(24)	5.27(24)
0.187	-0.437	0.437	12.76(14)	7.26(19)	0.015	-0.021	12.77(14)	7.24(19)	5.50(23)	5.53(23)
0.187	-0.437	-0.437	12.65(14)	7.39(19)	0.021	-0.021	12.67(14)	7.37(19)	5.26(24)	5.31(24)
0.187	-0.437	-0.313	12.80(14)	7.06(19)	0.008	-0.015	12.80(14)	7.04(19)	5.74(23)	5.76(23)
0.187	-0.437	-0.187	12.71(14)	7.41(19)	0.010	-0.001	12.72(14)	7.41(19)	5.31(23)	5.32(23)
0.187	-0.437	-0.063	12.36(14)	7.60(19)	0.011	0.010	12.37(14)	7.61(19)	4.76(24)	4.76(24)
0.187	-0.312	0.063	11.76(14)	7.47(19)	0.006	0.011	11.76(14)	7.48(19)	4.29(24)	4.28(24)
0.187	-0.312	0.187	11.91(14)	7.44(20)	0.015	0.009	11.93(14)	7.44(20)	4.48(24)	4.48(24)
0.187	-0.312	0.313	12.26(14)	7.16(19)	0.014	-0.005	12.27(14)	7.15(19)	5.10(24)	5.12(24)
0.187	-0.312	0.437	12.14(14)	7.48(19)	0.010	-0.011	12.15(14)	7.47(19)	4.66(23)	4.68(23)
0.187	-0.312	-0.437	11.87(14)	7.77(19)	0.001	-0.015	11.87(14)	7.75(19)	4.10(24)	4.12(24)
0.187	-0.312	-0.313	12.31(15)	6.98(19)	0.023	0.010	12.34(15)	6.99(19)	5.33(24)	5.34(24)
0.187	-0.312	-0.187	12.03(13)	7.37(18)	0.024	0.016	12.05(13)	7.39(18)	4.66(23)	4.66(23)
0.187	-0.312	-0.063	12.05(14)	7.40(19)	0.002	0.009	12.05(14)	7.41(19)	4.64(24)	4.64(24)
0.187	-0.187	0.063	11.67(14)	7.68(19)	0.017	0.041	11.69(14)	7.72(19)	4.00(24)	3.98(24)
0.187	-0.187	0.187	11.74(14)	7.60(19)	0.008	0.016	11.75(14)	7.62(19)	4.14(24)	4.13(24)
0.187	-0.187	0.313	12.11(14)	7.62(19)	0.001	-0.004	12.11(14)	7.61(19)	4.49(24)	4.50(24)
0.187	-0.187	0.437	11.82(14)	7.98(20)	0.007	-0.005	11.82(14)	7.98(20)	3.83(24)	3.84(24)
0.187	-0.187	-0.437	11.67(14)	8.19(19)	0.010	0.022	11.68(14)	8.21(19)	3.47(23)	3.46(23)
0.187	-0.187	-0.313	12.29(14)	7.58(19)	0.005	-0.005	12.30(14)	7.58(19)	4.71(24)	4.72(24)
0.187	-0.187	-0.187	11.91(14)	7.47(19)	0.004	0.017	11.91(14)	7.49(19)	4.43(24)	4.42(24)
0.187	-0.187	-0.063	11.75(13)	7.55(19)	0.018	0.036	11.77(13)	7.59(19)	4.20(23)	4.18(23)
0.187	-0.062	0.063	12.48(15)	7.68(20)	-0.000	0.041	12.48(15)	7.72(20)	4.80(25)	4.76(25)
0.187	-0.062	0.187	12.43(14)	7.79(19)	0.012	0.064	12.45(14)	7.85(19)	4.65(24)	4.59(24)
0.187	-0.062	0.313	12.03(15)	8.06(20)	0.010	0.016	12.04(15)	8.08(20)	3.97(25)	3.96(25)
0.187	-0.062	0.437	11.50(14)	8.12(19)	0.014	0.022	11.51(14)	8.14(19)	3.38(24)	3.37(24)
0.187	-0.062	-0.437	11.61(14)	8.11(19)	0.006	0.017	11.62(14)	8.13(19)	3.50(23)	3.49(23)
0.187	-0.062	-0.313	12.12(14)	8.11(19)	-0.002	0.015	12.12(14)	8.13(19)	4.01(24)	3.99(24)
0.187	-0.062	-0.187	12.35(14)	8.02(19)	0.005	0.026	12.36(14)	8.05(19)	4.33(24)	4.31(24)
0.187	-0.062	-0.063	12.54(14)	7.78(19)	-0.007	0.057	12.53(14)	7.83(19)	4.76(24)	4.70(24)

TABLE XVIII: H₂ r_s = 1.34. Part III.

k_x	k_y	k_z	μ^+	μ^-	$\delta\mu_s^+$	$\delta\mu_s^-$	$\bar{\mu}^+$	$\bar{\mu}^-$	Δ_k	$\overline{\Delta}_k$
0.312	0.062	0.063	13.88(14)	7.59(19)	0.002	0.035	13.89(14)	7.63(19)	6.29(24)	6.26(24)
0.312	0.062	0.187	12.98(14)	8.43(19)	-0.007	0.021	12.97(14)	8.45(19)	4.55(23)	4.52(23)
0.312	0.062	0.313	12.25(14)	7.87(19)	0.001	0.010	12.25(14)	7.88(19)	4.38(24)	4.37(24)
0.312	0.062	0.437	12.65(14)	7.58(19)	-0.002	0.010	12.64(14)	7.59(19)	5.06(24)	5.05(24)
0.312	0.062	-0.437	12.38(14)	7.75(19)	0.003	0.013	12.38(14)	7.76(19)	4.63(24)	4.62(24)
0.312	0.062	-0.313	12.17(14)	7.86(20)	0.004	0.020	12.18(14)	7.88(20)	4.31(24)	4.29(24)
0.312	0.062	-0.187	13.30(14)	8.11(19)	0.005	0.031	13.30(14)	8.14(19)	5.19(24)	5.16(24)
0.312	0.062	-0.063	13.80(14)	7.78(19)	-0.006	0.021	13.80(14)	7.80(19)	6.02(23)	6.00(23)
0.312	0.187	0.063	13.74(14)	7.53(19)	0.009	0.029	13.75(14)	7.56(19)	6.21(24)	6.19(24)
0.312	0.187	0.187	12.72(14)	7.98(19)	0.003	0.013	12.72(14)	7.99(19)	4.74(23)	4.73(23)
0.312	0.187	0.313	12.55(14)	7.85(19)	-0.003	0.009	12.55(14)	7.86(19)	4.70(23)	4.68(23)
0.312	0.187	0.437	12.55(14)	7.34(19)	0.010	-0.003	12.56(14)	7.34(19)	5.20(24)	5.22(24)
0.312	0.187	-0.437	12.48(14)	7.61(19)	0.013	0.003	12.49(14)	7.61(19)	4.87(24)	4.88(24)
0.312	0.187	-0.313	12.52(14)	7.83(19)	0.001	-0.001	12.52(14)	7.83(19)	4.69(24)	4.69(24)
0.312	0.187	-0.187	12.82(15)	8.15(20)	0.005	0.024	12.83(15)	8.17(20)	4.67(25)	4.66(25)
0.312	0.187	-0.063	13.53(14)	7.61(19)	0.008	0.043	13.54(14)	7.65(19)	5.92(24)	5.89(24)
0.312	0.312	0.063	13.12(14)	7.65(19)	0.007	0.015	13.12(14)	7.67(19)	5.46(23)	5.46(23)
0.312	0.312	0.187	12.83(14)	8.08(19)	0.006	-0.004	12.84(14)	8.08(19)	4.75(24)	4.76(24)
0.312	0.312	0.313	13.52(14)	7.91(18)	-0.003	-0.003	13.52(14)	7.91(18)	5.61(23)	5.61(23)
0.312	0.312	0.437	12.43(13)	7.40(19)	0.011	-0.006	12.44(13)	7.39(19)	5.03(23)	5.05(23)
0.312	0.312	-0.437	12.59(14)	7.16(19)	0.014	-0.010	12.60(14)	7.15(19)	5.43(24)	5.45(24)
0.312	0.312	-0.313	13.40(14)	7.54(19)	0.004	0.001	13.40(14)	7.54(19)	5.86(24)	5.87(24)
0.312	0.312	-0.187	13.10(14)	7.90(19)	0.007	0.007	13.10(14)	7.90(19)	5.20(23)	5.20(23)
0.312	0.312	-0.063	13.22(14)	7.57(19)	0.008	0.009	13.23(14)	7.58(19)	5.65(24)	5.65(24)
0.312	0.437	0.063	13.22(14)	7.46(19)	-0.003	0.012	13.21(14)	7.47(19)	5.76(23)	5.74(23)
0.312	0.437	0.187	13.24(14)	7.73(18)	0.018	0.004	13.26(14)	7.73(18)	5.51(23)	5.53(23)
0.312	0.437	0.313	13.34(14)	7.56(19)	0.021	-0.013	13.36(14)	7.55(19)	5.78(24)	5.81(24)
0.312	0.437	0.437	12.95(14)	6.95(19)	0.020	-0.017	12.97(14)	6.93(19)	6.00(23)	6.04(23)
0.312	0.437	-0.437	13.07(14)	6.66(19)	0.012	-0.014	13.08(14)	6.65(19)	6.41(24)	6.43(24)
0.312	0.437	-0.313	13.16(14)	7.53(19)	0.020	-0.005	13.18(14)	7.53(19)	5.63(24)	5.65(24)
0.312	0.437	-0.187	13.28(14)	7.79(19)	0.011	-0.015	13.29(14)	7.77(19)	5.49(24)	5.51(24)
0.312	0.437	-0.063	12.94(14)	7.68(19)	0.021	0.016	12.96(14)	7.70(19)	5.26(24)	5.26(24)
0.312	-0.437	0.063	12.55(14)	7.72(19)	0.010	0.019	12.56(14)	7.74(19)	4.83(23)	4.82(23)
0.312	-0.437	0.187	12.80(14)	7.75(19)	0.010	-0.006	12.82(14)	7.74(19)	5.05(23)	5.07(23)
0.312	-0.437	0.313	13.29(13)	7.14(18)	0.019	0.001	13.31(13)	7.14(18)	6.16(23)	6.18(23)
0.312	-0.437	0.437	12.82(14)	6.60(19)	0.017	-0.004	12.84(14)	6.60(19)	6.22(24)	6.24(24)
0.312	-0.437	-0.437	12.79(14)	6.62(19)	0.004	-0.009	12.79(14)	6.61(19)	6.17(24)	6.18(24)
0.312	-0.437	-0.313	13.07(14)	7.41(19)	0.016	-0.003	13.08(14)	7.40(19)	5.66(23)	5.68(23)
0.312	-0.437	-0.187	13.00(13)	7.78(19)	0.017	0.000	13.02(13)	7.78(19)	5.22(23)	5.24(23)
0.312	-0.437	-0.063	12.88(14)	7.66(19)	0.001	0.004	12.88(14)	7.67(19)	5.21(24)	5.21(24)
0.312	-0.312	0.063	12.86(14)	7.56(19)	0.007	0.020	12.86(14)	7.58(19)	5.30(24)	5.29(24)
0.312	-0.312	0.187	12.68(14)	7.93(19)	0.010	0.010	12.69(14)	7.94(19)	4.74(23)	4.74(23)
0.312	-0.312	0.313	13.04(14)	7.58(19)	0.003	-0.002	13.04(14)	7.58(19)	5.46(23)	5.47(23)
0.312	-0.312	0.437	12.25(14)	7.21(19)	0.010	-0.007	12.26(14)	7.21(19)	5.03(24)	5.05(24)
0.312	-0.312	-0.437	12.32(14)	7.21(19)	0.020	-0.004	12.34(14)	7.21(19)	5.11(23)	5.13(23)
0.312	-0.312	-0.313	12.92(14)	7.70(19)	0.002	-0.002	12.92(14)	7.70(19)	5.22(23)	5.23(23)
0.312	-0.312	-0.187	13.07(14)	7.98(19)	0.006	0.002	13.08(14)	7.98(19)	5.09(24)	5.09(24)
0.312	-0.312	-0.063	12.92(14)	7.62(20)	0.005	0.006	12.93(14)	7.63(20)	5.31(24)	5.30(24)
0.312	-0.187	0.063	13.13(14)	7.56(20)	-0.003	0.039	13.13(14)	7.60(20)	5.57(24)	5.53(24)
0.312	-0.187	0.187	13.01(14)	7.90(19)	0.000	-0.002	13.01(14)	7.89(19)	5.11(24)	5.12(24)
0.312	-0.187	0.313	12.40(14)	7.56(19)	0.014	0.008	12.41(14)	7.57(19)	4.84(23)	4.84(23)
0.312	-0.187	0.437	12.03(14)	7.66(19)	0.009	0.002	12.04(14)	7.66(19)	4.37(24)	4.38(24)
0.312	-0.187	-0.437	11.83(14)	7.69(19)	0.006	-0.001	11.84(14)	7.69(19)	4.14(24)	4.15(24)
0.312	-0.187	-0.313	12.43(14)	7.71(19)	0.016	0.005	12.45(14)	7.71(19)	4.73(24)	4.74(24)
0.312	-0.187	-0.187	13.23(14)	7.84(19)	-0.001	0.005	13.23(14)	7.84(19)	5.39(23)	5.39(23)
0.312	-0.187	-0.063	13.35(14)	7.73(19)	0.008	0.029	13.36(14)	7.76(19)	5.62(24)	5.60(24)
0.312	-0.062	0.063	13.70(15)	7.95(20)	-0.003	0.022	13.70(15)	7.97(20)	5.75(24)	5.72(24)
0.312	-0.062	0.187	13.38(14)	8.18(19)	-0.000	0.018	13.38(14)	8.20(19)	5.19(24)	5.17(24)
0.312	-0.062	0.313	12.00(14)	8.20(19)	0.006	0.017	12.01(14)	8.22(19)	3.80(24)	3.79(24)
0.312	-0.062	0.437	12.14(14)	7.60(19)	0.006	0.014	12.15(14)	7.61(19)	4.54(24)	4.53(24)
0.312	-0.062	-0.437	11.93(14)	7.84(19)	-0.003	0.007	11.93(14)	7.84(19)	4.09(24)	4.09(24)
0.312	-0.062	-0.313	12.03(14)	8.11(19)	0.010	0.008	12.04(14)	8.11(19)	3.93(24)	3.93(24)
0.312	-0.062	-0.187	13.41(14)	8.10(20)	-0.000	0.031	13.41(14)	8.14(20)	5.31(25)	5.27(25)
0.312	-0.062	-0.063	13.81(14)	7.82(19)	-0.000	0.020	13.81(14)	7.84(19)	5.99(24)	5.97(24)

TABLE XIX: H_2 $\mathbf{r}_s = 1.34$. Part IV.

k_x	k_y	k_z	μ^+	μ^-	$\delta\mu_s^+$	$\delta\mu_s^-$	$\bar{\mu}^+$	$\bar{\mu}^-$	Δ_k	$\bar{\Delta}_k$
0.438	0.062	0.063	14.63(14)	7.54(20)	-0.010	0.016	14.62(14)	7.55(20)	7.10(24)	7.07(24)
0.438	0.062	0.187	13.32(14)	8.24(19)	0.005	0.021	13.32(14)	8.26(19)	5.08(23)	5.07(23)
0.438	0.062	0.313	12.80(14)	8.38(19)	0.002	0.027	12.80(14)	8.40(19)	4.43(24)	4.40(24)
0.438	0.062	0.437	13.41(14)	8.30(20)	0.005	0.015	13.42(14)	8.32(20)	5.11(24)	5.10(24)
0.438	0.062	-0.437	13.54(14)	8.12(19)	0.003	0.010	13.55(14)	8.13(19)	5.42(24)	5.42(24)
0.438	0.062	-0.313	12.71(14)	8.36(19)	0.001	0.007	12.72(14)	8.36(19)	4.36(24)	4.35(24)
0.438	0.062	-0.187	13.04(14)	8.28(19)	-0.005	0.009	13.03(14)	8.29(19)	4.76(23)	4.75(23)
0.438	0.062	-0.063	14.66(14)	7.48(19)	0.004	0.030	14.66(14)	7.51(19)	7.17(24)	7.15(24)
0.438	0.187	0.063	14.09(14)	7.50(19)	0.005	0.009	14.10(14)	7.51(19)	6.59(24)	6.59(24)
0.438	0.187	0.187	13.22(14)	8.26(19)	-0.003	0.005	13.21(14)	8.27(19)	4.95(24)	4.94(24)
0.438	0.187	0.313	12.89(14)	8.26(19)	0.006	0.006	12.89(14)	8.27(19)	4.62(24)	4.62(24)
0.438	0.187	0.437	13.35(14)	7.99(19)	0.006	-0.004	13.35(14)	7.99(19)	5.36(24)	5.37(24)
0.438	0.187	-0.437	13.18(14)	8.02(19)	-0.002	-0.003	13.18(14)	8.01(19)	5.16(23)	5.17(23)
0.438	0.187	-0.313	13.08(14)	8.32(19)	0.006	0.012	13.09(14)	8.33(19)	4.77(23)	4.76(23)
0.438	0.187	-0.187	13.24(14)	8.34(19)	0.000	0.018	13.24(14)	8.36(19)	4.90(24)	4.88(24)
0.438	0.187	-0.063	14.36(14)	7.31(19)	-0.002	0.023	14.36(14)	7.34(19)	7.05(24)	7.02(24)
0.438	0.312	0.063	14.03(14)	7.65(19)	0.009	0.007	14.04(14)	7.66(19)	6.37(24)	6.38(24)
0.438	0.312	0.187	13.72(14)	8.18(19)	0.003	0.005	13.72(14)	8.18(19)	5.54(23)	5.54(23)
0.438	0.312	0.313	13.46(14)	7.75(19)	0.017	0.003	13.48(14)	7.75(19)	5.71(24)	5.72(24)
0.438	0.312	0.437	13.11(14)	7.61(19)	0.014	0.028	13.13(14)	7.64(19)	5.50(24)	5.49(24)
0.438	0.312	-0.437	12.82(14)	7.82(19)	0.027	0.010	12.84(14)	7.83(19)	5.00(23)	5.02(23)
0.438	0.312	-0.313	13.34(14)	7.98(19)	0.010	-0.003	13.35(14)	7.98(19)	5.36(24)	5.37(24)
0.438	0.312	-0.187	13.54(14)	8.21(18)	0.007	-0.001	13.54(14)	8.21(18)	5.32(23)	5.33(23)
0.438	0.312	-0.063	14.00(14)	7.75(19)	0.005	-0.000	14.01(14)	7.75(19)	6.25(23)	6.26(23)
0.438	0.437	0.063	14.25(14)	7.44(20)	0.001	0.007	14.25(14)	7.45(20)	6.80(24)	6.80(24)
0.438	0.437	0.187	14.41(14)	7.74(19)	0.001	-0.000	14.41(14)	7.73(19)	6.67(23)	6.67(23)
0.438	0.437	0.313	13.95(14)	7.21(19)	0.002	-0.009	13.95(14)	7.20(19)	6.74(24)	6.75(24)
0.438	0.437	0.437	13.30(14)	6.59(20)	0.017	-0.003	13.32(14)	6.59(20)	6.72(24)	6.74(24)
0.438	0.437	-0.437	13.23(14)	6.74(19)	0.015	0.005	13.24(14)	6.74(19)	6.49(24)	6.50(24)
0.438	0.437	-0.313	14.12(14)	7.38(19)	0.004	-0.001	14.12(14)	7.38(19)	6.74(24)	6.74(24)
0.438	0.437	-0.187	14.19(14)	7.61(19)	0.016	-0.003	14.21(14)	7.61(19)	6.58(24)	6.60(24)
0.438	0.437	-0.063	14.33(14)	7.50(20)	-0.000	0.002	14.33(14)	7.51(20)	6.83(24)	6.82(24)
0.438	-0.437	0.063	14.03(14)	7.43(19)	0.001	0.002	14.03(14)	7.44(19)	6.60(24)	6.60(24)
0.438	-0.437	0.187	14.20(14)	7.45(19)	0.014	-0.004	14.22(14)	7.44(19)	6.76(24)	6.77(24)
0.438	-0.437	0.313	13.91(14)	7.08(19)	0.015	-0.008	13.93(14)	7.07(19)	6.83(24)	6.85(24)
0.438	-0.437	0.437	12.96(14)	6.54(20)	0.020	0.008	12.98(14)	6.55(20)	6.42(24)	6.43(24)
0.438	-0.437	-0.437	13.10(14)	6.33(19)	0.008	-0.007	13.11(14)	6.32(19)	6.77(24)	6.79(24)
0.438	-0.437	-0.313	14.24(14)	7.06(19)	0.014	-0.003	14.26(14)	7.06(19)	7.18(24)	7.19(24)
0.438	-0.437	-0.187	14.01(14)	7.72(19)	0.002	-0.007	14.01(14)	7.72(19)	6.28(24)	6.29(24)
0.438	-0.437	-0.063	14.26(14)	7.28(19)	0.008	0.021	14.27(14)	7.30(19)	6.98(24)	6.97(24)
0.438	-0.312	0.063	14.25(14)	7.45(19)	0.011	0.023	14.26(14)	7.47(19)	6.81(24)	6.79(24)
0.438	-0.312	0.187	13.51(14)	7.97(19)	0.008	0.003	13.52(14)	7.98(19)	5.53(24)	5.54(24)
0.438	-0.312	0.313	13.21(14)	7.84(19)	0.008	-0.000	13.22(14)	7.84(19)	5.37(24)	5.38(24)
0.438	-0.312	0.437	12.52(14)	7.27(19)	0.005	-0.002	12.53(14)	7.27(19)	5.26(24)	5.26(24)
0.438	-0.312	-0.437	12.55(14)	7.17(20)	0.011	-0.001	12.57(14)	7.17(20)	5.39(24)	5.40(24)
0.438	-0.312	-0.313	13.29(13)	7.49(18)	0.008	0.003	13.30(13)	7.50(18)	5.80(23)	5.81(23)
0.438	-0.312	-0.187	13.82(14)	7.94(20)	0.016	0.021	13.84(14)	7.97(20)	5.88(24)	5.87(24)
0.438	-0.312	-0.063	14.39(14)	7.57(19)	0.010	0.002	14.40(14)	7.57(19)	6.82(24)	6.83(24)
0.438	-0.187	0.063	14.28(14)	7.58(19)	0.006	0.016	14.28(14)	7.60(19)	6.69(24)	6.68(24)
0.438	-0.187	0.187	13.23(14)	8.12(19)	0.006	0.022	13.24(14)	8.15(19)	5.10(23)	5.09(23)
0.438	-0.187	0.313	12.30(14)	8.25(19)	0.012	0.006	12.32(14)	8.26(19)	4.05(24)	4.06(24)
0.438	-0.187	0.437	12.35(14)	8.02(19)	0.002	0.006	12.35(14)	8.02(19)	4.34(23)	4.33(23)
0.438	-0.187	-0.437	12.16(14)	8.09(19)	0.016	-0.002	12.18(14)	8.09(19)	4.07(23)	4.09(23)
0.438	-0.187	-0.313	12.66(14)	8.02(20)	-0.001	0.009	12.66(14)	8.02(20)	4.64(24)	4.63(24)
0.438	-0.187	-0.187	13.16(14)	8.11(19)	0.027	0.018	13.18(14)	8.13(19)	5.04(24)	5.05(24)
0.438	-0.187	-0.063	14.26(14)	7.54(19)	0.007	0.015	14.27(14)	7.56(19)	6.72(24)	6.71(24)
0.438	-0.062	0.063	14.45(15)	7.58(20)	-0.003	0.018	14.45(15)	7.60(20)	6.87(25)	6.85(25)
0.438	-0.062	0.187	13.14(14)	8.42(19)	-0.004	0.022	13.13(14)	8.45(19)	4.71(24)	4.69(24)
0.438	-0.062	0.313	12.38(14)	8.35(19)	0.009	0.021	12.39(14)	8.37(19)	4.03(24)	4.02(24)
0.438	-0.062	0.437	12.71(14)	8.32(20)	0.006	-0.001	12.72(14)	8.32(20)	4.39(25)	4.40(25)
0.438	-0.062	-0.437	12.99(14)	8.20(19)	-0.004	0.011	12.99(14)	8.21(19)	4.79(24)	4.78(24)
0.438	-0.062	-0.313	12.65(14)	8.32(19)	0.009	0.012	12.66(14)	8.33(19)	4.33(24)	4.32(24)
0.438	-0.062	-0.187	13.24(14)	8.27(19)	0.011	0.034	13.25(14)	8.30(19)	4.97(24)	4.95(24)

-
- [1] W. Kohn, Phys. Rev. **110**, 857 (1958).
 - [2] V. Gorelov, C. Pierleoni and D.M. Ceperley, Contrib. to Plasma Phys. 2019;59:e201800185, (2019).
 - [3] R. C. Clay, III, J. McMinis, J. M. McMahon, C. Pierleoni, D. M. Ceperley, and M. A. Morales, Phys. Rev. B **89**, 184106 (2014).
 - [4] M. Holzmann, D. M. Ceperley, C. Pierleoni, and K. Esler, Phys. Rev. E **68**, 046707 (2003).